B4225

Ph.D. Thesis

New Methods for Modification of a Biomaterial Surface to Improve its Osseointegration

István Pelsőczi-Kovács DDS

2006

SZTE Egyetemi Könyvtár
szpcnzp
1225
13.

Ph.D. Thesis

New Methods for Modification of a Biomaterial Surface to Improve its Osseointegration

István Pelsőczi-Kovács DDS

University of Szeged, Faculty of Medicine
Albert Szent-Györgyi Medical and Pharmaceutical Center
Department of Dentistry and Oral Surgery

Graduate School of Clinical Science
Research in Dental Medicine

Head of the Program: Prof. Zoltán Rakonczay PhD., DSc.
Coordinators: Prof. András Fazekas PhD.
Dr. Kinga Turzó PhD.

2006

PUBLICATIONS RELATED TO THE THESIS

I. Bereznai M., **Pelsőczi K. I.**, Tóth Z., Turzó K., Radnai M., Bor, Z., Fazekas A.: Surface modifications induced by ns and sub-ps excimer laser pulses on titanium implant material. Biomaterials, 24; (23) 4197-4203, 2003
IF: 3,799

II. **Pelsőczi K. I.**, Bereznai M., Tóth Zs., Turzó K., Radnai M.,Bor Zs., Fazekas A.: Titán minták felületének módosítása excimer lézerrel a hatékonyabb osszeointegráció érdekében.
Fogorv. Szle, 97, (6) 231-237, 2004

III. **Pelsőczi K. I.**, Turzó K., Gergely C., Fazekas A., Dékány I., Cuisinier F.: Structural characterization of self-assembled polypeptide films and protein on titanium and silica surfaces by atomic force microscopy.
Biomacromolecules, 6; (6), 3345-3350, 2005
IF: 3,299

CONTENTS

1. Introduction

1.1. The role of dental implants in medical use

Implants are alloplastic materials used to substitute lost organs or parts of the body. Dental implants are increasingly applied to replace lost teeth. In this case an artificial root is inserted into the bone at the site of the missing tooth. Implant-supported prosthetic devices, connected via a retrievable fixation, to the implant, can restore the lost function of the chewing apparatus.

During recent decades the number of utilized implants has been increasing exponentially. There are several reasons for the constantly growing demand for implants. The standard of living has generally increased, and thus more and more people, even among the elderly generation, wish to wear an implant-supported fixed or removable prosthesis. Another reason is that even the best-fitting complete denture cannot provide the same stability, chewing comfort and improved aesthetic appearance as an implant-supported and/or retained prosthesis. Though in the last decades there has been a decrease in dental decay, the partial edentulousness is quiet frequent. In this case, applying the implant method instead of a conventional bridge the missing teeth can be replaced with an implant-borne crown, without preparation of neighbouring healthy natural teeth. Nevertheless, sporting accidents affecting the dentition and congenitally missing teeth are relatively frequent, and these patients also demand tooth-preserving procedures such as oral implants. Moreover, using osseous implants in the treatment of head and neck cancer patients, a long-term successful prosthetic restoration may be achieved after surgical process.

1.2. Titanium as a biomaterial for dental implants

Biomaterials are alloplastic or synthetic materials used to replace living organs or tissues, and are present for a long time in close contact with their bio-environment. A wide range of materials have been assessed or are already in use as endosseous implant materials [1,2,3], including metals (stainless steel, cobalt-chromium alloy, gold alloys, titanium (Ti), Ti alloys, tantalum, etc.), ceramics (alumina, hydroxylapatite, beta-tricalcium phosphate, bioglass, etc.) or polymers (poly(methyl methacrylate), poly(tetrafluoroethylene), poly(ethylene), polysulfone, etc.) [4]. On the basis of their biological and mechanical properties, the whole

spectrum of material types can be classified into three groups: biotolerated, bioinert and bioreactive materials [5], (Fig. 1).

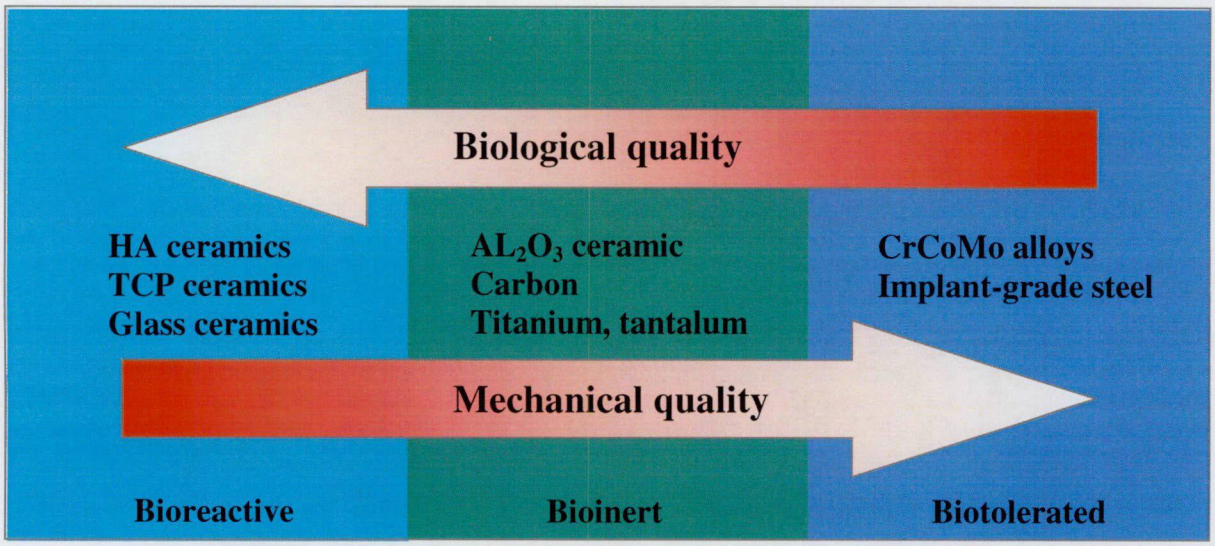

Fig. 1. Classification of dental implant materials from biological and mechanical aspect.

The best biological quality is to be expected from bioreactive materials, and biotolerated materials possess the best mechanical properties. Thanks to their physical and chemical properties, Ti and Ti alloys are nowadays the metals most commonly applied for such purposes, with an excellent osseointegration perspective, ensuring a predictable and long lifetime for dental implants [6-11].

Metallic Ti exists in a hexagonal closed packed structure called the α-phase at room temperature (25 °C), but shifts to a body-centred cubic crystal structure (the β-phase) at about 883 °C, and it melts at 1672 °C. Alloys of Ti with carbon, nitrogen and oxygen increase the stability of the α-phase, whereas vanadium stabilizes the β-phase. The two forms of Ti used for endosseous dental implants are "commercially pure" Ti (cpTi) and the most common Ti alloy Ti6Al4V. CpTi is available in different grades, which vary mostly in oxygen content. Grade 4 cpTi has the highest oxygen content, at 0.40%. Nitrogen, carbon, hydrogen and iron are also present, but do not vary much in concentration between grades. Ti alloys additionally contain approximately 6 wt% aluminium and 4 wt% vanadium. Aluminium increases the strength of the alloy and decreases its density. Vanadium acts to inhibit corrosion. Ti is a highly reactive metal: its exposure to air results in the rapid formation of a dense passive oxide layer. The surface

oxide, which forms on Ti, usually TiO_2, is of prime importance in the corrosion resistance of Ti. In air, the oxide begins to form in nanoseconds (10^{-9} s) and reaches a thickness of 20-100 Å in 1s (Fig. 2). It is very adherent to the parent Ti and impenetrable to oxygen. This oxide layer is capable of growing in time and this ability persists in the presence of a biological environment. The thickness and composition of this oxide probably change for a certain period after implantation. It is the nature of this surface layer that is thought to give Ti its excellent biocompatibility [4, 12-14]. Ti has a relatively large dielectric constant, ε = 50-170 (for alumina and dental porcelain ε = 4-10) (Fig. 2), and this provides a good condition for polar molecules to adsorb onto the surface and form van der Waal's bonds on TiO_2.

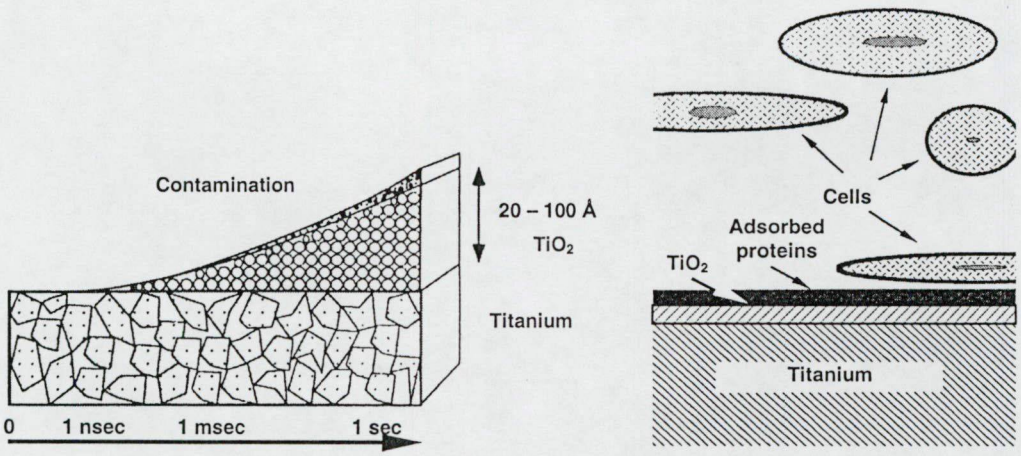

Fig. 2. Physical properties of Ti: heat of reaction ΔH = -912 kJ/mol, dielectric constant ε = 50-170.

In the early stages of bone healing, the adsorption of polar molecules is an important event. Ti has the advantage that its mechanical properties are closer to those of bone as compared with stainless steel or cobalt-chrome alloys [15].

The stoichiometric oxides of Ti, which contain Ti in the +4, +3 or +2 oxidation states, are TiO_2, Ti_2O_3 and TiO. The naturally abundant dioxide, TiO_2, exists in three crystalline forms: brookite (orthorhombic), anatase (tetragonal) and rutile (tetragonal). The surface of an implant may contain several different phases of TiO_2, reduced phases such as TiO or Ti_2O_3, different crystal faces and even amorphous phases. At higher temperatures, around 750 °C, brookite automatically reverts to the rutile structure. Rutile is the most common and well-known mineral of the three [16, 17].

1.3. Cellular and molecular reactions at the tissue-implant interface

The molecular or cellular reactions of the healing process take place at the tissue-implant interface, where the surface of the biomaterial is in intimate contact with the biological medium. In this process, the host bone and the alloplastic material are in permanent interaction with each other. From this point of view, the integration and the biocompatibility of the biomaterial must be regarded as continuously changing phenomena, the surface of material affecting the biological system and, at the same time, the host tissue interacting with the biomaterial. It is known that different materials will elicit different tissue responses. In recent decades, numerous materials have been developed as alloplastic materials, with varying degrees of success. The above-mentioned biotolerant materials initiate a special tissue response, and a fibrous capsule forms around the implant. These materials cannot fulfil the requirements of osseointegration, and therefore they cannot be used as materials for dental implants. In the case of bioinert materials (such as Ti), their stable oxide layer means that only a small number of metal ions are released from the surface. Although the surface oxide layer protects against corrosion, it cannot completely prevent the release of elements into the body. Previous studies have suggested that the rate of dissolution of Ti from cpTi is about 0.08 μg/day, which is approximately 10^4 times less than the normal daily intake. Accordingly Ti and its alloys are the most commonly used materials [4, 12]. Bioreactive materials, such as calcium phosphates, are generally applied as surface-coating materials, because of their chemical similarity to bone.

When a biomedical implant is brought into contact with living bone tissue, a series of complex processes occur over a broad range of time and area. These interactions are of major importance for the biological tissue-healing process. The earliest events at the interface, which occur within milliseconds after implantation, include the adsorption of water, ions and small biomolecules. Water may bind to the surface either as intact molecules or in dissociated form. Ions incorporated in the water layer can interact with the surface either directly or via a hydration shell. Different kinds of biomolecules (e.g. amino acids and carbohydrates) arrive at the interface from the blood and tissue fluid, and can interact directly with the surface or via a hydration layer. The actual nature of these early interactions constitutes important boundary conditions for later events, such as the interaction between the surface and larger biomolecules, e.g. proteins and enzymes, or cells. These initial processes are followed by the adsorption and exchange of larger biomolecules, such as proteins, which are known to have an inherent

tendency to deposit very rapidly on surfaces, which strongly influences the subsequent interactions of cells with the surface (Fig. 3).

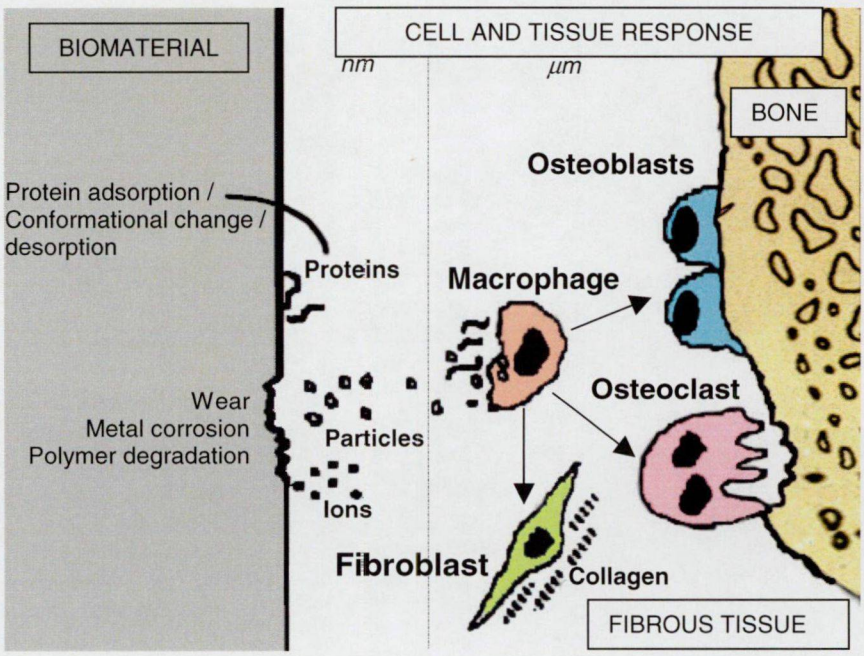

Fig. 3. Molecular and cellular interactions between biomaterial and host tissue.

Proteins can desorb (native or denaturated, intact or fragmented) or remain to mediate further tissue-implant interactions. Another consequence of these events is the release of metal ions or particles into tissues or electrochemical changes in the composition of the oxide film through the incorporation of various elements, e.g. Ca, P and S [18-20].

After the initial phases of molecular interactions of the bone-healing process, the symptoms of acute immune cell responses predominate during the first 4 days (Fig. 4). During the vascular response, a clot fills the gap between the implant and the bone, protecting the healing surfaces from the outside world. Cell reactions begin with the appearance of leucocytes that eliminate bacteria or foreign particles. Subsequently, lymphocytes and macrophages approach the surface. It is well known that macrophages have a significant role in the production of materials that regulate the migration of fibroblasts, and these cells will synthesize the new collagen. After the vascular response, fibroblasts appear, together with capillary proliferation or revascularization. As a result of the first stage of the bone-healing process, a collagen-rich fibrous tissue is formed, providing a scaffold for further processes.

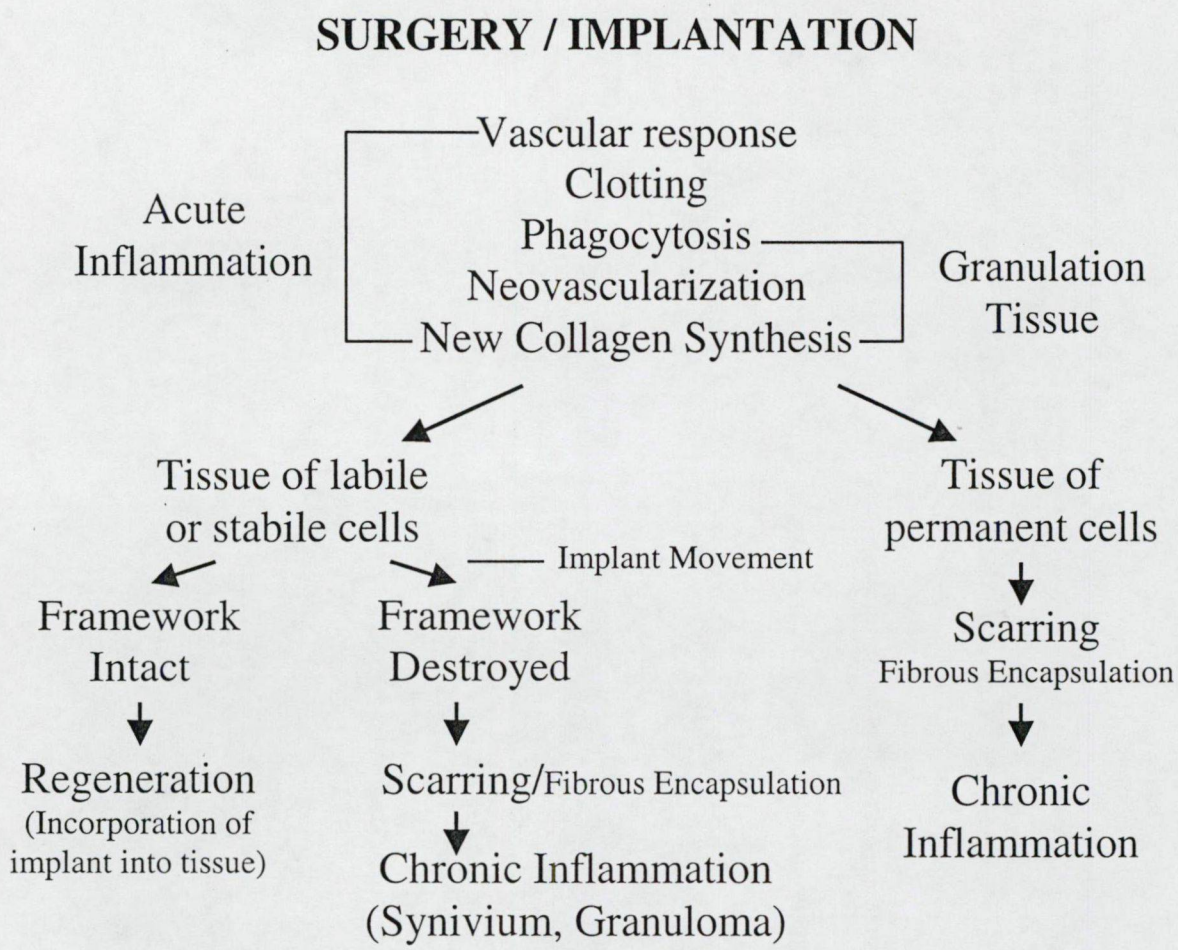

Fig. 4. Sequence processes of bone healing at the interface.

At the next, proliferation level, undifferentiated osteoprogenitor or mesenchymal cells are able to transform into osteogenic cells under the control of regulatory factors (such as non-collagenous proteins, osteopontin, bone sialoprotein or bone morphogenetic protein, etc.), and begin to build up the new bone in the following, differentiation stage. In this way, the regenerative capability of the surrounding bone tissue is basically determined by the presence and nature of the regulatory cells, such as macrophages or histiocytes and parenchymal cells, with respect to their capability for mitosis and migration, and by other factors, e.g. the vascularity, the oxygen saturation or the presence of regulatory proteins. Hence, a default of any of these results in a definable fibrous layer, permanently formed by fibroblasts, that surrounds an implant. This process, referred to as "fibrous encapsulation", should be avoided, as it leads to the failure of the implant. Another unfavourable condition is the premature (during

the healing period) loading of implants, which induces micro-motions and disrupts the newly formed tissue, likewise leading to the formation of a fibrous capsule [19, 21]. The wound-healing process is highly complex and involves numerous factors, including not only implant-related factors, such as material, surface chemistry and topography, but also other individual factors, such as the mechanical loading, the surgical technique, and the bone quality and quantity [18].

Normal bone regeneration depends mainly on the events described above. At the end of this process, differentiated osteogenic cells produce new bone, regulated by local growth factors in the ordinary way, ending with calcification. As mentioned above, the characteristics of the material and its chemical composition influence the initial reactions in the early stages of the bone-healing process. These interfacial characteristics therefore play an essential role in the osseointegration of the implant [22-24]. One aim of current implantology research is to attain a better understanding of the events at the interface, which is essential for the development of further strategies. The specific adsorption of proteins onto the surface and the subsequent cellular interactions are the key factors determining the interactions with the surrounding medium. Various biomolecules, which regulate the bone-healing process, have been identified at the interface [23, 25]. A number of them adsorb onto the surface and determine the osteogenic cellular response [26, 27]. The proteins involved in bone development and the adhesion of osteoblast cells can be divided into three groups: extracellular matrix proteins, cytoskeleton proteins and adhesion molecules. The extracellular matrix of bone is composed of 90% collagenic proteins (type I collagen 97% and type V collagen 3%) and of 10% non-collagenic proteins (osteocalcin 20%, osteonectin 20%, bone sialoproteins 12%, proteoglycans 10%, osteopontin, fibronectin, growth factors, bone morphogenetic proteins, etc.). All these proteins are synthesized by osteoblasts and most of them are involved in cell adhesion. Some of these proteins have chemotactic or adhesive properties, because they contain a special sequence named the RGD peptide (Arg-Gly-Asp) that is specific to the fixation of cell membrane receptors, e.g. integrin. The cell surface receptors recognize the RGD sequence and mediate the attachment [23, 25, 28].

...ctemi Könyvtár
SZEGED

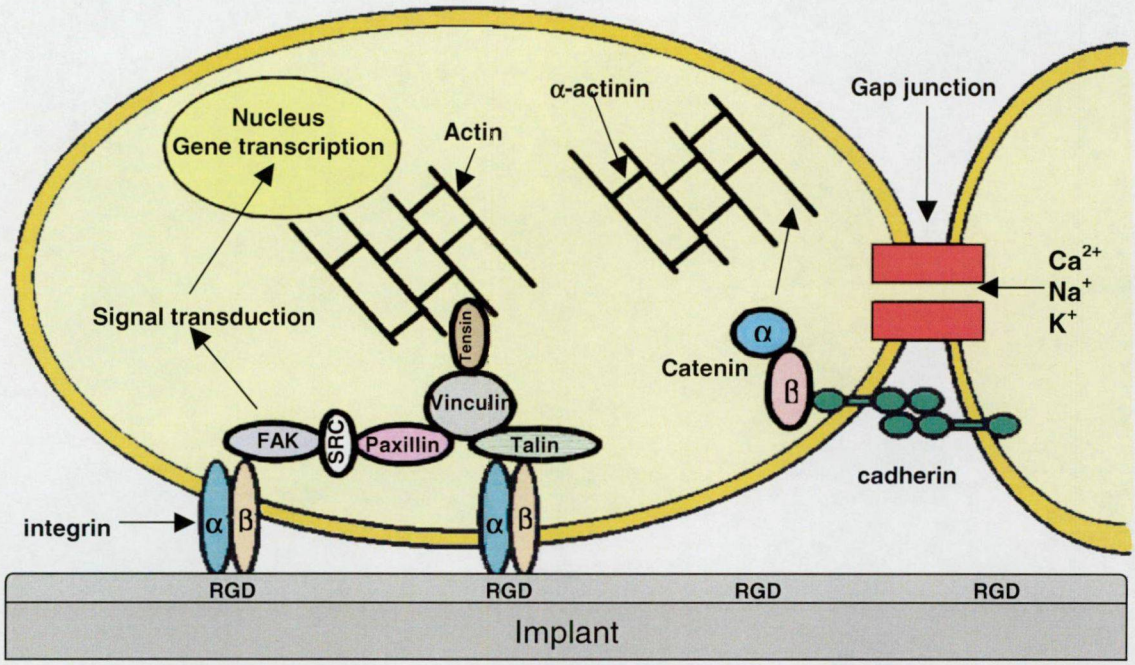

Fig. 5. Representation of the cell proteins involved in cell adhesion on a biomaterial.

On the internal faces of the cell, cytoskeleton proteins (talin, paxillin, vinculin and tensin) mediate the interactions between actin filaments and membrane receptor integrins. Actin has an essential role in the maintenance of cell shape and cell adhesion. Other important proteins are the adhesion molecules situated on the membrane of neighbouring cells. Adhesion molecules belong in different families. The four main classes are the selectins, the immunoglobulin superfamily, the cadherins and the integrins. Of these, only the cadherins and integrins have been described to date in osteoblastic cells. While the integrins are responsible for cell-substrate adhesion, the cadherins ensure cell-cell connection. The integrins have two types of sub-unit, α and β; each sub-unit is made up of a large extracellular domain, a transmembrane domain and a short cytoplasmic domain. It acts as an interfacer between the intra- and extracellular compartments and translates information about adhesion, spreading or cell migration, and consequently regulates cell growth and differentiation. The cadherins are transmembrane glycoproteins that interact with intracellular proteins [18, 23, 29, 30].

1.4. Biointegration of dental implants

The success and the long-term prognosis of dental implants depend mainly on three factors: first of all, on the anchorage of the artificial root in the host bone [31], i.e. on the osseointegration [32, 33], secondly on the peri-implant mucosal seal, and finally on the adequate loading of the implant, transmitted by the abutment, the biomechanical factor.

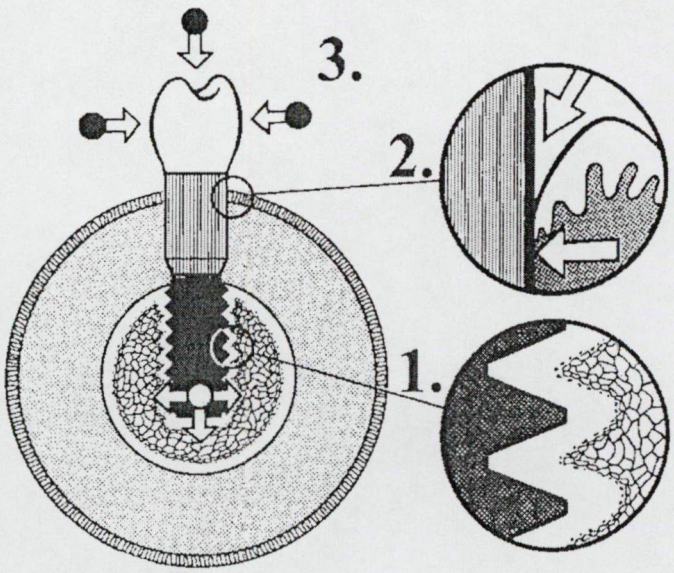

Fig. 6. Scheme of biointegration of a dental implant, representing osseointegration (1), mucosal seal (2) and biomechanical forces (3).

As regards osseointegration, which is the formation of a direct connection between the living bone and the surface of the load-carrying implant, strong links must be formed between the biomaterial and the surrounding bone tissue [22, 34-37]. This strong binding between the tissue and the implant can be ensured by connections in different size ranges: macro-mechanical, micro-mechanical and chemical connections [20, 38, 39]. The macro-mechanical connections relate to the geometrical design or the screw thread of the implant body, which is in the mm range. Micro-mechanical connections involve the roughness of the implant surface, which is detectable on a microscopic scale. The chemical connections between the implant surface and the host tissue develop at a nanoscopic level. During osseointegration, the normal wound-healing process is a two-sided event: besides the response of the host to the implant, the material affects the host. Hence, the newly formed bone grows from both sides simultaneously:

towards the bone (contact osteogenesis) and towards the biomaterial surface (distance osteogenesis) [31, 40]. Moreover, it has been reported [18] that the bone formation away from the implant surface proceeds at a rate about 30% higher than the rate of formation towards the implant. It is easy to see what an important role the biomaterial surface plays in bone healing.

The long-term benefits of dental implants additionally depend on the responses of the surrounding soft tissues: the connective tissues of the gingival attachment, and the gingival epithelium. Just as in the case of natural teeth, the presence of a healthy gingival attachment on an implant plays the role of a gate in the neck of an implant, blocking the way between the oral cavity and the inner milieu. Hence, the gingival attachment ensures an unperturbed healing period, thereby protecting against injuries coming from outside. The correct linkage of the ambient soft tissues is also influenced by the surface characteristics [41]. The soft tissue adhesion that forms around the neck of the dental implant measures about 3 mm in the corono-apical direction and consists of two zones: one of epithelium and one of connective tissue. Both tissues contribute to the establishment of a biological seal, which prevents oral bacteria and their products from penetrating into the body. The junctional epithelium covers about 2 mm of this surface, while the rest of it is utilized for the connective tissue adhesion.

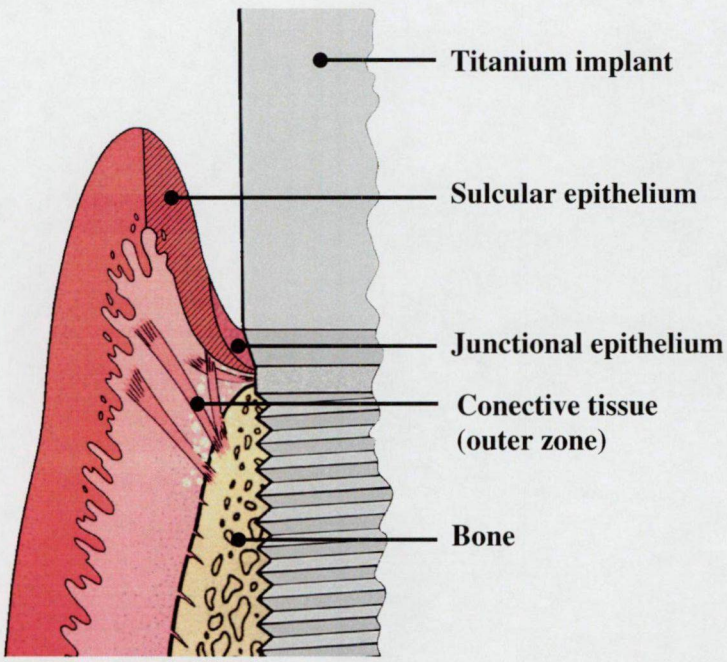

Fig. 7. Epithelial attachment on a Ti implant surface.

The connective tissue, located between the bony surface and the apical part of the junctional epithelium, can be divided into two zones. The inner zone is 50-100 μm thick, and is in direct contact with the implant surface. It is rich in fibres, with a few scattered cells and rare blood vessels. The rest of the connective tissue, the outer zone, is richer in cells and blood vessels, and is formed of fibres running in different directions [42]. The attachment of the epithelial cells occurs directly via a basal lamina and the formation of hemidesmosomes. Another possible attachment modality, which is an indirect epithelium-implant contact with a layer of amorphous material (consisting of glucosaminoglycans, glycoproteins and laminin), forms between the cell wall and the implant surface. In this way, the connective tissues surrounding dental implants do not become directly attached to the implant surface, but merely adhere to it. For bioinert and bioactive implant materials, a functional layer ensures the connection of the collagen fibres to the implant surface. In general, the connective tissue is rich in fibres that run parallel to the implant surface. The perpendicular attachment of connective fibres would be more favourable, resulting in a better support for the weak epithelial connection, as in the case of natural teeth. However a perpendicular fibre orientation has been observed in only a few investigations, when implants with a porous, rougher surface were used [43-45]. Although a rough surface would be favourable for the epithelial attachment, the neck of an implant must be polished in order to avoid pathogenic plaque accumulation [46].

The long-term function of an implant-supported prosthesis depends on numerous biomechanical factors. From a mechanical aspect, in the planning phase of the rehabilitation, the number, length and diameter of the implants must be included, and also their vertical and horizontal position in the jaw, anticipating the correct position of abutments in the normal occlusion scheme. These factors are very important from the point of view of further loading. Leverage factors that are generated by cantilevers can place enormous stress both on the implant and on the bone-implant interface. Leverage forces on implants further depend on the implant-abutment ratio of their vertical height. In patients with minimal bone loss, multiple long implants will easily support a prosthesis that has a relatively normal coronal height. However, in case involving advanced alveolar bone atrophy, it is a high requirement to fulfil the functional performance and also to restore perfectly the aesthetics and facial harmony. The engineering design for the implant-supported prosthesis must therefore consider the off-axis loading forces that are exerted on the implants and the bone by a variety of cantilevers [47].

1.5. Surface modifications of dental implants

Osseointegration is a relatively slow process (3-6 months in humans), when bone growths directly onto the surface of the alloplastic material, this taking place in a special space, the interface. Hence, there is major interest in increasing the speed of bone formation and degree of bone apposition, thereby reducing the healing time. It is particularly important in that case when patients suffered from any tumour or other bone diseases. In this way, the probability of long-term success may be increased, providing an added degree of patient comfort. Improved implant-bone bond strength and bone quality around implants would be of great significance in increasing the load-bearing capacity of the implant-bone interface. The important question arises as to how to attain a better integration by modification of the implant surface. It is widely agreed that the surface properties of an implant influence the interaction with the adjacent biological system. In order to regulate the bone formation and to achieve the desired biological responses, the surface properties can be modified by numerous methods. Surface modifications can be classified as produced by physicochemical or by biochemical methods [18, 48, 49].

1.5.1. Physicochemical methods

Surface energy, surface charge, surface composition and surface morphology are among the physicochemical characteristics, which can be altered in numerous ways. The surface energy (or surface wetting capability) plays an important role not only with regard to protein adsorption, but also with respect to cell attachment and spreading. This physical property can be measured by determination of the contact angles formed with the surface by different liquids. The surface charge influences both the molecular or cellular orientation and the cellular metabolic activity [50]. Bioreactive materials, such as calcium phosphate coatings, have been extensively applied because of their chemical similarity to bone [51, 52]. Protecting, bioactive ceramic oxide layer has been produced on titanium implants, in order to improve their surface properties [53, 54]. Various other types of physicochemical surface modifications have been reported, ranging from covalent and non-covalent coatings to other chemical reactions [49]. The best-known methods are etching, sand blasting, plasma spraying, film deposition, sol-gel process, vapor deposition, ion implantation and laser ablation.

Alterations in surface micromorphology and roughness have been used to influence the cell and tissue responses to implants, because the creation of mechanical interlocking

accelerates bone ingrowths [55-59]. This will increase the fixation and the stability of the implant. Larsson et al. carried out implantation in rabbit bone, their studies indicating that the surface roughness and the oxide thickness affect the rate of bone adhesion in the early stages (1-7 weeks) of implantation [38, 39].

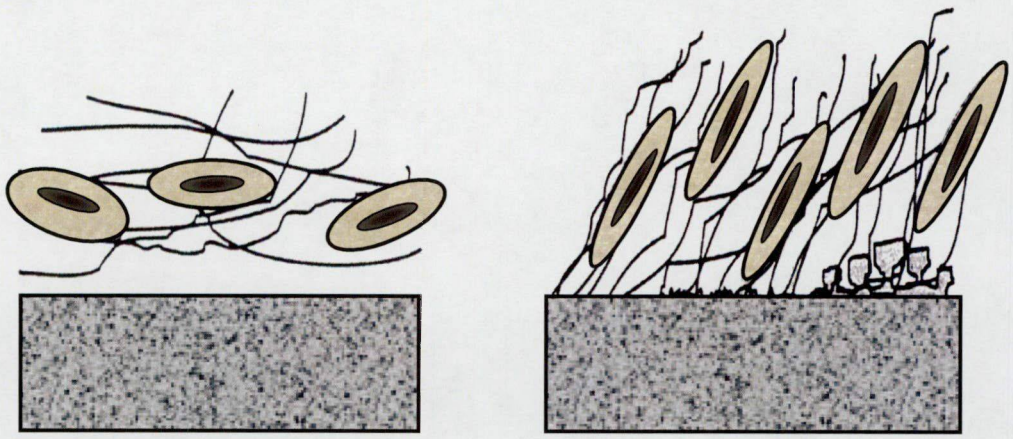

Fig. 8. Fibrins conduct osteogenic cells onto the surface.

Other authors suggest that the metabolic activity (the production of osteocalcin, prostaglandin E_2 (PGE_2) and transforming growth factor- β_1 (TGF-β_1) or alkaline phosphatase activity) of osteoblast-like cells is significantly increased on rough (sand-blasted, etched or plasma-sprayed) surfaces. It has been concluded that the surface roughness may modulate the activity of cells interacting with an implant and thereby affect the bone-healing process [50, 60]. As regards osseointegration, the mechanical roughness of the implant surface plays a significant role in anchoring cells (Fig. 8) and connecting the surrounding tissues together, thereby leading to a shorter healing period, as mentioned above. The area of contact can be enlarged by microstructuring the implant surface with one or other of the numerous methods referred to earlier [49, 56, 57, 61-63]. To increase the roughness of solid surfaces, a number of laser-based techniques have been applied in recent years [60, 65] and many authors have suggested that, for a perfect biointegration, the surface should be free from any contamination [34-36]. Besides the prompt intense heating of the surface, excimer laser illumination may further enhance the sterilizing effect in consequence of the high dose in the UV range. Recent studies on the laser machining of dental implants revealed that an appropriate structure with the least contamination could be achieved by means of laser treatment [66, 67]. After multipulse

irradiation with a focused Nd:YAG laser beam, a crown-like structure formation was observed on the titanium surface [68]. The efficient oxidation of Ti through Nd:YAG laser irradiation was reported in [69, 70]. The importance of these results lies in the fact, that they involve the processing of implant surfaces by means of laser technologies, which already have numerous industrial applications. However, these techniques must be further improved, since medical applications require high accuracy in the determination of both mechanical and chemical characteristics.

1.5.2. Biochemical methods

The goal of biochemical surface modification is to immobilize peptides, proteins or enzymes on biomaterials for the purpose of inducing specific cell and tissue responses or to control the tissue-implant interface with biomolecules [48, 71]. The immobilization methods consist of several processes ranging from physical adsorption (e.g. van der Waal's or electrostatic) to covalent attachment. In this respect, one possibility is to utilize the cell adhesion molecules described above (RGD peptides or integrin). These mediate the attachment of cells to the implant surface. The second approach to biochemical surface modification makes use of biomolecules: the growth factors (such as insulin-like growth factor (IGF), TGF, platelet-derived growth factor (PDGF) and extracellular matrix proteins etc.), which have osteotropic effects [72-75].

The anchoring of proteins to Ti surface was previously achieved by direct adsorption onto the surface [71], but such physical adsorption frequently induces denaturation and loss of the functional activity of the protein. To eliminate these problems, a surface modification by means of polyelectrolyte (PE) multilayers as self-assembled films is proposed in this work. PEs can be various polymers, proteins, different colloids and polypeptides. In our case, PE multilayers are formed by the alternating adsorption of polycations and polyanions from aqueous solution onto a charged, solid (glass or Ti) surface [76]. The alternating adsorption technique has been successfully applied in different fields. Its applications include surgical devices, implants and supporting materials (artificial organs, prostheses and sutures), drug delivery systems, carriers of immobilized enzymes and cells, stabilizing membrane proteins [77], biosensors, components of diagnostic assays, bioadhesives, ocular devices and materials for orthopaedic applications [78]. Polypeptide films can assemble spontaneously into well-

formed nanostructures in aqueous solution. This process is environment-friendly and various substrates can be covered with films of readily variable thickness [79]. The use of natural polymers can furnish other, also important advantages: they are non-toxic, non-antigenic and biocompatible [78]. Molecular self-assembly involves mostly the weak, non-covalent bonding. In order to attain the optimum strength between layers, it is proposed to apply charged poly(amino acids). Within the large number of candidate PEs, we were interested in biodegradable ones; accordingly, we studied the multilayers formed by the alternating adsorption of polycationic poly-L-lysine (PLL) and polyanionic poly-L-glutamic acid (PGA). To date, only a few studies have been carried out with this method, mainly by means of an *ex situ* build-up of films [80-82] or a partial *in situ* layering [30]. Besides the glass substrate used in the cited works, our study also included a PLL/PGA build-up on a Ti substrate, which is often used as an implant in medical interventions. PE films were deposited onto Ti and glass substrates by sequential adsorption in two ways: the build-up was performed either *in situ*, in the liquid cell of the atomic force microscope (*in situ* samples), or *ex situ*, outside the microscope, by an automatic immersion technique (dry samples). Previously published results [80, 83, 84] allow the expectation that PE multilayers should multiply the possibilities for the induction of cellular reactions if the cells are able to respond to bioactive molecules, e.g. signal transduction molecules embedded in the film.

2. Aims and questions to be answered

The aim of my research was to investigate two types of methods for surface modification: physicochemical and biochemical methods. I first investigated the microstructures of PE self-assembled films deposited on solid surfaces that might serve as future biomaterials. A second aim was to obtain results relating to excimer laser modifications, such as the polishing and structuring of Ti surfaces.

The challenging problems in my work may be summarized as follows.

- A structural characterization of the build-up process of PE (PLL/PGA) multilayers, by *in situ* optical waveguide light-mode spectroscopy (OWLS) and atomic force microscopy (AFM).
- Investigation of whether there are any differences in film surface characteristics between the two, *in situ* and *ex situ* build-up procedures.
- Examination of the film surface characteristics as a function of time. This is of great importance as concerns the industrial processing and clinical applicability of PE-modified implants.
- A study of how pH and rehydration affect the structure of such films, as hydration and a change in pH during the surgical process should not modify the applied coating.
- Visualization of the surface structures formed on Ti after excimer laser ablation (optical microscopy, scanning electron microscopy (SEM) and AFM).
- Investigations of the thickness of the oxide layer and the oxidation states of the laser-polished surface by means of X-ray photoelectron spectroscopy (XPS).
- Determination of any structural changes induced in the crystalline structure of the material by rapid laser annealing (X-ray diffraction (XRD) measurements).

The studies presented in this thesis were designed to answer the question of whether the two surface modification methods are applicable to dental implant materials, and in particular Ti. In the event of their applicability the next goal was to characterize these surfaces by using up-to-date surface science methods (SEM, XRD, XPS, AFM and OWLS).

Of course, achievement of the final, major aim, i.e. clinical application, and the processing of these surface modifications on an industrial scale necessitates biological testing. We have

already started cell-culture experiments and in the near future we plan animal testing. An account of these studies is not included here in consequence of space limitations.

3. Materials and methods

3.1. Materials

Microscope cover glass discs (Marienfeld, Germany) 14 mm in diameter were cleaned in a 3% solution of Hellmanex (D-79379, Hellma GmbH) and then in 0.1 M HCl solution for 15 minutes at boiling temperature, and finally rinsed in pure distilled water. Ti sample discs 1.5 mm thick and 15 mm in diameter were cut from commercially pure (grade IV) Ti rods (Dentaurum, Germany) used for the fabrication of dental implants. For the laser ablation 1.25 mm thick and 8 mm in diameter titanium sample discs were cut from commercially pure Ti rods (CP grade 1, <0.12% O, <0.05% N, <0.06% C, <0.013% H). In order to clean the surface, titanium samples were exposed to treatment in acetone or ethanol for 15 minutes in an ultrasonic bath and then sonicated in water three times for 10 minutes. PE solutions were prepared in an aqueous buffer solution of 25 mM TRIS (tris(hydroxymethyl)aminomethane, Sigma), 25 mM MES (2-(N-morpholino)ethanesulfonic acid, Sigma) and 100 mM NaCl (Fluka), pH 7.4. When the pH dependence was investigated, the buffer was adjusted to pH 5.0 or 9.0, with HCl or NaOH solution, respectively. The PE films were formed by the alternate adsorption of cationic PLL (MW = 30,000, Sigma Aldrich, P-2636) and anionic PGA (MW = 50,000, Sigma Aldrich, P-4886). The PE concentration was in all cases 1 mg/ml. Solutions were prepared with ultrapure water (Milli-Q-plus system, Millipore) and all buffer solutions were filtered before use.

3.2. Optical waveguide light-mode spectroscopy

OWLS is an optical technique, based on the confinement of a laser beam in a high refractive index layer of $Si_{0.8}Ti_{0.2}O_2$ (waveguide) by means of a grating coupler. The experimental details of the method are given elsewhere [85, 86]. The adsorption of a film onto such a waveguide perturbs the evanescent field and leads to changes in the effective refractive indices of the transverse electric (N_{TE}) and transverse magnetic (N_{TM}) modes. OWLS records with high precision ($\Delta N \sim 10^{-5}$) the changes in N_{TE} and N_{TM} up to a film thickness of roughly 350 nm. The measured N_{TE} and N_{TM} values depend on the refractive index profile of the film deposited on the wave-guiding layer. By means of the simultaneous measurement of two modes (p-polarized and s-polarized), the thickness and the refractive index of the adsorbed layer can

be calculated. The mode equations were resolved with a thin layer approximation, and the structural parameters, i.e. the refractive index and thickness (n_A and d_A) of each deposited layer, were obtained [86]. The PE multilayer film was then built up as follows: first, a 1 mg/ml PLL solution in 25 mM MES, 25 mM TRIS, 100 mM NaCl, pH 7.4 was injected for 15 minutes. Then, $(PLL/PGA)_n$, architectures were built up progressively up to $(PLL/PGA)_8$. PE depositions were always separated by a 15-minute long rinsing step.

3.3. *In situ* build-up of the PE film in the fluid cell of the AFM

The glass or Ti substrate was placed into the Nanoscope (Digital Instruments, Santa Barbara, USA) liquid cell closed by a silicone O-ring. The closed system joint for the liquid cell was described previously [87]. Buffer solution was then flowed through this system. PLL was injected first and left to adsorb for 15 minutes. After three rinses with buffer solution, PGA was injected in the same way. Images were taken 15 minutes after the last rinsing step. *In situ* imaging was performed following each deposition from the 4^{th} layer of PLL to the 8^{th} layer of PGA.

3.4. *Ex situ* build-up of the PE film outside the AFM

Both Ti and glass samples were placed in a special holder and were immersed alternately in PLL and PGA solutions by an automatic immersion device (Dept. of Colloid Chemistry, University of Szeged) at a constant speed. During each immersion period, the samples were kept in the solution for 15 minutes. Between two dips, the samples were rinsed three times with buffer solution. After formation of the last layer, the films (6, 8 or 10 bilayers) were rinsed in buffer and dried in a mild nitrogen-flow (high purity). Film-coated samples that had been aged for up to 1 month on the glass and for up to 2 months on the Ti substrate were studied by AFM. Rehydration was performed by wetting 6-week-old samples with buffer solution for at least 1 hour.

3.5. AFM measurements

The different surfaces were subjected to structural characterization with a Nanoscope III atomic force microscope (Digital Instruments, Santa Barbara, CA, USA) at Department of Colloid Chemistry at the University of Szeged. Silicon nitride tips (type MSCT-AUHW) were

purchased from Veeco Metrology Group (Santa Barbara, CA, USA). Cantilevers with spring constants of 0.01 and 0.03 N/m were used. Measurements were performed both in air and in a liquid cell. Height, deflection and friction images with areas of 10 × 10 μm and 5 × 5 μm were captured in contact mode, similarly as in other publications [80, 81, 87]. Lobo et al have pointed out that for the granulated structures of certain PE films, the tapping mode did not yield a good image contrast for the grains [88]. In these situations the contact and friction force modes must be used. As we expected such granulated structures and possible clustering, especially at high pH we employed contact mode AFM, furnishing the best image contrast with which to study the surface structure and morphology. However, in order to diminish the tip-sample interactions for *in situ* measurements, the AFM tips were silanized so as to transform the hydrophilic tip into a hydrophobic one, using a mixture of 5 ml of *n*-hexadecane, 5 drops of carbon tetrachloride and 5 drops of *n*-octadecyltrichlorosilane (Sigma Aldrich). Silanization allowed the imaging of both negative and positive surfaces. Several scans of each surface were performed in order to check the reproducibility of the images and to reveal possible tip damage. All images were taken at a scan rate of 1.97 Hz, with a resolution of 512 × 512 pixels, and 3D analysis was also performed.

The mean surface roughness (R_a) of a film was obtained by averaging the surface roughness (at least 5 independent measurements), defined as $R_a = \frac{1}{n}\sum_{j=1}^{n}\left|Z_j\right|$, the arithmetic average of the absolute values of the surface height deviations measured from the mean plane within the box cursor. The diameter of the grains was determined by performing section analysis in the Nanoscope software (Version 4.42, 1999).

Obtained data were analyzed by Student's *t* (unpaired, two-sample) test. A level of $p \leq 0.05$ was accepted as statistically significant.

3.6. Surface polishing with a ns ArF excimer laser

An ArF excimer laser (Lambda Physics EMG 201, wavelength: 193 nm, pulse duration: 18 ns, pulse energy: 100 mJ) was used for polishing. These experiments were performed at Department of Optics and Quantum Electronics in cooperation with Research Group on Laser Physics of the Hungarian Academy of Sciences. A square aperture that cut out the most

homogeneous part of the beam was imaged onto the surface of the samples by a fused silica lens (f = 5 cm). A 3.6 mm^2 area on the sample disc was illuminated by different series of laser pulses under atmospheric conditions. The fluence at the sample was monitored by calibrated energy measurement of a reference beam, coupled out by a fused silica plate.

In the experiments concerning laser polishing, two parameters were varied independently: the incident fluence was varied in the range 1.5-5 J/cm^2 by placing neutral filters in the beam path, and experiments were performed with 10, 100 or 1000 shots of excimer pulses.

3.7. Microstructuring by ns ArF excimer laser

For the local ablation of Ti surfaces, a similar set-up was used as in the case of the laser polishing experiments. A copper grid was placed in the beam path and its rectangular holes (0.29 mm^2 in area) were imaged by a fused silica lens with a focal length of 4 cm onto the sample surface. In this case a greater reduction of the beam was applied, and therefore the local average fluence was higher: 8.5 J/cm^2. 250, 500 and 1000 pulses were shot for local ablation experiments.

3.8. Microstructuring by 0.5 ps KrF excimer laser

Further microstructuring experiments were performed with ultrashort pulses of a KrF excimer laser (wavelength: 248 nm, pulse duration: 0.5 ps, pulse energy: 10 mJ). This laser system was described in detail in [89]. The only difference from the former optical set-up was that the titanium sample disc and the focal point of the lens were situated inside a low-pressure (10 Pa) vacuum chamber equipped with a transparent fused silica (Suprasil) window. Vacuum conditions were necessary because of the high power density, in order to avoid optical breakdown in air. In these experiments, 1000 pulses with a fluence of 2.4 J/cm^2 were applied.

3.9. Microscope investigations for laser treated samples

The surface morphology of the samples was first observed through an optical microscope (Nikon Optiphot 100S metallurgical microscope). High-resolution secondary electron images were recorded with a scanning electron microscope (Hitachi S-2400). For a better visualisation of the structures in depth, all samples were tilted at 75° in SEM. For

quantitative surface roughness determinations, AFM was applied (TopoMetrix Explorer TM, contact mode). The surface roughness characterised by the R_a value was determined by using TopoMetrix software.

3.10. X-ray photoelectron spectroscopy

One side of the Ti disk was polished by scanning over the whole surface area with laser pulses. The scanning speed was synchronised to the repetition rate of the laser, resulting in 10 overlapping laser shots with a fluence of 3.5 J/cm^2. This sample was used for XPS and XRD investigations. The chemical composition of the Ti surfaces was studied by XPS. The photoelectrons generated by Al K_α primary radiation (14 kV, 15 mA) were analysed with a hemispherical electron energy analyser (Kratos XSAM 800). Binding energies were normalised with respect to the position of the C (1s) peak. The changes in the XPS spectra were measured after 10 minutes of Ar^+ bombardment, repeated several times. Ar^+ was generated with ion gun energy of 3 kV and the incident ion beam current density was 4 μA/cm^2. Bombardment for 10 minutes removed about 10 nm from the surface of the material. Wide-range scans and higher-resolution narrow scans of the main characteristic peaks were recorded (Ti 2p, O 1s, and N 1s).

3.11. X-ray diffraction measurements

In order to compare the crystalline structures of the laser-treated samples with those of the non-irradiated materials XRD spectra were recorded, using Cu K_α radiation (λ = 0.154 nm). The XRD measurements were performed with a Philips PW 1830 X-ray generator (40 kV, 25 mA) with a powder diffractometer (PW 1877 Philips). The measured scan was taken between 2Θ values of 20° and 80°, with a step size of 0.02°.

4. Results and discussion

4.1. *In situ* PE deposition onto glass substrate measured by OWLS

The step-by-step build-up of a $(PLL/PGA)_8$ film was recorded *in situ* by OWLS (Fig 9A). This experiment served as a first check on the chosen experimental conditions, and the time domains necessary for the reproducible alternating adsorption of polypeptides forming the films to be further visualized by AFM. The thickness of the layers formed was calculated from the measured N_{TE} and N_{TM} values, as described in the Experimental section. The final thickness obtained was about 70 nm. A plot of the layer-by-layer growth of the film thickness (Fig. 9B) displays the well-known exponential growth of PLL/PGA film governed by polypeptide diffusion in and out, as explained previously [82].

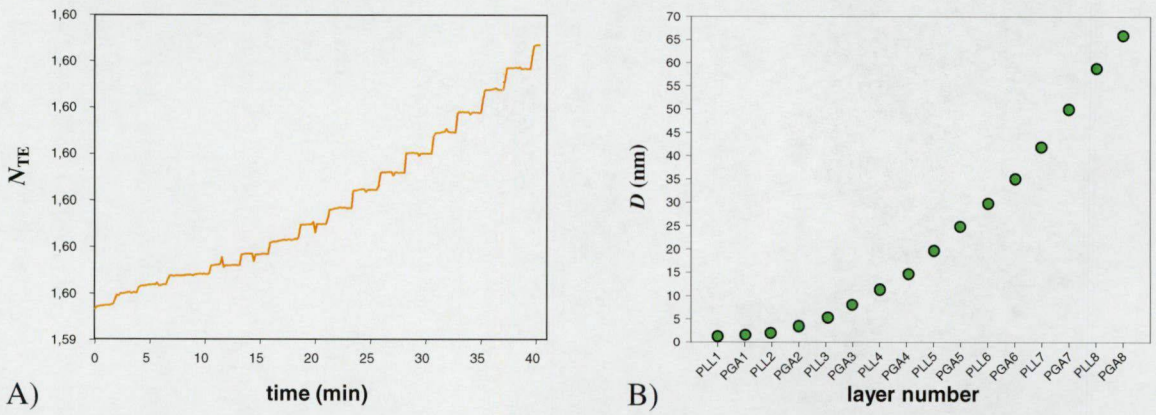

Fig. 9. OWLS measurements. A) N_{TE} values as a function of time; and B) film thickness (D) values as a function of layer number.

4.2. PE layers on glass substrate investigated by AFM

PLL/PGA films comprising up to 8 bilayers $(PLL/PGA)_8$ were successfully layered during *in situ* build-up in the liquid cell of the atomic force microscope. The AFM images exhibited a granular pattern similar to those found in other systems [81]. The same pattern was observed for samples prepared *ex situ*. The grain diameter was 270 ± 87 nm, in agreement with the values measured by Lavalle et al [82]. When not otherwise stated, the presented results will concern the film build-up under conditions close to physiological (150 mM ionic strength and pH 7.4).

SZTE Egyetemi Könyvtár SZEGED

The 3D images (Fig. 10.) demonstrated a significant morphological difference between the bare glass substrate and the $(PLL/PGA)_6$ film adsorbed on it.

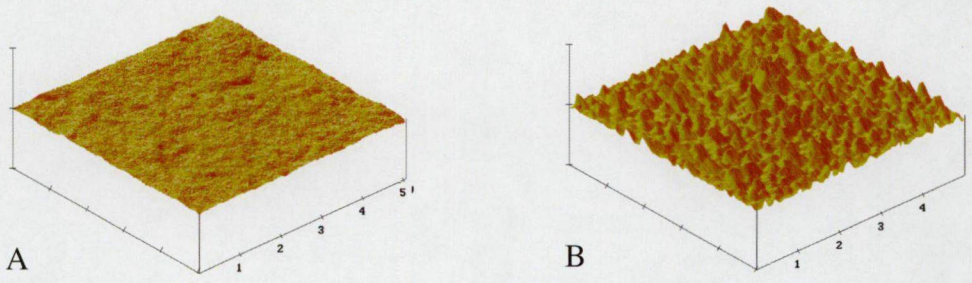

Fig. 10. 3D images of glass substrate and PE layers on it (*in situ* measurements). A) Bare glass, data scale: x = 1 μm/div and z = 20 nm/div; and B) $(PLL/PGA)_6$ PE film, data scale: x = 1 μm/div and z = 500 nm/div.

For the bare glass, a mean roughness value of $R_a = 0.5 \pm 0.2$ nm was obtained, while for $(PLL/PGA)_6$ the mean R_a was 17.7 ± 2.4 nm and for $(PLL/PGA)_8$ it was 16.9 ± 2.2 nm. For *in situ* deposition, the roughness was found to be independent of the number of layers (Fig. 11).

PLL/PGA films were also built up *ex situ*, by an automatic immersion method. Dry samples aged for 1 day, 1 week or 1 month was produced in this way. AFM images were then recorded. The structural characterization of these samples and their comparison with the result of the *in situ* measurements provided valuable information. Figure 11 depicts the changes in mean roughness of $(PLL/PGA)_5PLL$, $(PLL/PGA)_6$, $(PLL/PGA)_7PLL$ and $(PLL/PGA)_8$ films stored under dry conditions for up to 1 month.

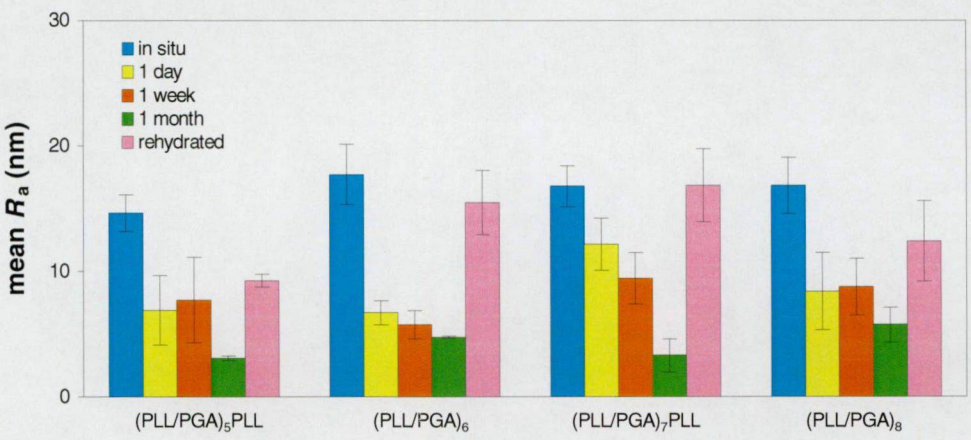

Fig. 11. Mean roughness values as a function of layer number and time for polypeptide films on a glass substrate. Rehydrated films were 6 weeks old.

In the *in situ* measurements, the roughness proved almost independent of the number of layers, whereas for the dry samples a significant variation was observed (see 1-day and the 1-week old samples for the $(PLL/PGA)_6$ and $(PLL/PGA)_7PLL$ films). The dry samples with both 6 and 8 bilayers indicated a large decrease in roughness in time as compared with the *in situ* values, except for the $(PLL/PGA)_7PLL$ film, where a smaller, but still significant decrement was observed. The chart reveals noteworthy decreases in R_a in all cases for the 1-month-old samples.

The PE films on a glass substrate also exhibited a significant time dependence, e.g. for the 1-day-old $(PLL/PGA)_7PLL$ film R_a was 12.2 ± 2.1 nm, while after 1 month it was 3.3 ±1.3 nm. Even after 1 day, a significant decrease in R_a was experienced, as observed for the $(PLL/PGA)_8$ films: the *in situ* value was 16.9 ± 2.2 nm, while for the 1-day-old sample it was 8.4 ± 3.1 nm.

Upon rehydration of a 6-week-old dry sample, the roughness values almost reached those measured *in situ*, independently of the nature of the last layer (Fig. 11). For the $(PLL/PGA)_6$ film, the mean R_a recovered to 15.5 ± 2.6 nm, while that for the $(PLL/PGA)_7PLL$ film did so to 16.9 ± 2.9 nm. The data prove that the PLL/PGA films possess a high capability to rehydrate and to recover their morphology when placed in a wet environment.

4.3. PE layers on Ti substrate investigated by AFM

PLL/PGA multilayers on Ti discs were also built up *in situ* in the liquid cell of the AFM. Typical AFM deflection images of the Ti substrate and $(PLL/PGA)_6$ and $(PLL/PGA)_8$ films may be seen in Fig. 12. The original rough-machined surface of the Ti disc can still be discerned even when the surface is covered totally by a PE film.

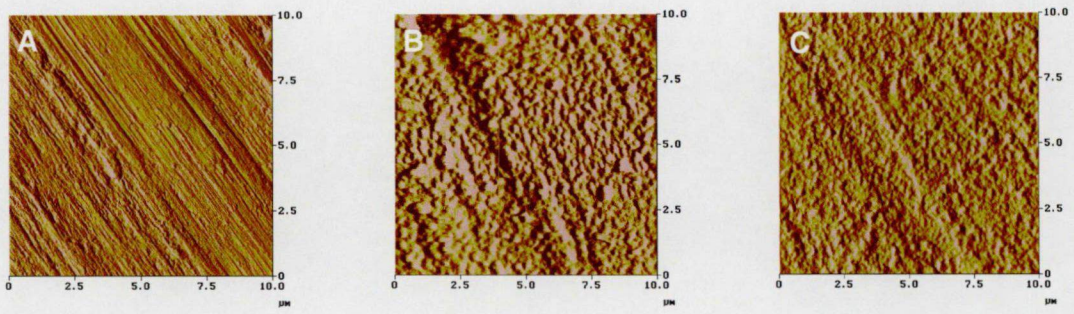

Fig. 12. AFM deflection images of Ti substrate and PE layers on Ti (*in situ* measurements). A) Bare Ti, z = 500 nm; B) $(PLL/PGA)_6$ multilayer, z = 800 nm; and C) $(PLL/PGA)_8$ film, z = 1.5 μm.

PLL/PGA films were also built up on a Ti substrate by the automatic immersion method. Dry samples aged of 1 day, 1 week, 1 month or 2 months were produced in this way. In the same way as for the glass substrate, a structural characterization was performed by AFM. The goal was to compare these samples with the samples prepared *in situ*, and to follow their variation in time, in order to provide information regarding their industrial applicability.

The same granular pattern was observed for the PE films prepared *ex situ*, demonstrating the lack of a dependence on the build-up procedure used (Fig. 13). The grain diameter, 303 ± 89 nm, was not significantly different from that obtained on glass.

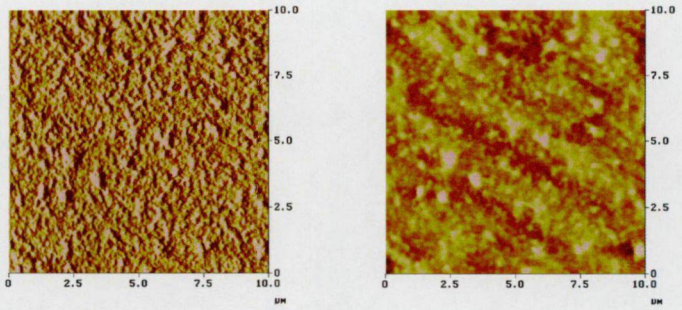

Fig. 13. AFM deflection and height images of a $(PLL/PGA)_9PLL$ film on a Ti substrate, 1-day-old sample, immersion build-up technique.

Figure 14A presents the mean roughness values for $(PLL/PGA)_7PLL$ and $(PLL/PGA)_8$ films, including the data on the *in situ*, *ex situ* and rehydrated samples. For *in situ* deposition, the roughness for $(PLL/PGA)_7PLL$ was 5.0 ± 0.6 nm, while for $(PLL/PGA)_8$ it was 6.1 ± 0.8 nm. Roughness value of bare Ti surface was 1.4 ± 0.5 nm (data not shown).

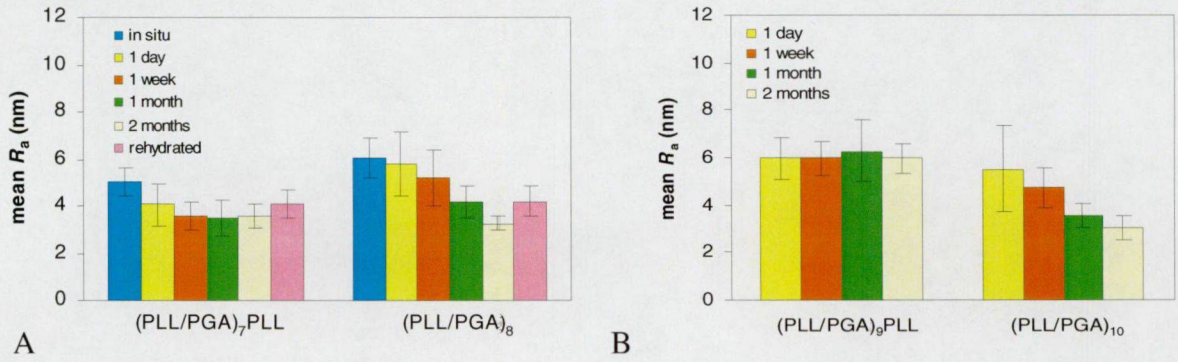

Fig. 14. Mean roughness values as a function of layer number and time for polypeptide films on a Ti. A) $(PLL/PGA)_7PLL$ and $(PLL/PGA)_8$ films, rehydration after 6 weeks. B) Dry samples of $(PLL/PGA)_9PLL$ and $(PLL/PGA)_{10}$ films.

PE films on a Ti substrate displayed a better stability in time up to 2 months as compared with glass substrate (Fig. 14A and Fig. 11). However, the 1-month-old samples of $(PLL/PGA)_7PLL$ and $(PLL/PGA)_8$ revealed almost the same roughness on the two different substrates. R_a for the $(PLL/PGA)_7PLL$ film on glass was 3.3 ± 1.3 nm, while that on the Ti substrate 3.5 ± 0.8 nm.

Figure 14B presents separately the mean roughness of thicker PE films (dry $(PLL/PGA)_9PLL$ and $(PLL/PGA)_{10}$) deposited *ex situ* on a Ti substrate. For the PLL-ended films, a significant (almost double) increase in R_a was found for all the dry samples: the typical R_a for a 1-week-old $(PLL/PGA)_7PLL$ sample was 3.6 ± 0.6 nm, while that for the $(PLL/PGA)_9PLL$ film was 5.9 ± 0.7 nm. In contrast for the PGA-ended films there was no such accentuated variation in roughness. The present data do not yield any explanation for this difference; however, the small error bars prove that there is a real increase in R_a due to the PLL. Additional studies are needed to explain this phenomenon.

Finally, when the 6-week-old samples were rehydrated, their roughness almost attained the *in situ* values: for $(PLL/PGA)_7PLL$, 4.1 ± 0.6 nm was measured, and for $(PLL/PGA)_8$ 4.2 ± 0.7 nm.

4.4. Structural characteristics of PE multilayers on Ti substrate as a function of pH

Since the degree of ionization of the PLL/PGA polypeptides is pH-sensitive, it may be expected that this parameter modulates the molecular organization of the films by altering the charge of both the polyanion and polycation. Weak PEs exhibit large variations in layer thickness and loops and tails above or below their pK_a as a result of incomplete charge compensation [90]. Morphological differences are observed when PLL/PGA films are deposited on a glass surface previously coated with strong PEs at pH 7.4 and pH 8.5 [30]. We were interested in following the pH dependence of the PLL/PGA film structures by AFM, after direct adsorption on a Ti surface. Accordingly, films were deposited *ex situ* on Ti at pH 5, pH 7.4 and pH 9. Analysis of the AFM images revealed a significant effect of pH on the roughness of the $(PLL/PGA)_7PLL$ and $(PLL/PGA)_8$ films: the values generally increased at acidic or basic pH (Fig. 15). There was also a noteworthy difference depending on the outermost layer of the PE film. When the outermost layer was PLL, high roughness values of 18.9 ± 4.2 nm and 11.2 ± 2.5 nm were obtained at low pH and high pH, respectively. In contrast, for the layers ending

in PGA R_a at pH 5 was much smaller, around 7.1 ± 1.5 nm, whereas at pH 9 there was no difference as compared with the PLL-ending film.

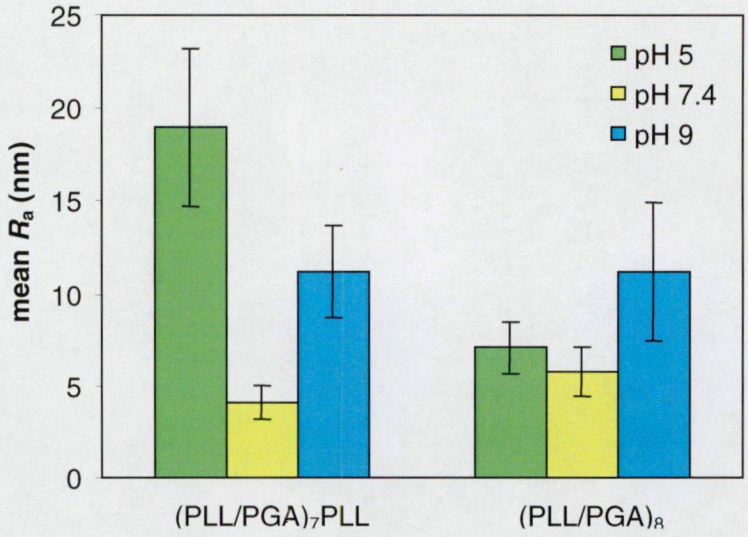

Fig. 15. pH dependence of mean roughness values for polypeptide films on a Ti substrate (1-day-old samples).

The high roughness values observed at acidic or basic pH are related to the degree of ionization of PGA and PLL. The pK_a values of PGA and PLL in aqueous solution are 4.9 and 9.8, respectively [91, 92]. At high pH, higher amounts of the only partly ionized PLL molecules are needed to neutralize the charges of the fully ionized PGA molecules. At low pH, where the PLL is totally, while the PGA is only partly ionized, the same interactions govern the build-up of the films as at high pH, but in the opposite sense. These processes lead to the observed increase in roughness. Our results are in good accordance with the formation of thicker layers at acidic or basic pH, as observed earlier [30].

4.5. Polishing of titanium surface

4.5.1. SEM and AFM analysis of laser-polished samples

ArF laser polishing was performed by applying 10 laser shots at a fluence of 1.5 J/cm^2. The efficiency of the polishing improved as the fluence was increased from 1.5 to 5 J/cm^2. As shown in the SEM micrograph in Fig. 16, the small scratches at intervals measuring <10 μm, were completely eliminated in the machined samples. Larger structures were merely reduced in

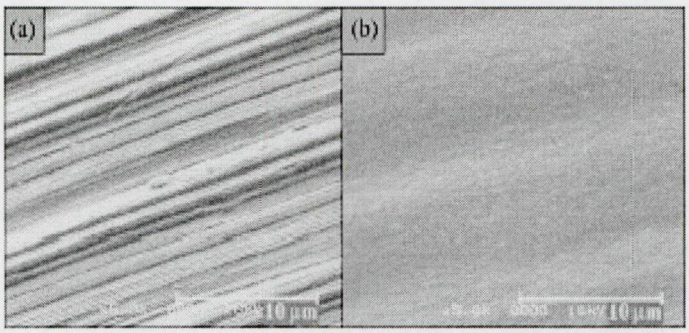

Fig. 16. SEM micrographs of: (a) non-irradiated machined and (b) ArF laser-polished titanium disk. The polishing was performed with 10 laser shots at a fluence of 3.5 J/cm^2.

height, but not completely removed, which resulted in a wavy surface (Fig. 16b). Sample surfaces subjected to a higher number of shots (100 or 1000) exhibited undesired waves, holes and plate-like formations (Fig. not shown).

The AFM surface topography pictures allowed a quantitative analysis of the surface roughness, as shown in Fig. 17. For the original machined samples, the roughness was R_a = 256 nm (Fig. 17a). The surface roughness of the laser-polished samples irradiated with 10 laser pulses with a fluence of ~5 J/cm^2 was significantly decreased, as revealed by the AFM micrographs (Fig. 17b): R_a = 25 nm.

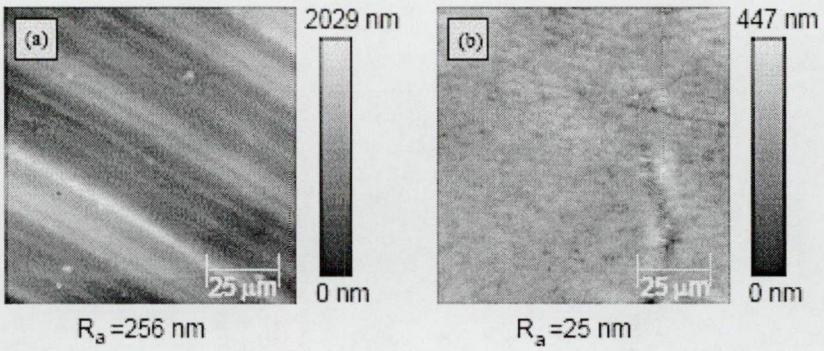

Figure 17. AFM surface topography images of: (a) non-irradiated and (b) ArF laser-polished titanium disk. The polishing was performed with 10 laser shots at a fluence of 5 J/cm^2. The surface roughness (Ra) for the non-irradiated and the laser-polished surface was 256 and 25 nm, respectively.

This value meets the requirements described in [93], where it was demonstrated that $R_a \leq 88$ nm for a titanium surface is optimum for the inhibition of plaque accumulation and maturation.

Both the SEM and the AFM studies confirmed that a titanium sample with Ra < ~1 μm can be effectively polished by homogeneous, 3-5 J/cm^2 fluence laser illumination. Polishing can occur via several mechanisms. During the applied laser irradiation, the surface material melts and evaporates. This was confirmed by the appearance of laser-induced plasma during polishing. Prior to resolidification, the molten surface can become smoothed. Another mechanism is described in [65]: the absorbed laser light heats the emergent sharp peaks of the rough surface more efficiently than the valleys, where the heat diffusion is more effective. The result is more material removal on the hills, and finally the surface will be smoother.

4.5.2. XPS investigation of the surface chemistry

The XPS survey spectra illustrated in Fig. 18 confirmed the presence of oxygen, nitrogen and carbon on both non-irradiated and laser-treated samples. These elements are typically observed on titanium implant surfaces [94]. Trace amounts of phosphorus and chlorine could also be detected as in [95, 96].

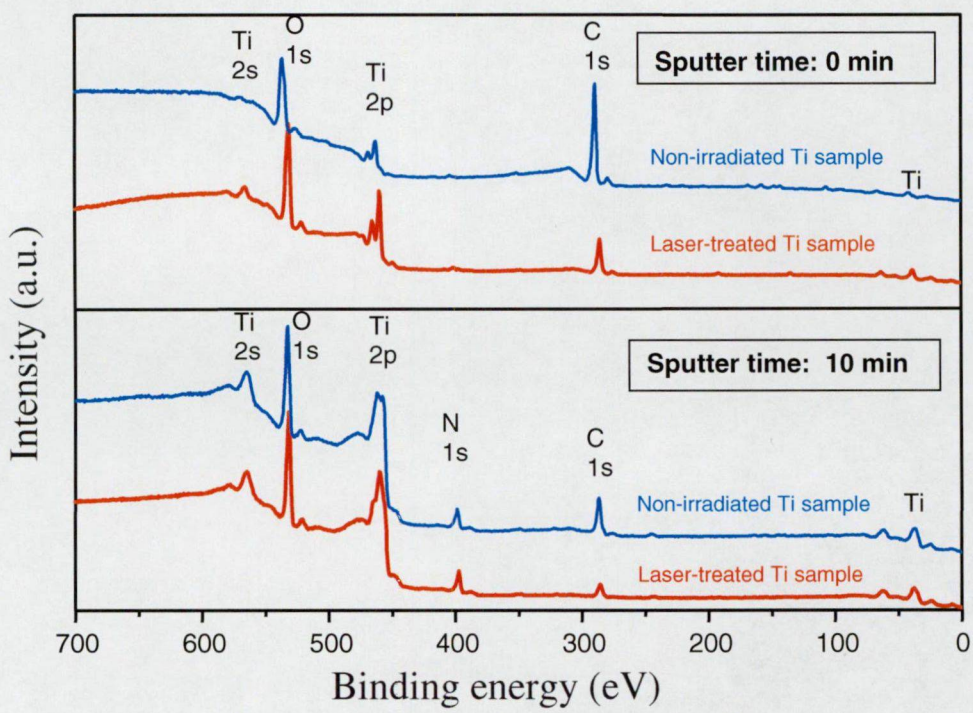

Figure 18. XPS survey spectra of non-irradiated and ArF-laser polished (10 laser shots at 3.5 J/cm^2) titanium disks. Upper part: spectra recorded without Ar^+ sputter; lower part: spectra after 10 min of Ar^+ bombardment.

SZTE Egyetemi Könyvtár SZEGED

The upper part of Fig. 18 depicts spectra recorded without any sputter, while the lower part presents spectra after 10 minutes of bombardment. In general, the laser treatment altered the surface chemistry in only a few respects. The substantial drop in the C 1s signal demonstrates that the excimer laser illumination effectively cleans the titanium surface. The C 1s signal indicates the presence of carbonaceous contamination, due to carbon-containing molecules remaining after chemical cleaning or adsorbed later on air-exposed surfaces [96, 97].

Representative high-resolution Ti 2p spectra of non-irradiated and laser-treated titanium samples after 10, 20 and 30 minutes of Ar^+ sputtering are to be seen in Fig. 19. The core level spectra after a single Ar^+ bombardment are similar, with three characteristic peaks, at 464.7, 459 and 455.6 eV. The positions of the Ti $2p_{1/2}$ and Ti $2p_{3/2}$ peaks correspond to those measured in TiO_2 [98]. The shoulder appearing at the lowest binding energy can be assigned to Ti $2p_{3/2}$ in TiN [99]. This reveals that, besides a thin TiO_2 layer, TiN impurities (probably originating from the basic material [100]) are also present on the sample surface. The presence of N was supported by the concomitant increment of the N 1s peak during Ar^+ sputtering. This can also be seen from a comparison of the curves corresponding to sputtering times of 0 and 10 minutes in Fig. 19.

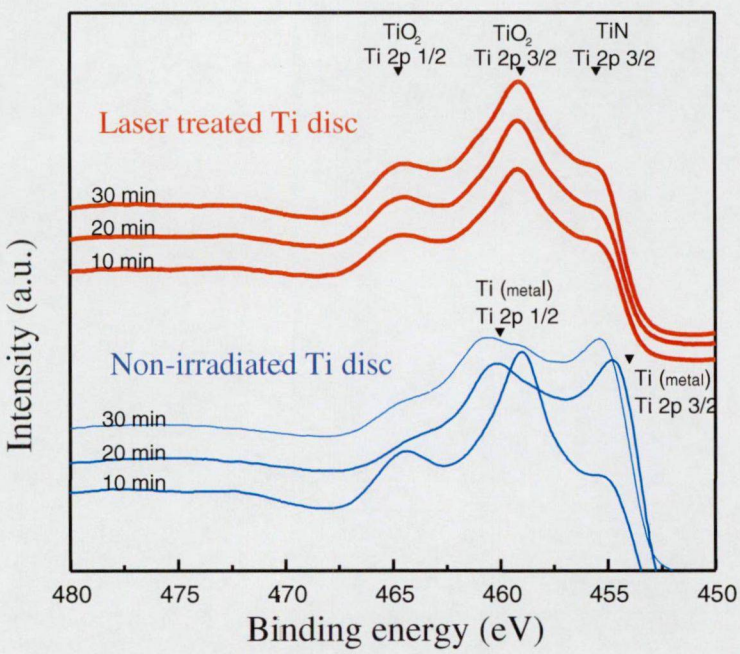

Fig. 19. High-resolution XPS spectra showing Ti 2p lines of nonirradiated and ArF laser-treated titanium samples (after 10, 20 and 30 min of Ar^+ sputtering).

It is interesting to compare the spectra in Fig. 19 that were measured after a second and a third Ar^+ sputter. The spectrum of the non-irradiated titanium surface includes peaks at binding energies of around 460 and 454 eV, corresponding to pure Ti metal [99, 101], while that of the laser-treated sample still exhibits the group of three peaks indicating the oxidized state of titanium as mentioned above, even after the second and third Ar^+ bombardments. Consequently, laser-polishing thickens the oxide layer at least 2-fold, which may favour the use of laser techniques to achieve better osseointegration [38, 39, 61].

4.5.3. XRD analysis

Rapid laser annealing by a series of ns laser pulses may alter the crystalline structure of the implant in the heat-affected zone. At room temperature the hexagonal α form of titanium is stable, while above 1158 K this phase changes to cubic β-titanium. It is essential to preserve the original crystal structure of the implant in order to avoid stress formation in it. The changes in crystal structure were followed by comparing the XRD spectra of the non-irradiated and laser-polished probes (Fig. 20). The XRD spectrum of the non-irradiated probe mainly shows the peaks of α-titanium [69, 102], but the peaks at $2\theta = 31.61°$, 34.59°, 36.13°, 47.53° and 56.29° demonstrate that other crystalline form(s) are present as well. Diffraction peaks at 34.59° and 38.42° can be attributed to surface contamination, since laser treatment resulted in significant decreases in intensity of these peaks. The XRD spectrum of the laser-polished probe reveals the intensity characteristics of pure α-titanium [103], indicated at the bottom of Fig. 20. The origins of the non-α-titanium peaks in the non-irradiated probes have not yet been clarified. The increase in the peak measured at 38.42° for the non-irradiated probe might possibly be assigned to the strong diffraction at 38.48° originating from the (110) plane of β-titanium, but this assumption cannot be true, since other peaks characteristic of β-titanium (e.g. at 55.54° and 69.60°) are completely missing from both diffraction curves. Titanium oxides such as anatase or rutile cannot furnish these non-α-titanium peaks either, because other strong characteristic titanium oxide peaks are absent from the spectra (e.g. the highest-intensity peaks at 25.32° and 27.37°, respectively, for anatase and rutile [102]).

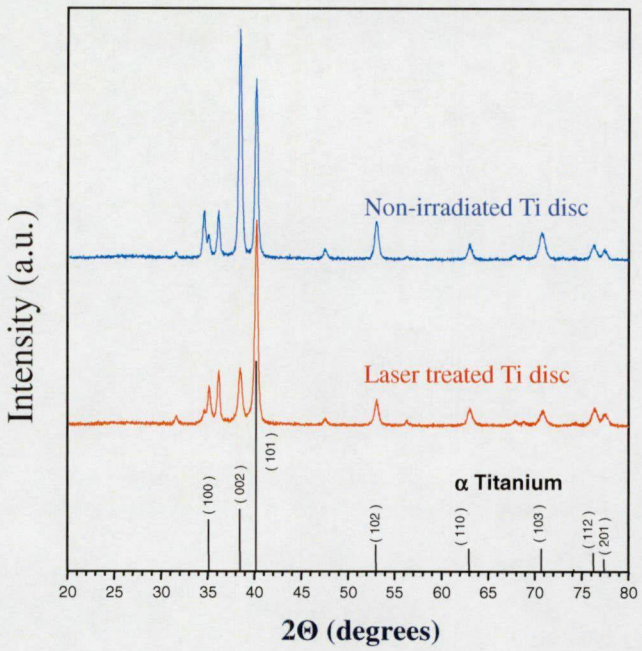

Fig. 20. XRD spectra of non-irradiated and ArF laser-polished probes. The relative intensities of pure α-titanium are indicated at the bottom.

Diffraction peaks of crystalline nitrides or carbides of titanium [104, 105] can likewise not be correlated with these locations. These diffraction peaks probably originate from crystalline forms of non-stoichiometric titanium compounds, e.g. oxides, nitrides or carbides, which were indicated by XPS. As X-ray diffraction is a bulk technique, it is naturally not possible to exclude with certainty the presence of a thin layer of some other material with a crystalline or amorphous structure. As concerns applicability, we can conclude that laser treatment results in cleaning of the surface and maintenance of the crystal structure of the titanium probe in α form.

4.6. Microstructuring of Ti surface by laser ablation

4.6.1. Surface patterning by ns excimer pulses

Holes at a characteristic distance of about 25 μm from each other were successfully ablated into the titanium surface by imaging a grid with ArF excimer laser pulses, as revealed by the SEM images in Fig. 21a,b. The surface was ablated locally at those sites where the fluence exceeded the ablation threshold. Increase of the number of pulses led to the ablation of holes with a higher aspect ratio. At the same time, rims formed around the edges of the holes as can be seen in Fig. 21a,b. After 250 shots at a fluence of 8.5 J/cm^2, the depth of the holes was about 10 μm and the height of the rims was at most 8 μm. From the depth of the ablated holes,

the effective evaporated thickness proved to be approximately 40 nm per pulse. Formation of the separate craters was possible because the heat diffusion length (for a pulse duration of 18 ns this is ~800 nm for titanium) was shorter than the distance between the holes.

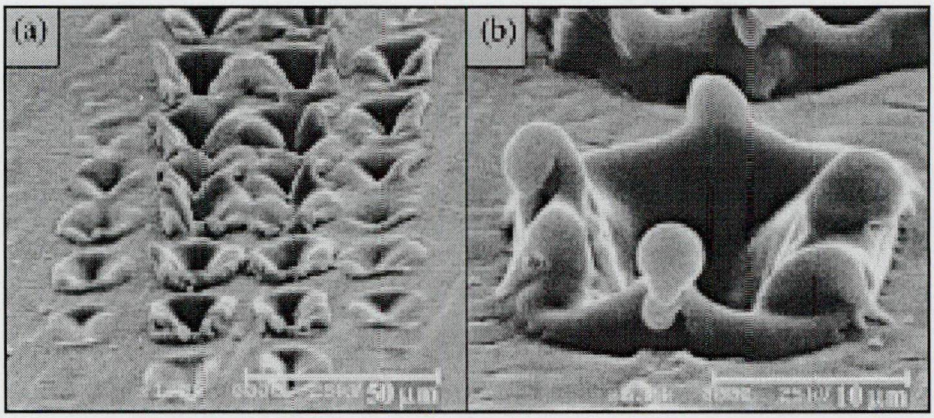

Fig. 21. SEM micrographs at different magnifications of ablated holes formed in a titanium surface after 250 shots of the ArF excimer laser. The fluence applied was 8.5 J/cm^2.

In nature, the holes resemble the drilled patterns made by other pulsed laser sources (e.g. Nd:YAG lasers) operated at longer wavelengths [68]. The temperature distribution in metals is determined mostly by the heat conduction and not by the wavelength-dependent absorption. The adsorption penetration depths at 193, 248 and 1064 nm are 13.5, 12.7, and 253.3 nm, respectively. These values are 1-2 orders of magnitude smaller then the above-mentioned heat diffusion length. It is common in these techniques that the ablation occurs via extensive evaporation and melting. In the applied fluence range, plasma is formed and the underlying molten layer is propelled out as a radial hydrodynamic flow due to the high recoil plasma pressures. During this process, rims are formed at the edges [68]. This is an inconvenient effect, since the rims may break away from the implant surface during the implanting procedure and contaminate the surrounding biological tissues.

4.6.2. Surface patterning by sub-ps excimer pulses

The debris-free processing of holes with high aspect ratios, which are commonly produced in the short-wavelength excimer laser ablation of specific polymers and ceramics, can not be reproduced in the case of metals with relatively high thermal conductivities. Similarly as

in drilling with ns length pulses of Q-switched Nd:YAG lasers, at an excimer pulse duration of 18 ns, the heat-affected zone is defined by the thermal diffusion length and not by the absorption penetration depth of the laser light. In this case the molten depth may approach 1 μm and the melt flows out from the high-pressure zones of high-temperature laser plasma. One possibility to overcome the problems of rim formation is to decrease the extent of heat diffusion. The application of 0.5 ps laser pulses allows a heat diffusion length of 4.3 nm. In this case the absorption penetration depth will determine the precision of laser processing. A number of authors have investigated the pulse duration requirements for the melting-free and burr-free drilling of metals [65, 106-110]. The highest process efficiency and hole quality can be achieved by using sub-ps pulse durations. On repetition of the surface patterning experiments with a 0.5 ps KrF excimer laser, rim formation could be eliminated completely, as illustrated in the SEM micrograph in Fig. 22. The laser fluence here was 2.4 J/cm^2 and 1000 shots had to be administered.

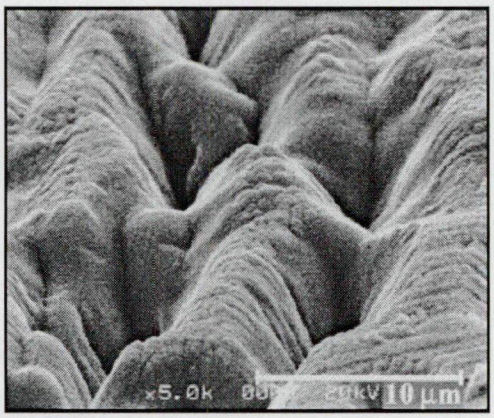

Figure 22. SEM micrograph of ablated holes formed in a titanium surface after 1000 shots of the 0.5 ps KrF excimer laser. The fluence applied was 2.4 J/cm^2.

The coherence properties of the applied 0.5 ps laser system led to less accurate imaging of the mask pattern on the sample surface. The topography of the ablated structure practically reproduces the intensity distribution in the image plane, which is distorted by interference phenomena. Accordingly, the ablated holes do not possess sharp and well-defined borders. The aspect ratio of the holes is sufficient for the required purpose, since the contact interface of the osseointegrating tissues was enlarged significantly.

5. Conclusions

The organization of multilayer films formed by electrostatically self-assembled PLL/PGA films was studied by means of OWLS. My results demonstrated that these layers grow in an exponential way on the glass substrate, and the final thickness of the PE multilayer was about 70 nm after 8th bilayer.

AFM measurements provided a structural characterization of the $(PLL/PGA)_i$ auto-assembled layers adsorbed on glass and Ti substrates in an irreversible way. A comparison was also made between the frequently used *ex situ* and the rarely used *in situ* buildup methods. Independently of the buildup procedure the films show granular patterns on both glass and Ti substrates, up to 10 bilayers. In all cases the grain diameters are between 200 and 400 nm.

The two substrates show different behaviour with increasing number of layers. On the glass the PE film is generally rougher. Unlike *in situ* examination a significant decrease of the roughness occurs on the dry (1 day-, 1 week-, and 1 month-old) glass samples. Contrarily on Ti a better stability can be observed in time and the dry sample values are closer to the *in situ* values, mostly in cases when PLL was the last layer. Consequently, surface modification with PLL ended 8 bilayers, and dry packing of the PE modified dental implants may be suggested in the course of industrial manufacturing.

Upon rehydration of dry samples the roughness values on glass almost reach the values measured *in situ*, while for titanium they exceed those. The stability and rehydration capability of PLL/PGA multilayer coatings built on Ti by immersion is of prime importance concerning their biomedical applications. In case of PE films built on Ti substrate a significant pH effect can be observed. The high roughness values observed at extreme pH's are related to the degree of ionization of PGA and PLL which means that the pH affect the structure of films. Therefore, any change in physiological pH, during the surgical process, can modify the applied coating.

Excimer laser processing modified the morphology of the Ti surface. Effective polishing was achieved by homogeneous illumination with ns laser pulses in the 3-5 J/cm^2 fluence range, as revealed by SEM and AFM studies. Holes about 20 μm diameter and 10 μm in depth with rims around the edges were ablated into the Ti surface with pulses of ns ArF excimer laser at a fluence of 8.5 J/cm^2. To avoid the formation of these fragile rims, 0.5 ps excimer pulse duration laser fluence of 2.4 J/cm^2 and increased number of shots were applied, whereby the melting- and rim-free ablation of Ti was attained.

The XPS measurements demonstrate that polishing with an excimer laser cleans the surface of Ti and thickens the oxide layer at least 2-fold, which may be favourable from the aspect of osseointegration. The XRD data confirmed that the laser polishing process did not alter the original crystalline structure.

However, industrial application of sub-ps excimer laser ablation is not yet available, considering its benefits for the surface improvement, utilization of this new method for modification of an implant surface can be recommended.

6. Acknowledgements

First and foremost I would like to thank Prof. András Fazekas and Dr. Kinga Turzó (University of Szeged, Department of Dentistry and Oral Surgery) for their valuable help and encouraging support, Dr. Csilla Gergely (Université Montpellier II, Groupe d'Étude des Semiconducteurs) and Dr. Frederic Cuisinier (Université Montpellier I, UFR Odontologie) for their help, which added so much to my work, Dr. Hector Flores (Facultad de Estomatología, Universidad Autónoma de San Luis Potosí) and Dr. Márta Szekeres (Department of Colloid Chemistry, University of Szeged) for their help in the AFM measurements. I am grateful to Dr. Zsolt Tóth and Miklós Bereznai (Research Group on Laser Physics, University of Szeged) for his help in laser polishing and laser ablation process. I also wish to thank Dr. Gábor Laczkó (Department of Experimental Physics, University of Szeged) for valuable discussions, Dr. Albert Oszkó from the Department of Solid-State and Radiochemistry at the University of Szeged for the XPS measurements, Dr. Ágnes Patzkó from the Department of Colloid Chemistry at the University of Szeged for the XRD measurements, and Prof. Sándor Szatmári for providing access to the 0.5 ps KrF laser facility at the Department of Experimental Physics, University of Szeged.

This work was supported by the SIMI-NAS Project of the 5th FWP of the European Commission (Growth Programme, Project no: GRD3-2001-61801) and the GVOP-3.2.1.-2004-04-0408/3.0 project funded by the Hungarian Ministry of Economy and the EC.

7. References

[1] Williams DF. Implants in dental and maxillofacial surgery. Biomaterials 1981;2:133

[2] Lemons JE. Dental implant biomaterials. J Am Dental Assoc 1990;121:716-719.

[3] Lemons JE. Dental Implants. In Ratner BD, Hoffman AS, Schoen FJ, Lemons JE (Eds.) Biomaterials Science. Academic Press, New York, 1996.

[4] Wataha JC. Materials for endosseous dental implants. J Oral Rehab 1996;23:79-90

[5] Spiekerman H, Donath K, Hassel T, Jovanovic S, Richter J. Implantology. In Rateitschak KH, Wolf HF (Eds.) Color Atlas of Dental Medicine. Georg Thieme Verlag, Stuttgart, 1995.

[6] Meffert RM, Langer B, Fritz ME. Dental implants: a review. J Periodontol 1992;63:859-870.

[7] Brånemark PI, Adell R, Albrektsson T, Lekholm U, Lundkvist S, Rockler B. Osseointegrated titanium fixtures in the treatment of edentulousness. Biomaterials 1983;4:25-28.

[8] Albrektsson T. The response of bone to titanium implants. CRC Critical Reviews in Biocompatibility 1985;1:53.

[9] Alberktsson T, Brånemark PI, Hansson HA, Lundström I. Osseointegrated titanium implants. Requirements for ensuring a long-lasting direct bone-to-implant enchorage in man. Acta Orthop Scand 1991;17:132-139.

[10] Morra M, Cassinelli C, Cascardo G, Cahalan P, Cahalan L, Fini M, Giardino R. Biomaterials 2003;24:4639-4654.

[11] El Ghannam, A.; Starr, L.; Jones, J. J Biomed Mater Res 1998;41:30-40.

[12] Lautenschlager EP, Monaghan P. Titanium and titanium alloys as dental materials. Int Dental Journal 1993;43:245-253.

[13] Michel R. Trace metal analysis in biocompatibility testing. CRC Critical Reviews in Biocompatibility 1987;3:235.

[14] Williams DF. Titanium and titanium alloys. In Williams DF (Ed.) Biocompatibility of Implant Materials. CRC Press, Boca Raton, FL, 1981.

[15] Long M, Rack HJ. Titanium alloys in total joint replacement – a materials science respective. Biomaterials 1998;19:1621-1639.

[16] Egdell RG, Jones FH. Structure and reactivity of oxide surfaces: new perspectives from scanning tunnelling microscopy. J Mater Chem 1998;3:469-484.

[17] Pang CL, Raza H, Haycock SA, Thorton G. Imaging reconstructed TiO_2 surfaces with non-contact atomic force microscopy. Appl Surf Sci 2000;4:233-238.

[18] Puleo DA, Nanci A. Understanding and controlling the bone-implant interface Biomaterials 1999;20:2311-2321.

[19] Spector M, Lalor PA. *In vivo* assessment of tissue compatibility. In Ratner BD, Hoffman AS, Schoen FJ, Lemons JE (Eds.) Biomaterials Science. Academic Press, New York, 1996.

[20] Kasemo B, Lausmaa J. Biomaterials and interfaces. In Naert I, Steenberghe D, Worthington P (Eds.) Osseointegration in oral rehabilitation. Quintessence Publishing Co., 1993.

[21] Divinyi T. Fogászati Implantológia. Springer-Verlag, Budapest, 1994.

[22] Morra M, Cassinelli C. Organic surface chemistry on titanium surfaces via thin film deposition. J Biomed Mater Res 1997;37:198-206.

[23] Anselme K. Osteoblast adhesion on biomaterials. Biomaterials 2000 ;21:667-681.

[24] Schwartz Z, Boyan BD. Underlying mechanisms at the bone-biomaterial interface. J Cell Biochem 1994;56:340-347.

[25] Schakenraad JM. Cells:their surfaces and interactions with materials. In Ratner BD, Hoffman AS, Schoen FJ, Lemons JE (Eds.) Biomaterials Science. Academic Press, New York, 1996.

[26] Zeng H, Chittur KK, Lacefield WR. Analysis of bovine serum albumine adsorption on calcium phosphate and titanium surfaces. Biomaterials 1999;20:377-384.

[27] Green RJ, Davies MC, Roberts CJ, Tendler SJB. Competitive protein adsorption as observed by surface plasmon resonance. Biomaterials 1999;20:385-391.

[28] Huang S, Ingber DE. The structural and mechanical complexity of cell-growth control. Nature Cell Biol 1999;1:131-138.

[29] Courtney J, Lamba M, Sundaram S, Forbes CD. Biomaterials for blood-contacting applications. Biomaterials 1994;15:737-744.

[30] Gergely C, Bahi S, Szalontai B, Flores H, Schaaf P, Voegel JC, Cuisinier FJG. Human serum albumin self-assembly on weak polyelectrolyte multilayer films structurally modified by pH changes. Langmuir 2004;20:5575-5582.

[31] Davies JE. Mechanisms of endosseous integration. Int J Prosthodont 1998;11:391-401.

[32] Adell R, Leckholm U, Rockler B, Brånemark PI. A 15-year study of osseointegrated implants in the treatment of the edentulous jaw. Int J Oral Surg 1981;10:387-416.

[33] Brånemark PI. Osseointegration and its experimental background. J Prosthet Dent 1983;50:399-410.

[34] Binon PP, Weir DJ, Marshall SJ. Surface analysis of an original Brånemark implant and three related clones. Int J Oral Max Imp 1992;7:168-175.

[35] Olefjord I, Hansson S. Surface analysis of four dental implant systems. Int J Oral Max Imp 1993;8:32-40.

[36] Cochran DL. A comparison of endosseous dental implant surfaces. J Periodontology 1999;70:1523-1539.

[37] Uitto VJ, Larjava H, Peltonen J, Brunette DM. Expression of fibronectin and integrins in cultured periodontal-ligament epithelial-cells. J Dent Res 1992;71:1203-1211.

[38] Larsson C, Thomsen P, Lausmaa J, Rodahl M, Kasemo B, Ericson LE. Bone response to surface modified titanium implants: studies on electropolished implants with different oxide thickness and morphology. Biomaterials 1994;15:1062-1074.

[39] Larsson C, Thomsen P, Aronsson BO, Rodahl M, Lausmaa J, Kasemo B, Ericson LE. Bone response to surface modified titanium implants: studies on the early tissue response to machined and electropolished implants with different oxide thicknesses. Biomaterials 1996;17:605-616.

[40] Davies JE, Lowenberg B, Shiga A. The bone-titanium interface in vitro. J Biomed Mater Res 1990;24:1289-1306.

[41] Hansson H, Albrektsson T, Brånemark PI. Structural aspects of the interface between tissue and titanium implants. J Prosth Dent 1983;50:108-113.

[42] Vogel G. Biological aspects of a soft tissue seal. In Lang NP, Karring T, Lindhe J (Eds.) Proceedings of the 3rd European Workshop on Periodontology. Quintessenz Verlags-GmbH, Berlin, 1999.

[43] Akagawa Y, Matsumoto T, Nikai H, Takata T, Tsuru H. Correlation between clinical and histological evaluations of the periimplant gingiva around the single-crystal sapphire endosseous implant. J Oral Rehab 1989;16:581-587.

[44] Cochran DL, Hermann JS, Schenk RK, Higginbottom FL, Buser D. Biological width around titanium implants. A histometric analysis of the implanto-gingival junction around unloaded and loaded nonsubmerged implants in the canine mandible. J Periodont 1997;68:186-198.

[45] Hashimoto M, Akagawa Y, Nikai H, Tsuru H. Ultrastructure of the periimplant junctional epithelium on single-crystal sapphire endosseous dental implant loaded with functional stress. J Oral Rehab 1989;16:261-270.

[46] Quirinen M, Bollen CM, Papaioannou W, Van Eldere J, van Steenberghe D. The influence of titanium abutment surface roughness on plaque accumulation and gingivitis: short-term observations. Int J Oral Max Imp 1996;11:169-178.

[47] Brunski JB, Skalak R. Biomechanics of osseointegration and dental prosthesis. In Naert I, van Steenberghe D, Worthington P. Osseointegration in Oral Rehabilitation. Quintessence Publishing Co., London, 1993.

[48] Ito Y, Kajihara M, Imanishi Y. Materials for enhancing cell adhesion by immobilization of cell-adhesive peptide. J Biomed Mater Res 1991;25:1325-1337.

[49] Ratner BD, Hoffman AS. Thin films, Grafts, and Coatings. In Ratner BD, Hoffman AS, Schoen FJ, Lemons JE (Eds.) Biomaterials Science. Academic Press, New York, 1996.

[50] Meyle J. Cell adhesion and spreading on different implant surfaces. In Lang N, Karrig T, Lindhe J. Proceedings of the 3rd European Workshop on Periodontology, Quintessenz Verlags-GmbH, Berlin, 1999.

[51] Rohanizadeh R, LeGeros RZ, Harsono M, Bendavid A. Adherent apatite coating on titanium substrate using chemical deposition. J Biomed Mater Res A. 2005;72:428-438.

[52] Sun L, Berndt CC, Gross KA, Kucuk A. Material fundamentals and clinical performance of plasma-sprayed hydroxyapatite coatings: a review. J Biomed Mater Res 2001;58:570-592.

[53] Szabo G, Kovacs L, Vargha K. Possibilities for improvement of the surface properties of dental implants (2). The use of ceramic oxides in surface coating for titanium and tantalum implants. Fogorv Sz 1995;88:73-77.

[54] Hench LL. Ceramics, glasses and glass-cements. In In Ratner BD, Hoffman AS, Schoen FJ, Lemons JE (Eds.) Biomaterials Science. Academic Press, New York, 1996.

[55] Joob-Fancsaly A, Huszar T, Divinyi T, Rosivall L, Szabo G. The effect of the surface morphology of Ti-implants on the proliferation activity of fibroblasts and osteoblasts. Fogorv Sz 2004;97:251-255.

[56] Buser D, Sehenk RK, Steinemann S, Fiorellini JP, Fox H, Stitch H. Influence of surface characteristics on bone integration of titanium implants: a histometric study in miniature pigs. J Biomed Mater Res 1991; 25:889-902.

[57] Wong M, Eulenberger J, Schenk RK, Hunziker E. Effect of surface topography on the osseointegration of implant materials in trabecular bone. J Biomed Mater Res 1995; 29:1567-1575.

[58] Cochran DL, Schenk RK, Lussi A, Higginbottom FL, Buser D. Bone response to unloaded and loaded titanium implants with a sandblasted and acid-etched surface: a histometric study in the canine mandible. J Biomed Mater Res 1998; 40:1-11.

[59] Santis D, Guerriero C, Nocini PF, Ungersbock A, Richards G, Gotte P, Armato U. Adult human bone cells from jaw bones cultured on plasma-sprayed or polished surfaces of titanium or hydroxyapatite discs. J Mater Sci Mater Med 1996;7:21-28.

[60] Joob-Fancsaly A, Divinyi T, Fazekas A, Peto G, Karacs A. Surface treatment of dental implants with high-energy laser beam. Fogorv Sz 2000;93:169-180.

[61] Eriksson C, Lausmaa J, Nygren H. Interactions between human whole blood and modifed TiO_2-surfaces: Influence of surface topography and oxide thickness on leukocyte adhesion and activation. Biomaterials 2001;22:1987-1996.

[62] Wennerberg A, Ektessabi A, Albrektsson T, Johansson L, Andersson B. A 1-year follow-up of implants of differing surface roughness placed in rabbit bone. Int J Oral Max Imp 1997;12:486-494.

[63] Boyan BD, Batzer R, Kieswetter K, Liu Y, Cochran DL, Szmuckler-Moncler SS, Dean DD, Schwartz Z. Titanium surface roughness alters responsiveness of MG63 osteoblast-like cells to 1 alpha,25-(OH)(2)D-3. J Biomed Mater Res 1998;39:77-85.

[64] Rupp F, Scheideler L, Rehbein D, Axmann D, Geis-Gerstorfer J. Roughness induced dynamic changes of wettability of acid etched titanium implant modifications. Biomaterials 2004;25:1429-1438.

[65] Bäuerle D. Laser Processing and Chemistry. Berlin, Heidelberg, New York, Tokyo: Springer-Verlag, 2000.

[66] Gaggl A, Schultes G, Müller WD, Kärcher H. Scanning electron microscopical analysis of laser-treated titanium implant surfaces – a comparative study. Biomaterials 2000;21:1067-1073.

[67] Pető G, Karacs A, Pászti Z, Guczi L, Divinyi T, Joób A. Surface treatment of screw shaped titanium dental implants by high intensity laser pulses. Appl Surf Sci 2001;7524:1-7.

[68] György E, Mihailescu IN, Serra P, Pérez del Pino A, Morenza JL. Crown-like structure development on titanium exposed to multipulse Nd:YAG laser irradiation. Appl Phys A 2002;74:755-759.

[69] Perez del Pino, Serra P, Morenza JL. Oxidation of titanium through Nd:YAG laser irradiation. Appl Surf Sci 2002;197-198:887-890.

[70] Nánai L, Vajtai R, George TF. Laser-induced oxidation of metals: state of art. Thin Solid Films 1997;298:160-164.

[71] Hoffman AS, Biologically Functional Materials. In Ratner BD, Hoffman AS, Schoen FJ, Lemons JE (Eds.) Biomaterials Science. Academic Press, New York, 1996.

[72] Dee KC, Rueger DC, Andersen TT, Bizios R. Conditions which promote mineralization at the bone-implant interface: a model in vitro study. Biomaterials 1996;17:209-215.

[73] Lynch SE, Buser D, Hernandez RA, Weber HP, Stich H, Fox CH, Williams RC. Effects of the platelet-derived growth factor/insulin-like growth factor-I combination on bone regeneration around titanium dental implants. Results of a pilot study in beagle dogs. J Periodontol 1991;62:710-716.

[74] Rezania A, Thomas CH, Branger AB, Waters CM, Healy KE. The detachment strength and morphology of bone cells contacting materials modified with a peptide sequence found within bone sialoprotein. J Biomed Mater Res 1997;37:9-19.

[75] Puleo DA. Biochemical surface modification of Co-Cr-Mo. Biomaterials 1996;17:217-222.

[76] Decher G, Hong JD, Schmitt J. Buildup of ultrathin multilayer films by a self-assembly process: consecutively alternating adsorption of anionic and cationic polyelectrolytes on charged surfaces. Thin Solid Films 1992;210:831-835.

[77] Zhang S, Zhao X. Design of molecular biological materials using peptide motifs. J Mater Chem 2004;14:2082-2086.

[78] Angelova N, Hunkeler D. Rationalizing the design of polymeric biomaterials. Reviews Elsevier Science 1999;17:409-421.

[79] Sano M, Lvov Y, Kunitake T. Formation of ultrathin polymer layers on solid substrates by means of polymerization-induced epitaxy and alternate adsorption. Annu Rev Mater Sci 1996;26:153-187.

[80] Ram MK, Bertoncello P, Ding H, Paddeu S, Nicolini C. Cholesterol biosensors prepared by layer-by-layer technique. Biosensors & Bioelectronics 2001;16:849-856.

[81] Boura C, Menu P, Payan E, Picart C, Voegel JC, Muller S, Stoltz JF. Endothelial cells grown on thin polyelectrolyte mutlilayered films: an evaluation of a new versatile surface modification. Biomaterials 2003;24:3521-3530.

[82] Lavalle P, Gergely C, Cuisinier FJG, Decher G, Schaaf P, Voegel JC, Picart C. Comparison of the structure of polyelectrolyte multilayer films exhibiting a linear and an exponential growth regime: an in situ atomic force microscopy study. Macromolecules 2002;35:4458-4465.

[83] Chluba J, Voegel JC, Decher G, Erbacher P, Schaaf P, Ogier J. Peptide hormone covalently bound to polyelectrolytes and embedded into multilayer architectures conserving full biological activity. Biomacromolecules 2001;2:800-805.

[84] Tryoen-Toth P, Vautier D, Haikel Y, Voegel JC, Schaaf P, Chluba J, Ogier J. Viability, adhesion, and bone phenotype of osteoblast-like cells on polyelectrolyte multilayer films. J Biomed Mater Res 2002;60:657-667.

[85] Picart C, Ladam G, Senger B, Voegel JC, Schaaf P, Cuisinier FJG, Gergely C. Determination of structural parameters characterizing thin films by optical methods: a comparison between scanning angle reflectometry and optical waveguide lightmode spectroscopy. J. Chem. Phys 2001;115:1086-1095.

[86] Picart C, Gergely C, Senger B, Arntz Y, Voegel JC, Schaaf P, Cuisinier FJG. Measurement of film thickness up to several hundreds of nanometers using optical waveguide lightmode spectroscopy. Biosensors and Bioelectronics 2004;20:553-561.

[87] Menchaca JL, Jachimska B, Cuisinier FJG, Perez E. In situ surface structure study of polyelectrolyte multilayers by liquid-cell AFM. Colloids and Surfaces A 2003;222:185-194.

[88] Lobo RFM, Pereira-da Silva MA, Raposo M, Faria RM, Oliveira ON. The morphology of layer-by-layer films of polymer/polyelectrolyte studied by atomic force microscopy. Nanotechnology 2003;14:101-108.

[89] Szatmari S, Schäfer FP. Simplified laser system for the generation of 60 fs pulses at 248 nm. Opt Commun 1988;68:196-202.

[90] Shiratori SS, Rubner MF. pH-Dependent Thickness Behavior of Sequentially Adsorbed Layers of Weak Polyelectrolytes. Macromolecules 2000,33:4213-4219.

[91] Cheng Y, Corn RM. Ultrathin polypeptide multilayer films for the fabrication of model lquid/liquid electrochemical interfaces. J Phys Chem B 1999;103:8726-8731.

[92] Cantor R, Schimmel PR. In *Biophysical Chemistry*. Freeman WH (Ed) San Francisco, 1980, p.2.

[93] Rimondini L, Faré S, Brambilla E, Felloni A, Consonni C, Brossa F, Carrassi A. The effect of surface roughness on early in vivo plaque colonization on titanium. J Periodontol 1997;68:556-562.

[94] Ameen AP, Short RD, Johns R, Schwach G. The surface analysis of implant materials 1. The surface composition of a titanium dental implant material. Clin Oral Implan Res 1993;4:144-150.

[95] Brånemark PI, Zarb GA, Albrektsson T. Gewebeintegrierter Zahnersatz. Berlin, Chicago, London, Rio de Janeiro, Tokio: Quintessenz Verlags-GmbH, 1985. p. 109-111.

[96] Lausmaa J, Kasemo B. Surface spectroscopic characterization of titanium implant materials. Appl Surf Sci 1990;44:133-146.

[97] Sawase T, Hai K, Yoshida K, Baba K, Hatada R, Atsuta M. Spectroscopic studies of three osseointegrated implants. J Dentistry 1998;26:119-124.

[98] Kilpadi DV, Raikar GN, Liu J, Lemons JE, Vohra Y, Gregory JC. Effect of surface treatment on unalloyed titanium implants: Spectroscopic analyses. J Biomed Mater Res 1998;40:646-659.

[99] NIST XPS Database, 2000 (http://srdata.nist.gov/xps)

[100] Park JY, Gemmell CH, Davies JE. Platelet interactions with titanium: modulation of platelet activity by surface topography. Biomaterials 2001;2671-2682.

[101] Arys A, Philippart C, Dourov N, He Y, Le QT, Pireaux JJ. Analysis of titanium dental implants after failure of osseointegration: combined histological, electron microscopy, and X-ray photoelectron spectroscopy approach. J Biomed Mater Res 1998;43:300-312.

[102] Sul YT, Johansson CB, Petronis S, Krozer A, Jeong Y, Wennerberg A, Albrektsson T. Characteristics of the surface oxides on turned and electrochemically oxidized pure titanium implants up to dielectric breakdown: the oxide thickness, micropore configurations, surface roughness, crystal structure and chemical composition. Biomaterials 2002;23:491-501.

[103] Sailer R, McCarthy G. ICCD Grant-in-Aid. North Dakota USA: Fargo, 1993

[104] Voevodin AA, Capano MA, Laube SJP, Donley MS, Zabinski JS. Design of a Ti/TiC/DLC functionally gradient coating based on studies of structural transitions in Ti–C thin films. Thin Solid Films. 1997;298:107-115.

[105] Zehnder T, Patscheider J. Nanocomposite TiC/a–C:H hard coatings deposited by reactive PVD. Surface and Coatings Technol. 2000;133-134:138-144.

[106] Kruger J, Kautek W. The femtosecond pulse laser: a new tool for micromachining. Laser Physics 1999;9:30-40.

[107] Banks PS, Feit MD, Rubenchik AM, Stuart BC, Perry MD. Material effects in ultra-short pulse laser drilling of metals. Appl Phys A 1999;69:S377-380.

[108] Zhu X, Naumov AY, Villeneuve DM, Corkum PB. Influence of laser parameters and material properties on micro drilling with femtosecond laser pulses. Appl Phys A 1999;69:S367-371.

[109] Tonshoff HK, Momma C, Ostendorf A, Nolte S, Kamlage G. Microdrilling of metals with ultrashort laser pulses. J Laser Appl 2000;12:23-27.

[110] Békési J, Klein-Wiele JH, Simon P. Efficient submicron processing of metals with femtosecond UV pulses. Appl Phys A 2003;76:355-357.

I.

Available online at www.sciencedirect.com
SCIENCE DIRECT®
Biomaterials 24 (2003) 4197–4203
Biomaterials
www.elsevier.com/locate/biomaterials

Surface modifications induced by ns and sub-ps excimer laser pulses on titanium implant material

M. Bereznai[a,*], I. Pelsöczi[b], Z. Tóth[c], K. Turzó[b], M. Radnai[b], Z. Bor[a], A. Fazekas[b]

[a] Department of Optics and Quantum Electronics, University of Szeged, Dóm tér 9., Szeged, H-6720, Hungary
[b] Department of Dentistry and Oral Surgery, University of Szeged, Tisza Lajos krt. 64., Szeged, H-6720, Hungary
[c] Research Group on Laser Physics, Hungarian Academy of Sciences, Dóm tér 9., Szeged, H-6720, Hungary

Received 21 December 2002; accepted 8 April 2003

Abstract

Medical implants used in oral and orthopaedic surgery are mainly produced from titanium. Their biological behaviour, e.g. osseointegration, essentially depends on both the chemical composition and the morphology of the surface. Modifications achieved by excimer laser irradiation of titanium samples were investigated in order to improve their surface characteristics so as to facilitate biointegration. To enlarge the effective interfacial area of bone–implant contact, holes were ablated by laser pulses of ns or sub-ps length. During ns ablation, crown-like projecting rims formed around the borders of the holes. Ultra-short (0.5 ps) KrF excimer laser pulses were successfully applied to avoid these undesirable formations. Since a smooth dental implant surface is necessary to maintain a healthy connection with the soft tissues, laser polishing of samples was investigated, too. Irradiation with a series of ns laser pulses resulted in effective smoothing, as measured with atomic force microscope. X-ray photoelectron spectroscopy analysis of the laser-polished titanium surface revealed that laser treatment led to a decrease of the surface contamination and in thickening of the oxide layer. X-ray diffraction measurements demonstrated that the original α-titanium crystal structure was preserved.
© 2003 Elsevier Science Ltd. All rights reserved.

Keywords: Titanium; Osseointegration; Laser ablation; Surface modification; Surface roughness

1. Introduction

Dental implants are frequently applied to replace lost teeth. A wide variety of materials have been used to produce endosseous implants [1–3]. Titanium and its alloys are currently the most commonly used dental and orthopaedic implant materials, meeting the most important requirements [4–6]. The properties of titanium and of its surface, which is covered by a native oxide layer, are appropriate to allow its use as a biocompatible material [7,8].

The long-term benefits of dental implants depend on the responses of the different surrounding host tissues (the alveolar bone, the conjunctival part of the oral soft tissues and the gingival epithelium). As regards osseointegration, i.e. the formation of a direct connection between the living bone and the surface of load-carrying implants, the important question arises as to how to attain better integration by modification of the implant surface morphology. Many authors have suggested that the surface should be free from any contamination [9–12]. Another important property of the implant surface is its morphology [13]. The mechanical roughness of the implant surface plays a significant role in anchoring cells and connecting together the surrounding tissues, thereby leading to a shorter healing period. The area of contact can be enlarged by microstructuring the implant surface. Rough titanium surfaces display advantages over smooth ones, e.g. a shorter bone-healing period [14–17].

The presence of a healthy gingival attachment on an implant is also influenced by the surface characteristics [18]. Connective tissues surrounding dental implants do not become directly attached to the implant surface, but merely adhere to it. For bioinert and bioactive implant materials, a glycoprotein layer ensures the connection of the collagen fibres to the implant surface. Although a rough surface would be favourable for the epithelial

*Corresponding author. Tel.: +36-62-544-653; fax: +36-62-544-658.
E-mail address: bereznai@physx.u-szeged.hu (M. Bereznai).

0142-9612/03/$ - see front matter © 2003 Elsevier Science Ltd. All rights reserved.
doi:10.1016/S0142-9612(03)00318-1

attachment, the neck part of an implant has to be polished in order to avoid pathogenic plaque accumulation [19].

To increase the roughness of solid surfaces, a number of laser-based techniques have been applied in recent years [20]. Besides the prompt intense heating of the surface, excimer laser illumination may further enhance the sterilising effect in consequence of the high dose in the UV range.

Recent studies on the laser machining of dental implants revealed that an appropriate structure with the least contamination could be achieved by means of laser treatment [21,22]. After multipulse irradiation with a focused Nd:YAG laser beam, a crown-like structure formation was observed on the titanium surface [23]. The efficient oxidation of titanium through Nd:YAG laser irradiation was reported in [24,25]. The importance of these results lies in the fact that they involve laser technologies for the processing of implant surfaces which already have numerous industrial applications. However, these techniques must be further improved, since medical applications require high accuracy in both mechanical and chemical characteristics.

The aim of the present study was to obtain results relating to excimer laser modifications, such as the polishing and structuring of titanium surfaces. The thickness of the oxide layer and the changes in the oxidation states of the laser-polished surface were investigated by means of X-ray photoelectron spectroscopy (XPS). Structural changes caused in the crystalline structure by rapid laser annealing were examined by X-ray diffraction (XRD) measurements. Optical microscopy, scanning electron microscopy (SEM) and atomic force microscopy (AFM) was applied to visualise the surface structures formed by local excimer laser ablation.

2. Material and methods

2.1. Titanium samples

Titanium sample discs 1.25 mm thick and 8 mm in diameter were cut from commercially pure titanium rods (CP grade 1, <0.12% O, <0.05% N, <0.06% C, <0.013% H), used for the fabrication of dental implants. Concentric scratches 0.1–2 μm in depth were observable on the surface of the machined samples. Before laser treatment, all samples were cleaned ultrasonically in a distilled water—detergent mixture, and then rinsed in pure distilled water and finally in absolute ethanol.

2.2. Surface polishing with a ns ArF excimer laser

An ArF excimer laser (Lambda Physics EMG 201, wavelength: 193 nm, pulse duration: 18 ns, pulse energy: 100 mJ) was used for polishing. A square aperture that cut out the most homogeneous part of the beam was imaged onto the surface of the samples by a fused silica lens ($f = 5$ cm). A 3.6 mm^2 area on the sample disc was illuminated by different series of laser pulses under atmospheric conditions. The fluence at the sample was monitored by calibrated energy measurement of a reference beam, coupled out by a fused silica plate.

In the experiments concerning laser polishing, two parameters were varied independently: the incident fluence was varied in the range 1.5–5 J/cm^2 by placing neutral filters in the beam path, and experiments were performed with 10, 100 or 1000 shots of excimer pulses.

2.3. Microstructuring

2.3.1. Nanosecond ArF excimer laser ablation

For the local ablation of titanium surfaces, a similar set-up was used as in the case of the laser polishing experiments. A copper grid was placed in the beam path and its rectangular holes (0.29 mm^2 in area) were imaged by a fused silica lens with a focal length of 4 cm onto the sample surface. In this case a greater reduction of the beam was applied, and therefore the local average fluence was higher: 8.5 J/cm^2. 250, 500 and 1000 pulses were shot for local ablation experiments.

2.3.2. Laser ablation with 0.5 ps KrF excimer pulses

Further microstructuring experiments were performed with ultrashort pulses of a KrF excimer laser (wavelength: 248 nm, pulse duration: 0.5 ps, pulse energy: 10 mJ). This laser system was described in detail in [26]. The only difference from the former optical set-up was that the titanium sample disc and the focal point of the lens were situated inside a low-pressure (10 Pa) vacuum chamber equipped with a transparent fused silica (Suprasil) window. Vacuum conditions were necessary because of the high power density, in order to avoid optical breakdown in air. In these experiments, 1000 pulses with a fluence of 2.4 J/cm^2 were applied.

2.4. Microscopic investigations

The surface morphology of the samples was first observed through an optical microscope (Nikon Optiphot 100S metallurgical microscope). High-resolution secondary electron images were recorded with a scanning electron microscope (Hitachi S-2400). For a better visualisation of the structures in depth, all samples were tilted at 75° in SEM. For quantitative surface roughness determinations, AFM was applied (TopoMetrix Explorer TM, contact mode). The surface roughness characterised by the mean roughness (R_a) value was determined by using TopoMetrix software. R_a gives the average deviation of the surface height relative to the mean height.

2.5. X-ray photoelectron spectroscopy

One side of the titanium disk was polished by scanning over the whole surface area with laser pulses. The scanning speed was synchronised to the repetition rate of the laser, resulting in 10 overlapping laser shots with a fluence of 3.5 J/cm^2. This sample was used for XPS and XRD investigations. The chemical composition of the titanium surfaces was studied by XPS. The photoelectrons generated by Al K_α primary radiation (14 kV, 15 mA) were analysed with a hemispherical electron energy analyser (Kratos XSAM 800). Binding energies were normalised with respect to the position of the C (1 s) peak. The changes in the XPS spectra were measured after 10 min of Ar^+ bombardment, repeated several times. Ar^+ was generated with an ion gun energy of 3 kV and the incident ion beam current density was 4 μA/cm^2. Bombardment for 10 min removed about 10 nm from the surface of the material. Wide-range scans and higher-resolution narrow scans of the main characteristic peaks were recorded (Ti 2p, O 1 s, and N 1 s).

2.6. X-ray diffraction measurements

In order to compare the crystalline structures of the laser-treated samples with those of the non-irradiated materials XRD spectra were recorded, using Cu K_α radiation ($\lambda = 0.154$ nm). The XRD measurements were performed with a Philips PW 1830 X-ray generator (40 kV, 25 mA) with a powder diffractometer (PW 1877 Philips). The measured scan was taken between 2Θ values of 20° and 80°, with a step size of 0.02°.

3. Results and discussion

3.1. Surface polishing

3.1.1. Microscopic analysis of laser-polished samples

ArF laser polishing was performed by applying 10 laser shots at a fluence of 1.5 J/cm^2. The efficiency of the polishing improved as the fluence was increased from 1.5 to 5 J/cm^2. As shown in the SEM micrograph in Fig. 1, the small scratches at intervals measuring <10 μm, were completely eliminated in the machined samples. Larger structures were merely reduced in height, but not completely removed, which resulted in a wavy surface (Fig. 1b). Sample surfaces subjected to a higher number of shots (100 or 1000) exhibited undesired waves, holes and plate-like formations (Fig. 2).

The AFM surface topography pictures allowed a quantitative analysis of the surface roughness, as shown in Fig. 3. For the original machined samples, the roughness was $R_a = 256$ nm (Fig. 3a). The surface roughness of the laser-polished samples irradiated with 10 laser pulses with a fluence of ~ 5 J/cm^2 was

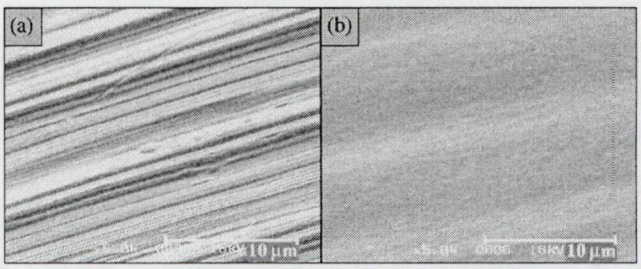

Fig. 1. SEM micrographs of: (a) non-irradiated machined and (b) ArF laser-polished titanium disk. The polishing was performed with 10 laser shots at a fluence of 3.5 J/cm^2.

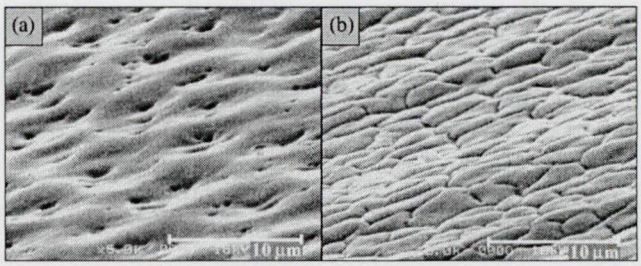

Fig. 2. SEM micrographs of structures formed on titanium surfaces illuminated with (a) 100 or (b) 1000 ArF laser shots at a fluence of 1.5 J/cm^2.

significantly decreased, as revealed by the AFM micrographs (Fig. 3b): $R_a = 25$ nm. This value meets the requirements described in [27], where it was demonstrated that $R_a \leqslant 88$ nm for a titanium surface is optimum for the inhibition of plaque accumulation and maturation.

Both the SEM and the AFM studies confirmed that a titanium sample with $R_a < \sim 1$ μm can be effectively polished by homogeneous, 3–5 J/cm^2 fluence laser illumination. Polishing can occur via several mechanisms. During the applied laser irradiation, the surface material melts and evaporates. This was confirmed by the appearance of laser-induced plasma during polishing. Prior to resolidification, the molten surface can become smoothed. Another mechanism is described in [20]: the absorbed laser light heats the emergent sharp peaks of the rough surface more efficiently than the valleys, where the heat diffusion is more effective. The result is more material removal on the hills, and finally the surface will be smoother.

3.1.2. XPS measurement of the surface chemistry

The XPS survey spectra illustrated in Fig. 4 confirmed the presence of oxygen, nitrogen and carbon on both non-irradiated and laser-treated samples. These elements are typically observed on titanium implant surfaces [28]. Trace amounts of phosphorus and chlorine could also be detected as in [29,30]. The upper part of Fig. 4 depicts spectra recorded without any Ar^+ sputter, while the lower part presents spectra after

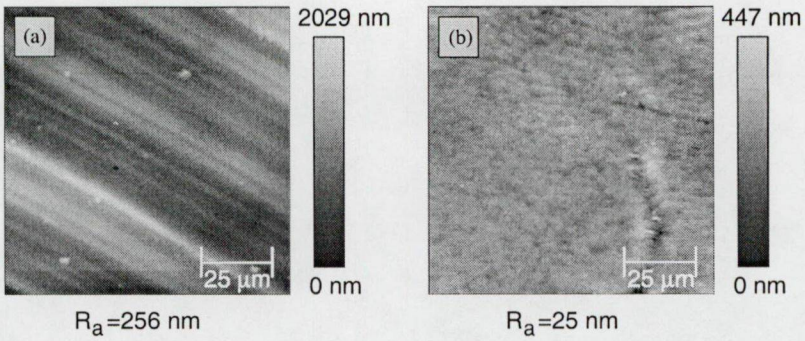

Fig. 3. AFM surface topography images of: (a) non-irradiated and (b) ArF laser-polished titanium disk. The polishing was performed with 10 laser shots at a fluence of 5 J/cm^2. The surface roughness (R_a) for the non-irradiated and the laser-polished surface was 256 and 25 nm, respectively.

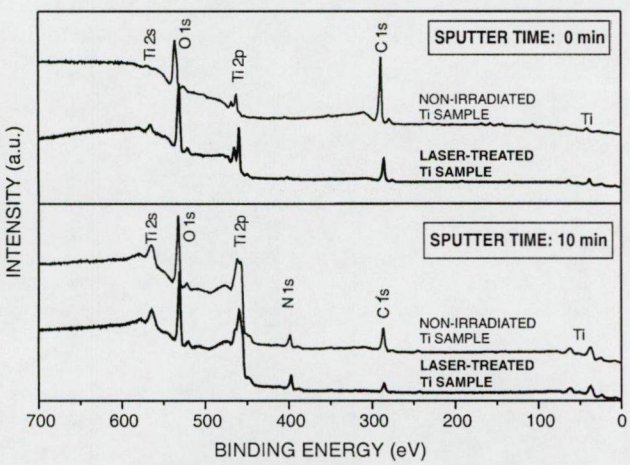

Fig. 4. XPS survey spectra of non-irradiated and ArF-laser polished (10 laser shots at 3.5 J/cm^2) titanium disks. Upper part: spectra recorded without Ar^+ sputter; lower part: spectra after 10 min of Ar^+ bombardment.

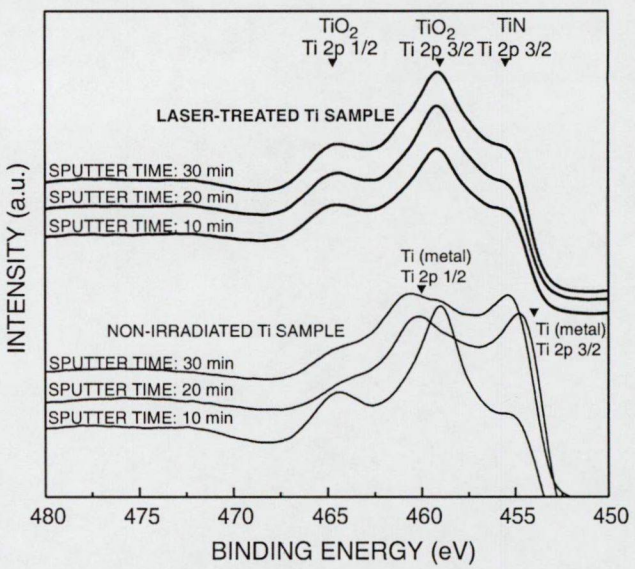

Fig. 5. High-resolution XPS spectra showing Ti 2p lines of non-irradiated and ArF laser-treated titanium samples (after 10, 20 and 30 min of Ar^+ sputtering).

10 min of Ar^+ bombardment. In general, the laser treatment altered the surface chemistry in only a few respects. The substantial drop in the C 1s signal demonstrates that the excimer laser illumination effectively cleans the titanium surface. The C 1s signal indicates the presence of carbonaceous contamination, due to carbon-containing molecules remaining after chemical cleaning or adsorbed later on air-exposed surfaces [30,31].

Representative high-resolution Ti 2p spectra of non-irradiated and laser-treated titanium samples after 10, 20 and 30 min of Ar^+ sputtering are shown in Fig. 5. The core level spectra after a single Ar^+ bombardment are similar, with three characteristic peaks, at 464.7, 459 and 455.6 eV. The positions of the Ti $2p_{1/2}$ and Ti $2p_{3/2}$ peaks correspond to those measured in TiO_2 [32]. The shoulder appearing at the lowest binding energy can be assigned to Ti $2p_{3/2}$ in TiN [33]. This reveals that, besides a thin TiO_2 layer, TiN impurities (probably originating from the basic material [34]) are also present on the sample surface. The presence of N was supported by the concomitant increment of the N 1s peak during Ar^+ sputtering. This can also be seen from a comparison of the curves corresponding to sputtering times of 0 and 10 min in Fig. 5.

It is interesting to compare the spectra in Fig. 5 that were measured after a second and a third Ar^+ sputter. The spectrum of the non-irradiated titanium surface includes peaks at binding energies of around 460 and 454 eV, corresponding to pure Ti metal [33,35], while that of the laser-treated sample still exhibits the group of three peaks indicating the oxidised state of titanium as mentioned above, even after the second and third Ar^+ bombardments. Consequently, laser-polishing thickens the oxide layer at least 2-fold, which may favour the use of laser techniques to achieve better osseointegration [13].

3.1.3. XRD analysis

Rapid laser annealing by a series of ns laser pulses may alter the crystalline structure of the implant in the heat-affected zone. At room temperature the hexagonal

α form of titanium is stable, while above 1158 K this phase changes to cubic β-titanium. It is essential to preserve the original crystal structure of the implant in order to avoid stress formation in it. The changes in crystal structure were followed by comparing the XRD spectra of the non-irradiated and laser-polished probes (Fig. 6). The XRD spectrum of the non-irradiated probe mainly shows the peaks of α-titanium [24,36], but the peaks at $2\theta = 31.61°$, 34.59°, 36.13°, 47.53° and 56.29° demonstrate that other crystalline form(s) are present as well. Diffraction peaks at 34.59° and 38.42° can be attributed to surface contamination, since laser treatment resulted in significant decreases in intensity of these peaks. The XRD spectrum of the laser-polished probe reveals the intensity characteristics of pure α-titanium [37], indicated at the bottom of Fig. 6. The origins of the non-α-titanium peaks in the non-irradiated probes have not yet been clarified. The increase in the peak measured at 38.42° for the non-irradiated probe might possibly be assigned to the strong diffraction at 38.48° originating from the (1 1 0) plane of β-titanium, but this assumption cannot be true, since other peaks characteristic of β-titanium (e.g. at 55.54° and 69.60°) are completely missing from both diffraction curves. Titanium oxides such as anatase or rutile cannot furnish these non-α-titanium peaks either, because other strong characteristic titanium oxide peaks are absent from the spectra (e.g. the highest-intensity peaks at 25.32° and 27.37°, respectively, for anatase and rutile [36]). Diffraction peaks of crystalline nitrides or carbides of titanium [38,39] can likewise not be correlated with these locations. These diffraction peaks probably originate from crystalline forms of non-stoichiometric titanium compounds, e.g. oxides, nitrides or carbides, which were indicated by XPS. As X-ray diffraction is a bulk technique, it is naturally not possible to exclude with certainty the presence of a thin layer of some other material with a crystalline or amorphous structure. As concerns applicability, we can conclude that laser treatment results in cleaning of the surface and maintenance of the crystal structure of the titanium probe in α form.

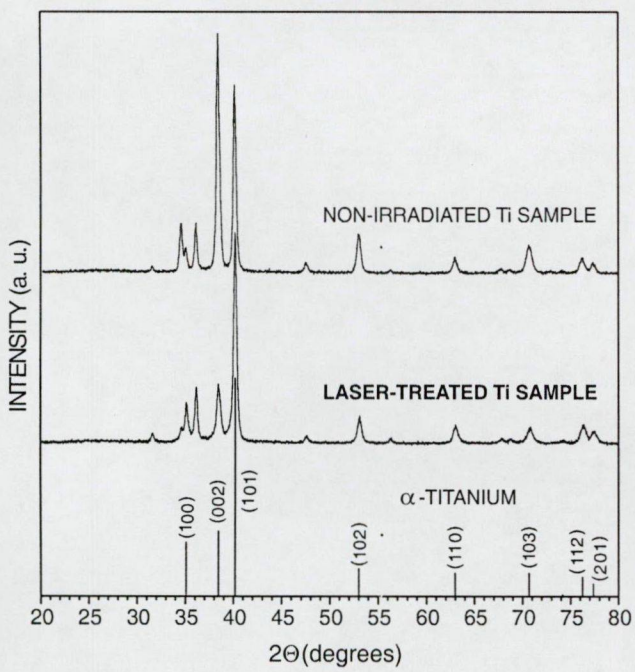

Fig. 6. XRD spectra of non-irradiated and ArF laser-polished probes. The relative intensities of pure α-titanium are indicated at the bottom.

3.2. Microstructuring

3.2.1. Surface patterning by ns excimer pulses

Holes at a characteristic distance of about 25 μm from each other were successfully ablated into the titanium surface by imaging a grid with ArF excimer laser pulses, as revealed by the SEM images in Figs. 7a and b. The surface was ablated locally at those sites where the fluence exceeded the ablation threshold. Increase of the number of pulses led to the ablation of holes with a higher aspect ratio. At the same time, rims formed around the edges of the holes as can be seen in Figs. 7a and b. After 250 shots at a fluence of 8.5 J/cm^2, the depth of the holes was about 10 μm and the height of the rims was at most 8 μm. From the depth of the ablated holes, the effective evaporated thickness proved to be approximately 40 nm per pulse. Formation of the separate craters was possible because the heat diffusion length (for a pulse duration of 18 ns this is ~800 nm for titanium) was shorter than the distance between the holes.

In nature, the holes resemble the drilled patterns made by other pulsed laser sources (e.g. Nd:YAG lasers) operated at longer wavelengths [23]. The temperature distribution in metals is determined mostly by the heat conduction and not by the wavelength-dependent absorption. The absorption penetration depths at 193, 248 and 1064 nm are 13.5, 12.7, and 253.3 nm, respectively. These values are 1–2 orders of magnitude smaller then the above-mentioned heat diffusion length. It is common in these techniques that the ablation occurs via extensive evaporation and melting. In the applied

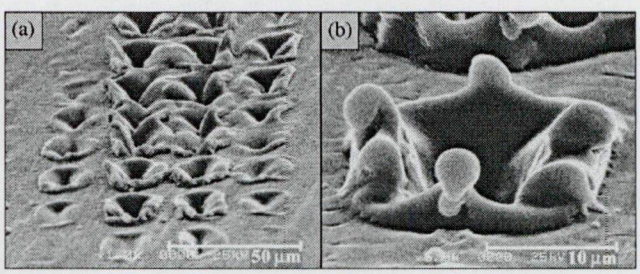

Fig. 7. SEM micrographs at different magnifications of ablated holes formed in a titanium surface after 250 shots of the ArF excimer laser. The fluence applied was 8.5 J/cm^2.

fluence range, plasma is formed and the underlying molten layer is propelled out as a radial hydrodynamic flow due to the high recoil plasma pressures. During this process, rims are formed at the edges [23]. This is an inconvenient effect, since the rims may break away from the implant surface during the implanting procedure and contaminate the surrounding biological tissues.

3.2.2. Surface patterning by sub-ps excimer pulses

The debris-free processing of holes with high aspect ratios, which are commonly produced in the short-wavelength excimer laser ablation of specific polymers and ceramics, cannot be reproduced in the case of metals with relatively high thermal conductivities. Similarly as in drilling with ns length pulses of Q-switched Nd:YAG lasers, at an excimer pulse duration of 18 ns, the heat-affected zone is defined by the thermal diffusion length and not by the absorption penetration depth of the laser light. In this case the molten depth may approach 1 μm and the melt flows out from the high-pressure zones of high-temperature laser plasma. One possibility to overcome the problems of rim formation is to decrease the extent of heat diffusion. The application of 0.5 ps laser pulses allows a heat diffusion length of 4.3 nm. In this case the absorption penetration depth will determine the precision of laser processing. A number of authors have investigated the pulse duration requirements for the melting- and burr-free drilling of metals [20,40–44]. The highest process efficiency and hole quality can be achieved by using sub-ps pulse durations. On repetition of the surface patterning experiments with a 0.5 ps KrF excimer laser, rim formation could be eliminated completely, as illustrated in the SEM micrograph in Fig. 8. The laser fluence here was 2.4 J/cm^2 and 1000 shots had to be administered.

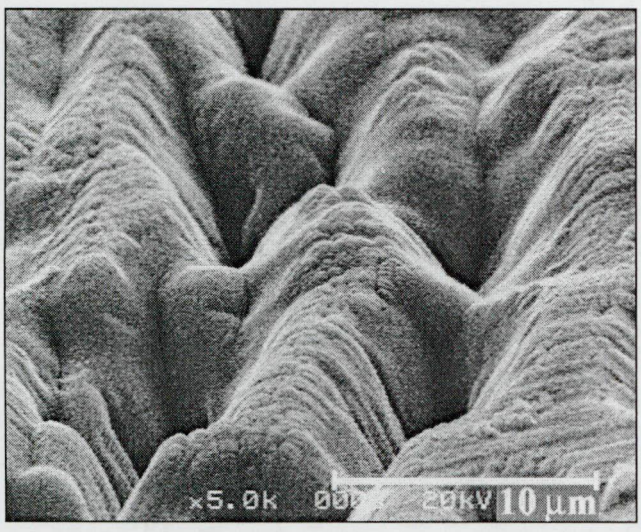

Fig. 8. SEM micrograph of ablated holes formed in a titanium surface after 1000 shots of the 0.5 ps KrF excimer laser. The fluence applied was 2.4 J/cm^2.

The coherence properties of the applied 0.5 ps laser system led to less accurate imaging of the mask pattern on the sample surface. The topography of the ablated structure practically reproduces the intensity distribution in the image plane, which is distorted by interference phenomena. Accordingly, the ablated holes do not possess sharp and well-defined borders. The aspect ratio of the holes is sufficient for the required purpose, since the contact interface of the osseointegrating tissues was enlarged significantly.

4. Conclusions

The chemical composition and morphology of the titanium surface were modified by excimer laser processing. Effective polishing was achieved by homogeneous illumination with ns laser pulses in the 3–5 J/cm^2 fluence range, as revealed by SEM and AFM studies. Carbonaceous contamination was removed, as indicated by XPS and XRD measurements, demonstrating that polishing with an excimer laser cleans the surface of titanium. The XRD data confirmed that the laser polishing process did not alter the original crystalline structure, while the XPS measurements proved that pulsed laser oxidation in air resulted in an increased thickness of the surface oxide layer.

Holes about 20 μm diameter and 10 μm in depth with rims around the edges were ablated into the titanium surface with pulses of ns ArF excimer laser. To avoid the formation of these fragile rims, we applied an excimer pulse duration of 0.5 ps, whereby the melting- and rim-free ablation of titanium was attained.

Acknowledgements

The authors thank Albert Oszkó from the Department of Solid-State and Radiochemistry at the University of Szeged for the XPS measurements, Dr. Ágnes Patzkó from the Department of Colloid Chemistry at the University of Szeged for the XRD measurements, and Prof. Sándor Szatmári for providing access to the 0.5 ps KrF laser facility at the Department of Experimental Physics, University of Szeged. The optical microscope used was purchased with World Bank—OTKA support (OTKA-W015254).

References

[1] Williams DF. Implants in dental and maxillofacial surgery. Biomaterials 1981;2:133.
[2] Lemons JE. Dental implant biomaterials. J Am Dental Assoc 1990;121:716–9.
[3] Craig RG. In: Powers JM, Craig RG, editors. Restorative dental materials. St. Louis: Mosby Inc.; 1989. p. 169.

SZTE Egyetemi Könyvtár SZEGED 13.

[4] Meffert RM, Langer B, Fritz ME. Dental implants: a review. J Periodontol 1992;63:859–70.
[5] Brånemark PI, Adell R, Albrektsson T, Lekholm U, Lundkvist S, Rockler B. Osseointegrated titanium fixtures in the treatment of edentulousness. Biomaterials 1983;4:25–8.
[6] Albrektsson T. The response of bone to titanium implants. CRC Crit Rev Biocompat 1985;1:53.
[7] Lautenschlager EP, Monaghan P. Titanium and titanium alloys as dental materials. Int Dental J 1993;43:245–53.
[8] Michel R. Trace metal analysis in biocompatibility testing. CRC Cri Rev Biocompat 1987;3:235.
[9] Binon PP, Weir DJ, Marshall SJ. Surface analysis of an original Brånemark implant and three related clones. Int J Oral Max Implants 1992;7:168–75.
[10] Olefjord I, Hansson S. Surface analysis of four dental implant systems. Int J Oral Max Implants 1993;8:32–40.
[11] Cochran DL. A comparison of endosseous dental implant surfaces. J Periodontol 1999;70:1523–39.
[12] Uitto VJ, Larjava H, Peltonen J, Brunette DM. Expression of fibronectin and integrins in cultured periodontal-ligament epithelial-cells. J Dent Res 1992;71:1203–11.
[13] Eriksson C, Lausmaa J, Nygren H. Interactions between human whole blood and modifed TiO_2-surfaces: influence of surface topography and oxide thickness on leukocyte adhesion and activation. Biomaterials 2001;22:1987–96.
[14] Buser D, Schenk RK, Steinmann S, Fiorellini JP, Fox CH, Stich H. Influence of surface characteristics on bone integration of titanium implants—a histomorphometric study in miniature pigs. J Biomed Mater Res 1991;25:889–902.
[15] Wong M, Eulenberger J, Schenk R, Hunziker E. Effect of surface-topology on the osseointegration of implant materials in trabecular bone. J Biomed Mater Res 1995;29:1567–75.
[16] Wennerberg A, Ektessabi A, Albrektsson T, Johansson L, Andersson B. A 1-year follow-up of implants of differing surface roughness placed in rabbit bone. Int J Oral Max Implants 1997; 12:486–94.
[17] Boyan BD, Batzer R, Kieswetter K, Liu Y, Cochran DL, Szmuckler-Moncler SS, Dean DD, Schwartz Z. Titanium surface roughness alters responsiveness of MG63 osteoblast-like cells to 1 alpha,25-(OH)(2)D-3. J Biomed Mater Res 1998;39:77–85.
[18] Hansson H, Albrektsson T, Brånemark PI. Structural aspects of the interface between tissue and titanium implants. J Prosth Dent 1983;50:108–13.
[19] Quirinen M, Bollen CM, Papaioannou W, Van Eldere J, van Steenberghe D. The influence of titanium abutment surface roughness on plaque accumulation and gingivitis: short-term observations. Int J Oral Max Implants 1996;11:169–78.
[20] Bäuerle D. Laser processing and chemistry. Berlin, Heidelberg. New York, Tokyo: Springer; 2000.
[21] Gaggl A, Schultes G, Müller WD, Kärcher H. Scanning electron microscopical analysis of laser-treated titanium implant surfaces—a comparative study. Biomaterials 2000;21:1067–73.
[22] Petö G, Karacs A, Pászti Z, Guczi L, Divinyi T, Joób A. Surface treatment of screw shaped titanium dental implants by high intensity laser pulses. Appl Surf Sci 2001;7524:1–7.
[23] György E, Mihailescu IN, Serra P, Pérez del Pino A, Morenza JL. Crown-like structure development on titanium exposed to multipulse NdYAG laser irradiation. Appl Phys A 2002;74:755–9.
[24] Perez del Pino, Serra P, Morenza JL. Oxidation of titanium through Nd:YAG laser irradiation. Appl Surf Sci 2002; 197–198:887–90.
[25] Nánai L, Vajtai R, George TF. Laser-induced oxidation of metals: state of art. Thin Solid Films 1997;298:160–4.
[26] Szatmari S, Schäfer FP. Simplified laser system for the generation of 60 fs pulses at 248 nm. Opt Commun 1988;68:196–202.
[27] Rimondini L, Faré S, Brambilla E, Felloni A, Consonni C, Brossa F, Carrassi A. The effect of surface roughness on early in vivo plaque colonization on titanium. J Periodontol 1997;68: 556–62.
[28] Ameen AP, Short RD, Johns R, Schwach G. The surface analysis of implant materials 1. The surface composition of a titanium dental implant material. Clin Oral Implants Res 1993;4: 144–50.
[29] Brånemark PI, Zarb GA, Albrektsson T. Gewebeintegrierter zahnersatz. Berlin, Chicago, London, Rio de Janeiro, Tokio: Quintessenz Verlags-GmbH; 1985. p. 109–11.
[30] Lausmaa J, Kasemo B. Surface spectroscopic characterization of titanium implant materials. Appl Surf Sci 1990;44:133–46.
[31] Sawase T, Hai K, Yoshida K, Baba K, Hatada R, Atsuta M. Spectroscopic studies of three osseointegrated implants. J Dent 1998;26:119–24.
[32] Kilpadi DV, Raikar GN, Liu J, Lemons JE, Vohra Y, Gregory JC. Effect of surface treatment on unalloyed titanium implants: spectroscopic analyses. J Biomed Mater Res 1998;40:646–59.
[33] NIST XPS Database, 2000 (http://srdata.nist.gov/xps).
[34] Park JY, Gemmell CH, Davies JE. Platelet interactions with titanium: modulation of platelet activity by surface topography. Biomaterials 2001;22:2671–82.
[35] Arys A, Philippart C, Dourov N, He Y, Le QT, Pireaux JJ. Analysis of titanium dental implants after failure of osseointegration: combined histological, electron microscopy, and X-ray photoelectron spectroscopy approach. J Biomed Mater Res 1998; 43:300–12.
[36] Sul YT, Johansson CB, Petronis S, Krozer A, Jeong Y, Wennerberg A, Albrektsson T. Characteristics of the surface oxides on turned and electrochemically oxidized pure titanium implants up to dielectric breakdown: the oxide thickness, micropore configurations, surface roughness, crystal structure and chemical composition. Biomaterials 2002;23:491–501.
[37] Sailer R, McCarthy G. ICCD grant-in-aid. North Dakota, USA: Fargo; 1993.
[38] Voevodin AA, Capano MA, Laube SJP, Donley MS, Zabinski JS. Design of a Ti/TiC/DLC functionally gradient coating based on studies of structural transitions in Ti–C thin films. Thin Solid Films 1997;298:107–15.
[39] Zehnder T, Patscheider J. Nanocomposite TiC/a–C:H hard coatings deposited by reactive PVD. Surf Coatings Technol 2000;133–134:138–44.
[40] Kruger J, Kautek W. The femtosecond pulse laser: a new tool for micromachining. Laser Phys 1999;9:30–40.
[41] Banks PS, Feit MD, Rubenchik AM, Stuart BC, Perry MD. Material effects in ultra-short pulse laser drilling of metals. Appl Phys A 1999;69:S377.
[42] Zhu X, Naumov AY, Villeneuve DM, Corkum PB. Influence of laser parameters and material properties on micro drilling with femtosecond laser pulses. Appl Phys A 1999;69:S367–71.
[43] Tonshoff HK, Momma C, Ostendorf A, Nolte S, Kamlage G. Microdrilling of metals with ultrashort laser pulses. J Laser Appl 2000;12:23–7.
[44] Békési J, Klein-Wiele JH, Simon P. Efficient submicron processing of metals with femtosecond UV pulses. Appl Phys A 2003;76:355–7.

II.

Structural Characterization of Self-Assembled Polypeptide Films on Titanium and Glass Surfaces by Atomic Force Microscopy

István Pelsöczi,† Kinga Turzó,*,† Csilla Gergely,‡ András Fazekas,† Imre Dékány,§ and Frederic Cuisinier∥

Department of Dentistry and Oral Surgery, University of Szeged, Tisza Lajos krt. 64, H-6720 Szeged, Hungary, Université Montpellier II, Groupe d'Étude des Semiconducteurs, Place Eugène Bataillon, F-34095 Montpellier, France, Department of Colloid Chemistry, University of Szeged, Aradi vértanúk tere 1, H-6720 Szeged, Hungary, and INSERM U595, Université Louis Pasteur, 11 rue Humann, F-67085 Strasbourg, France

Received May 26, 2005; Revised Manuscript Received July 26, 2005

Chemically modified biomaterial surfaces (titanium and glass) covered with polyelectrolyte self-assembled films formed by the alternating adsorption of cationic poly-L-lysine (PLL) and anionic poly-L-glutamic acid (PGA) were structurally characterized by atomic force microscopy. Complementary information concerning the thickness and layer-by-layer growth of the films was provided by optical waveguide light-mode spectroscopy. The frequently used ex situ and the rarely used in situ build-up methods were compared. Important aspects of the industrial applicability of these films, their stability in time, and possible differences in their morphology were investigated. The films revealed a granular pattern, with grain diameters of 270 ± 87 nm for glass (up to 8 bilayers) and 303 ± 89 nm for titanium (up to 10 bilayers), independently of the build-up procedure. Both surfaces displayed a rehydration capability, the titanium surface exhibiting a better stability in time. The high roughness values observed at acidic or basic pH are related to the degree of ionization of PGA and PLL.

1. Introduction

This work addresses the implantological problem of how to make the surface of a biomaterial biocompatible. The success and long-term prognosis of endosseous implants depend primarily on the anchorage of the implant in the host bone,[1] i.e., the osseointegration.[2] The good osseointegration of alloplastic materials in contact with bone tissue requires the formation of strong links between the biomaterial and the surrounding bone tissue.[3]

Thanks to their good integration, physical properties and predictable, long lifetime, titanium (Ti) and its alloys are nowadays widely used in implantology.[4,5] The surface of an implant is in immediate contact with the biological medium; its interfacial characteristics (topography, chemistry or surface energy) and surface improvement therefore play essential roles in biointegration.[3,6] One solution with which to improve the surface of an implant has proved to be modification of the surface chemistry by the formation of polyelectrolyte (PE) multilayer films that are nanometer-sized and can be biofunctionalized toward targeted properties. This is certainly one of the driving forces for the increasing interest in this field. PE film coatings modify the solid/liquid interface in such a way as to ensure a proper environment for the adsorption of proteins, which is a key factor determining the interactions between the implant and the surrounding medium. Thus, the distribution of functional groups on the surface of the biomaterial and the macromolecular structure are properties that it is essential to study,[7−9] and this was our main aim.

PE multilayers are formed by the alternating adsorption of polycations and polyanions from aqueous solution onto a charged, solid surface.[10] The alternating adsorption technique has been successfully applied in different fields of science, as a consequence of its numerous practical applications. It can be automated, it involves the use of aqueous solutions, it is environment-friendly, and various substrates can be covered with films of readily variable thickness.[11,12]

Within the large number of candidate PEs, we were interested in biodegradable ones; accordingly, we studied multilayers formed by the alternating adsorption of polycationic poly-L-lysine (PLL) and polyanionic poly-L-glutamic acid (PGA). Previously published results[13−15] allow the expectation that PE multilayers should multiply the possibilities for the induction of cellular reactions if the cells are able to respond to bioactive molecules, e.g., signal transduction molecules embedded in the film.

It has been suggested that the self-assembling approach offers many advantages in the construction of PE coatings. We were interested in the validity of this for the chosen (PLL/PGA) system, i.e., in the effects of the applied procedure,

* To whom correspondence should be addressed. Tel: +36-62-545299. Fax: +36-62-545282. E-mail: turzo@stoma.szote.u-szeged.hu.
† Department of Dentistry and Oral Surgery, University of Szeged.
‡ Université Montpellier II.
§ Department of Colloid Chemistry, University of Szeged.
∥ Université Louis Pasteur.

10.1021/bm050360k CCC: $30.25 © 2005 American Chemical Society
Published on Web 09/07/2005

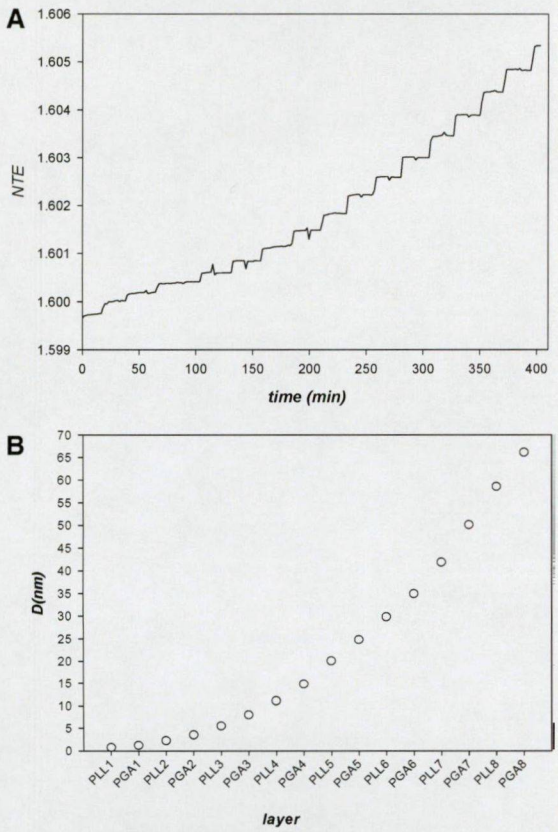

Figure 1. OWLS measurements. (A) N_{TE} values as a function of time and (B) film thickness (D) values as a function of layer number.

for the grains. In these situations, the contact and friction force modes must be used. As we expected such granulated structures and possible clustering, especially at high pH, we employed contact mode AFM, furnishing the best image contrast with which to study the surface structure and morphology. However, to diminish the tip−sample interactions for in situ measurements, the AFM tips were silanized so as to transform the hydrophilic tip into a hydrophobic one, using a mixture of 10 mL of *n*-hexadecane, 5 drops of carbon tetrachloride, and 5 drops of *n*-octadecyltrichlorosilane (Sigma Aldrich). Silanization allowed the imaging of both negative and positive surfaces. Several scans of each surface were performed in order to check the reproducibility of the images and to reveal possible tip damage. All images were taken at a scan rate of 1.97 Hz, with a resolution of 512 × 512 pixels, and 3D analysis was also performed.

The mean surface roughness (R_a) of a film was obtained by averaging the surface roughness (at least 5 independent measurements), defined as $R_a = 1/n\sum_{j=1}^{n} |Z_j|$, the arithmetic average of the absolute values of the surface height deviations measured from the mean plane within the box cursor. The diameter of the grains was determined by performing section analysis in the Nanoscope software (Version 4.42, 1999).

3. Results and Discussion

3.1. In Situ PE Deposition Measured by OWLS. The step-by-step build-up of a $(PLL/PGA)_8$ film was recorded in situ by OWLS (Figure 1A). This experiment served as a first check on the chosen experimental conditions, and the time domains necessary for the reproducible alternating

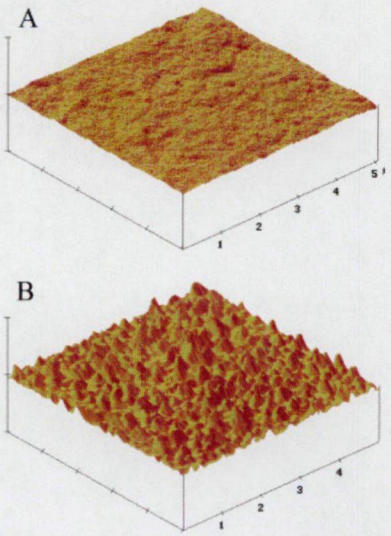

Figure 2. 3D images of glass substrate and PE layers on it (in situ measurements). (A) Bare glass, data scale: $x = 1$ μm/div and $z =$ 20 nm/div and (B) $(PLL/PGA)_6$ PE film, data scale: $x = 1$ μm/div and $z = 500$ nm/div.

adsorption of polypeptides forming the films to be further visualized by AFM. The thickness of the layers formed was calculated from the measured N_{TE} and N_{TM} values, as described in the Experimental Section. The final thickness obtained was about 70 nm. A plot of the layer-by-layer growth of the film thickness (Figure 1B) displays the well-known exponential growth of the PLL/PGA film governed by polypeptide diffusion in and out, as explained previously.[17]

3.2. PE Layers on a Glass Substrate. PLL/PGA films comprising up to 8 bilayers $(PLL/PGA)_8$ were successfully layered during in situ build-up in the liquid cell of the atomic force microscope. The AFM images exhibited a granular pattern similar to those found in other systems.[16] The same pattern was observed for samples prepared ex situ. The grain diameter was 270 ± 87 nm, in agreement with the values measured by Lavalle et al.[17] When not otherwise stated, the presented results will concern the film build-up under conditions close to physiological (150 mM ionic strength and pH 7.4).

The 3D images (Figure 2) demonstrated a significant morphological difference between the bare glass substrate and the $(PLL/PGA)_6$ film adsorbed on it.

For the bare glass, a mean roughness value of $R_a = 0.5 \pm$ 0.2 nm was obtained, whereas for $(PLL/PGA)_6$ the mean R_a was 17.7 ± 2.4 nm, and for $(PLL/PGA)_8$, it was 16.9 ± 2.2 nm. For in situ deposition, the roughness was found to be independent of the number of layers (Figure 3).

PLL/PGA films were also built-up ex situ, by an automatic immersion method. Dry samples aged for 1 day, 1 week, or 1 month were produced in this way. AFM images were then recorded. The structural characterization of these samples and their comparison with the result of the in situ measurements provided valuable information. Figure 3 depicts the changes in mean roughness of $(PLL/PGA)_5PLL$, $(PLL/PGA)_6$, $(PLL/PGA)_7PLL$, and $(PLL/PGA)_8$ films stored under dry conditions for up to 1 month.

In the in situ measurements, the roughness proved almost independent of the number of layers, whereas for the dry

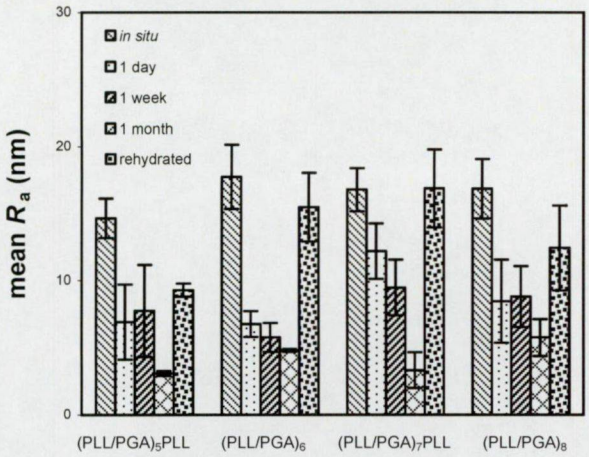

Figure 3. Mean roughness values as a function of layer number and time for polypeptide films on a glass substrate. Rehydrated films were 6 weeks old.

samples, a significant variation was observed (see 1-day and 1-week old samples for the (PLL/PGA)$_6$ and (PLL/PGA)$_7$PLL films). The dry samples with both 6 and 8 bilayers indicated a large decrease in roughness in time as compared with the in situ values, except for the (PLL/PGA)$_7$PLL film, where a smaller, but still significant decrease was observed. The chart reveals noteworthy decreases in R_a in all cases for the 1-month-old samples.

The PE films on a glass substrate also exhibited a significant time dependence, e.g., for the 1-day-old (PLL/PGA)$_7$PLL film R_a was 12.2 ± 2.1 nm, whereas after 1 month, it was 3.3 ±1.3 nm. Even after 1 day, a significant decrease in R_a was experienced, as observed for the (PLL/PGA)$_8$ films: the in situ value was 16.9 ± 2.2 nm, whereas for the 1-day-old sample, it was 8.4 ± 3.1 nm.

Upon rehydration of a 6-week-old dry sample, the roughness values almost reached those measured in situ, independently of the nature of the last layer. For the (PLL/PGA)$_6$ film, the mean R_a recovered to 15.5 ± 2.6 nm, whereas that for the (PLL/PGA)$_7$PLL film did so to 16.9 ± 2.9 nm. The data prove that the PLL/PGA films possess a high capability to rehydrate and to recover their morphology when placed in a wet environment.

3.3. PE Layers on a Ti Substrate. PLL/PGA multilayers on Ti disks were also built up in situ in the liquid cell of the atomic force microscope. Typical AFM deflection images of the Ti substrate and (PLL/PGA)$_6$ and (PLL/PGA)$_8$ films may be seen in Figure 4. The original rough-machined surface of the Ti disk can still be discerned even when the surface is covered totally by a PE film.

PLL/PGA films were also built up on a Ti substrate by the automatic immersion method. Dry samples aged 1 day, 1 week, 1 month, or 2 months were produced in this way. In the same way as for the glass substrate, a structural characterization was performed by AFM. The goal was to compare these samples with the samples prepared in situ, to follow their variation in time, and to provide information regarding their industrial applicability.

The same granular pattern was observed for the PE films prepared ex situ, demonstrating the lack of a dependence on the build-up procedure used (Figure 5). The grain diameter,

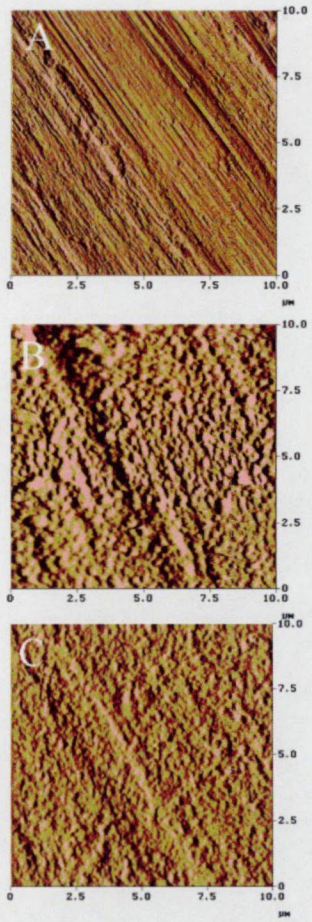

Figure 4. AFM deflection images of Ti substrate and PE layers on Ti (in situ measurements). (A) Bare Ti, z = 500 nm; (B) (PLL/PGA)$_6$ multilayer, z = 800 nm; and (C) (PLL/PGA)$_8$ film, z = 1.5 μm.

303 ± 89 nm, was not significantly different from that obtained on glass.

Figure 6A presents the mean roughness values for (PLL/PGA)$_7$PLL and (PLL/PGA)$_8$ films, including the data on the in situ, ex situ, and rehydrated samples. For in situ deposition, the roughness for (PLL/PGA)$_7$PLL was 5.0 ± 0.6 nm, whereas for (PLL/PGA)$_8$ it was 6.1 ± 0.8 nm.

PE films on a Ti substrate displayed a better stability in time up to 2 months as compared with glass substrate (Figures 6A and 3). However, the 1-month-old samples of (PLL/PGA)$_7$PLL and (PLL/PGA)$_8$ revealed almost the same roughness on the two different substrates. R_a for the (PLL/PGA)$_7$PLL film on glass was 3.3 ± 1.3 nm, whereas that on the Ti substrate was 3.5 ± 0.8 nm.

Figure 6B presents separately the mean roughness of thicker PE films (dry (PLL/PGA)$_9$PLL and (PLL/PGA)$_{10}$) deposited ex situ on a Ti substrate. For the PLL-ended films, a significant (almost double) increase in R_a was found for all of the dry samples: the typical R_a for a 1-week-old (PLL/PGA)$_7$PLL sample was 3.6 ± 0.6 nm, whereas that for the (PLL/PGA)$_9$PLL film was 5.9 ± 0.7 nm. In contrast for the PGA-ended films, there was no such accentuated variation in roughness. The present data do not yield any explanation for this difference; however, the small error bars prove that there is a real increase in R_a due to the PLL. Additional studies are needed to explain this phenomenon.

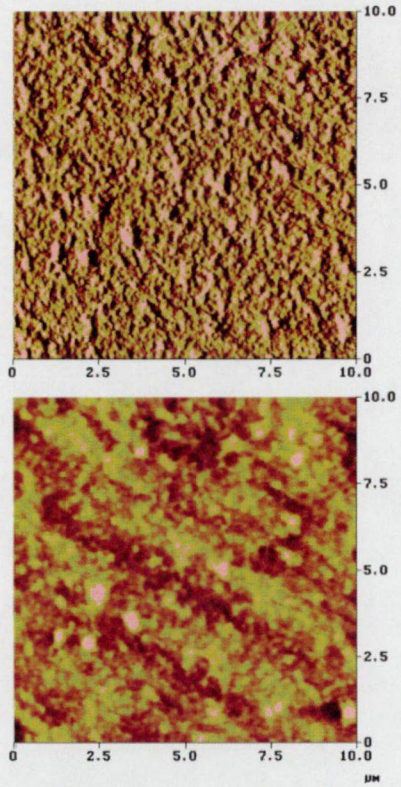

Figure 5. AFM deflection and height images of a $(PLL/PGA)_9PLL$ film on a Ti substrate, 1-day-old sample, immersion build-up technique.

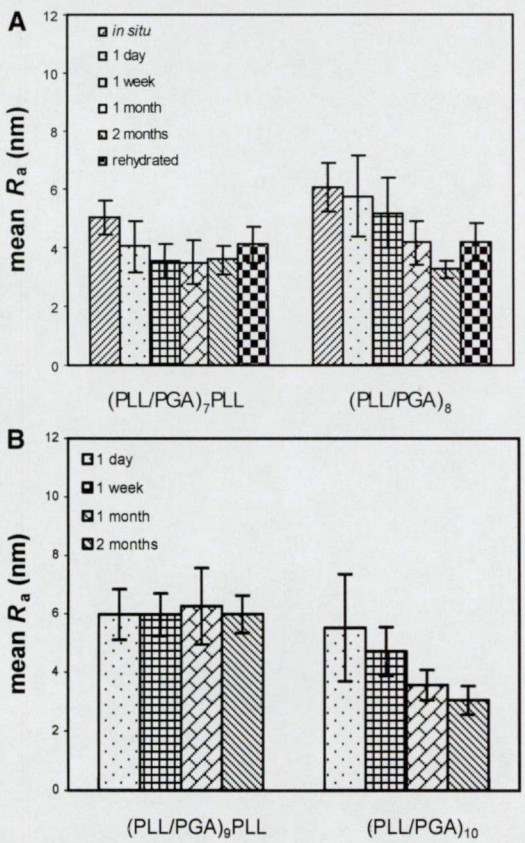

Figure 6. Mean roughness values as a function of layer number and time for polypeptide films on a Ti. (A) $(PLL/PGA)_7PLL$ and $(PLL/PGA)_8$ films, rehydration after 6 weeks. (B) Dry samples of $(PLL/PGA)_9PLL$ and $(PLL/PGA)_{10}$ films.

Finally, when the 6-week-old samples were rehydrated, their roughnesses almost attained the in situ values: for $(PLL/PGA)_7PLL$, 4.1 ± 0.6 nm was measured, and for $(PLL/PGA)_8$, 4.2 ± 0.7 nm was measured.

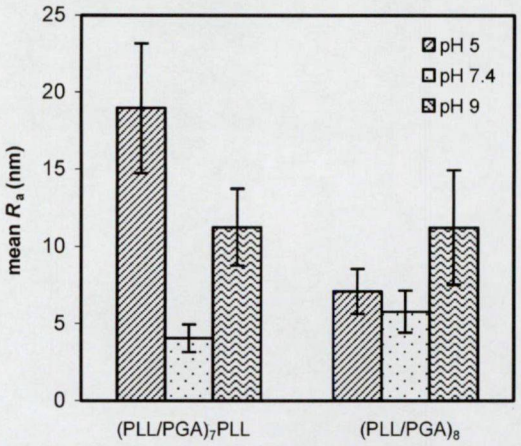

Figure 7. pH dependence of mean roughness values for polypeptide films on a Ti substrate (1-day-old samples).

3.4. Structural Characteristics of PE Multilayers on a Ti Substrate as a Function of pH. Since the degree of ionization of the PLL/PGA polypeptides is pH-sensitive, it may be expected that this parameter modulates the molecular organization of the films by altering the charge of both the polyanion and polycation. Weak PEs exhibit large variations in layer thickness and loops and tails above or below their pK_a as a result of incomplete charge compensation.[22] Morphological differences are observed when PLL/PGA films are deposited on a glass surface previously coated with strong PEs at pH 7.4 and pH 8.5.[8] We were interested in following the pH dependence of the PLL/PGA film structures by AFM, after direct adsorption on a Ti surface. Accordingly, films were deposited ex situ on Ti at pH 5, 7.4, and 9. Analysis of the AFM images revealed a significant effect of pH on the roughness of the $(PLL/PGA)_7PLL$ and $(PLL/PGA)_8$ films: the values generally increased at acidic or basic pH (Figure 7). There was also a noteworthy difference depending on the outermost layer of the PE film. When the outermost layer was PLL, high roughness values of 18.9 ± 4.2 and 11.2 ± 2.5 nm were obtained at low pH and high pH, respectively. In contrast, for the layers ending in PGA, R_a at pH 5 was much smaller, around 7.1 ± 1.5 nm, whereas at pH 9 there was no difference as compared with the PLL-ending film.

The high roughness values observed at acidic or basic pH are related to the degree of ionization of PGA and PLL. The pK_a values of PGA and PLL in aqueous solution are 4.9 and 9.8, respectively.[23,24] At high pH, higher amounts of the only partly ionized PLL molecules are needed to neutralize the charges of the fully ionized PGA molecules. At low pH, where the PLL is totally ionized, and the PGA is only partly ionized, the same interactions govern the build-up of the films as at high pH, but in the opposite sense. These processes lead to the observed increase in roughness. Our results are in good accordance with the formation of thicker layers at acidic or basic pH, as observed earlier.[8]

4. Conclusions

The final thickness of the $(PLL/PGA)_8$ film in situ was found to be about 70 nm by OWLS. Structural characteriza-

tion of the $(PLL/PGA)_i$ self-assembled layers adsorbed on glass and Ti substrates deposited irreversibly in two ways: in situ or ex situ was achieved by means of AFM investigations.

The films on both glass and Ti substrates exhibited granular patterns with a grain diameter of 270 ± 87 nm on glass and 303 ± 89 nm on Ti, independently of the build-up procedure used.

With glass as the substrate, the roughness values of the dried samples decreased as compared with those obtained for the PE films built in situ, depending on the time that had passed. This effect was much less accentuated for the Ti surfaces, and the PE films revealed a better stability in time up to a 2 month period relative to those on glass. The roughness values for the dry PE films built ex situ on Ti were closer to the in situ values. However, on Ti a significant increase in R_a was observed for the $(PLL/PGA)_9PLL$ film. PLL seems to be the key factor in this growth: when PGA was added in the next layer, R_a resumed a value of about 3.5 nm.

Upon the rehydration of dry samples, the roughness values almost attained those measured in situ for both glass and Ti. For a Ti substrate, a significant pH effect was observed. The high roughness values observed at acidic or basic pH are related to the different degrees of ionization of PGA and PLL.

The technique of alternating adsorption of the polypeptides PLL and PGA proved to be a successful method with which to coat the Ti surface of a possible implant material and is accompanied by a number of advantages. It can be automated, it uses aqueous solutions of biodegradable polypeptides, and it can provide films with controlled surface charge and finely tuneable thickness and roughness. The demonstrated time stability and good rehydration capability of PLL/PGA multilayer films built on Ti by immersion are of prime importance as concerns their biomedical applications, providing stable coatings at the solid−liquid interface.

Acknowledgment. The authors thank Hector Flores (Faculty of Dentistry, Université Louis Pasteur, Strasbourg) and Dr. Márta Szekeres (Department of Colloid Chemistry, University of Szeged) for their help in the AFM measurements. We are grateful to Dr. Gábor Laczkó (Department of Biophysics, University of Szeged) for valuable discussions. This work was supported by the SIMI-NAS Project of the 5th FWP of the European Commission (Growth Program, Project no: GRD3-2001-61801) and the GVOP-3.2.1.-2004-04-0408/3.0 Project funded by the Hungarian Ministry of Economy and the EC.

References and Notes

(1) Davies, J. E. *Int. J. Prosthodont.* **1998**, *11*, 391−401.
(2) Adell, R.; Leckholm, U.; Rockler, B.; Branemark P. I. *Int. J. Oral Surg.* **1981**, *10*, 387−416.
(3) Morra, M.; Cassinelli, C. *J. Biomed. Mater. Res.* **1997**, *37*, 198−206.
(4) Morra, M.; Cassinelli, C.; Cascardo, G.; Cahalan, P.; Cahalan, L.; Fini, M.; Giardino, R. *Biomaterials* **2003**, *24*, 4639−4654.
(5) El Ghannam, A.; Starr, L.; Jones, J. *J. Biomed. Mater. Res.* **1998**, *41*, 30−40.
(6) Anselme, K. *Biomaterials* **2000**, *21*, 667−681.
(7) Courtney, J.; Lamba, M.; Sundaram, S.; Forbes, C. D. *Biomaterials* **1994**, *15*, 737−744.
(8) Gergely, C.; Bahi, S.; Szalontai, B.; Flores, H.; Schaaf, P.; Voegel, J. C.; Cuisinier, F. J. G. *Langmuir* **2004**, *20*, 5575−5582.
(9) Puleo, D. A.; Nanci, A. *Biomaterials* **1999**, *20*, 2311−2321.
(10) Decher, G.; Hong, J. D.; Schmitt, J. *Thin Solid Films* **1992**, *210*, 831−835.
(11) Sano, M.; Lvov, Y.; Kunitake, T. *Annu. Rev. Mater. Sci.* **1996**, *26*, 153−187.
(12) Angelova, N.; Hunkeler, D. *Rev. Elsevier Sci.* **1999**, *17*, 409−421.
(13) Chluba, J.; Voegel J. C.; Decher, G.; Erbacher, P.; Schaaf, P.; Ogier, J. *Biomacromolecules* **2001**, *2*, 800−805.
(14) Tryoen-Toth, P.; Vautier, D.; Haikel, Y.; Voegel, J. C.; Schaaf, P.; Chluba, J.; Ogier, J. *J. Biomed. Mater. Res.* **2002**, *60*, 657−667.
(15) Ram, M. K.; Bertoncello, P.; Ding, H.; Paddeu, S.; Nicolini, C. *Biosens. Bioelectron.* **2001**, *16*, 849−856.
(16) Boura, C.; Menu, P.; Payan, E.; Picart, C.; Voegel, J. C.; Muller, S.; Stoltz, J. F. *Biomaterials* **2003**, *24*, 3521−3530.
(17) Lavalle, P.; Gergely, C.; Cuisinier, F. J. G.; Decher, G.; Schaaf, P.; Voegel, J. C.; Picart, C. *Macromolecules* **2002**, *35*, 4458−4465.
(18) Picart, C.; Ladam, G.; Senger, B.; Voegel, J. C.; Schaaf, P.; Cuisinier, F. J. G.; Gergely, C. *J. Chem. Phys.* **2001**, *115*, 1086−1095.
(19) Picart, C.; Gergely, C.; Senger, B.; Arntz, Y.; Voegel, J. C.; Schaaf, P.; Cuisinier, F. J. G. *Biosens. Bioelectron.* **2004**, *20*, 553−561.
(20) Menchaca, J. L.; Jachimska, B.; Cuisinier, F. J. G.; Perez, E. *Colloids Surf. A* **2003**, *222*, 185−194.
(21) Lobo, R. F. M.; Pereira-da Silva, M. A.; Raposo, M.; Faria, R. M.; Oliveira Jr., O. N. *Nanotechnol.* **2003**, *14*, 101−108.
(22) Shiratori, S. S.; Rubner, M. F. *Macromolecules* **2000**, *33*, 4213−4219.
(23) Cheng, Y.; Corn, R. M. *J. Phys. Chem. B* **1999**, *103*, 8726−8731.
(24) Cantor, R.; Schimmel, P. R. In *Biophysical Chemistry*; W. H. Freeman: San Francisco, 1980; p 2.B

BM050360K

III.

FOGORVOSI SZEMLE ■ 97. évf. 6. sz. 2004. 231–237.

Szegedi Tudományegyetem Általános Orvostudományi Kar, Fogászati és Szájsebészeti Klinika,*
Szegedi Tudományegyetem Természettudományi Kar Optikai és Kvantumelektronikai Tanszék**
Szegedi Tudományegyetem Természettudományi Kar MTA Lézerfizikai Tanszéki Kutatócsoport***

Titán-minták felületének módosítása excimer lézerrel a hatékonyabb osszeointegráció érdekében

DR. PELSŐCZI KOVÁCS ISTVÁN*, DR. BEREZNAI MIKLÓS**, DR. TÓTH ZSOLT***, DR. TURZÓ KINGA*, DR. RADNAI MÁRTA*, DR. BOR ZSOLT**, DR. FAZEKAS ANDRÁS*

A fogászatban és az ortopédiában használatos titán-implantátumoknak az őket körülvevő szövetekkel való kapcsolata, biointegrációja nagymértékben függ felszínük morfológiájától és annak fizikai-kémiai tulajdonságaitól. Ezért a gyártási technológiában fontos feltétel az implantátumok felületének olyan eljárással való kialakítása, amellyel jól irányítható módon, kívánt formájú mikro szerkezet alakítható ki. Ehhez, a széles körben alkalmazott „homokfúvás + savazás" és a „plazma-ráfúvásos" technikák mellett kézenfekvőként kínálkozik a lézeres felületkezelési módszer. A kívánatos felületi morfológia kialakításához az implantátumok alapanyagául szolgáló titánból készült próbatestek felületét excimer lézeres kezelésnek vetettük alá. Alapvető célunk az volt, hogy a titán próbatesteken olyan felszíneket alakítsunk ki, amelyek egyrészt a csontránövés, másrészt a hámtapadás kialakulása és fenntarthatósága számára biztosítanak optimális feltételeket. Ennek érdekében – az elsőként megfogalmazott cél elérésére – nanoszekundumos (18 ns, ArF) és szubpikoszekundumos (0,5 ps, KrF) lézer-impulzusokkal ablációs lyukakat hoztunk létre a próbatestek felületén. A nanoszekundumos lézerkezelés hatására kráterek keletkeztek, amelyek széle körül csepp formájú alakzatból álló, peremszerű, horgas kitüremkedések jelentek meg, amelyek alakjukból következően mechanikus hatásra sérülékenyek. Ha a felület kezelését KrF ultrarövid lézer-impulzusokkal végeztük, akkor a kráterek körül nem képződött ilyen sérülékeny perem. A másodikként megfogalmazott cél, a lágyszövetekkel való egészséges kapcsolat kialakulásának és fenntarthatóságának érdekében a mintákat ArF lézerrel políroztuk. Atomi erő mikroszkóppal (AFM) végzett vizsgálataink azt bizonyítják, hogy a nanoszekundumos lézer-besugárzás hatékony felületi simítást eredményez, ami kedvez a hámtapadás kialakulásának, de főleg a plakk-mentesítés lehetőségének, mely utóbbi alapvető feltétele a periimplantáris szulkusz egészséges állapotának. A röntgen fotoelektron spektroszkópiás (XPS) vizsgálataink azt mutatták, hogy a lézerkezelés a mikrostrukturális, morfológiai alakításon túl a felületi szennyeződés csökkenését és az oxid-réteg megvastagodását is eredményezi. Röntgen diffrakciós (XRD) vizsgálataink azt igazolták, hogy a kezelés hatására az eredeti, α-titán kristályszerkezet nem szenved károsodást, illetve nem változik meg.

Kulcsszavak: titán, osszeointegráció, excimer lézeres abláció, felszíni módosítás, felületi érdesség

A hiányzó fogak pótlására használt fogászati implantátumokat többféle alapanyagból lehet előállítani [1–3]. Ezek közül a tiszta titán a leggyakrabban használt, mivel ez rendelkezik optimális tulajdonságokkal [4–6]. A titán-oxidáció magas entalpiájának (ΔH = -912 kJ/mol) köszönhetően, a fém felületén 20–100 Å vastag natív titán-dioxid réteg alakul ki spontán, pár másodperc alatt. Ez biztosítja az anyag korrózióállóságát, méltán emelve a fémet a legkiválóbb bioanyagok közé [7, 8].

A dentális implantáció hosszú távú sikere nagymértékben függ a befogadó szövetek (környező kemény és lágy szövetek) válaszreakcióitól. Az osszeointegráció szempontjából – amely az implantátum felszíne és az élő csont között kialakuló direkt kapcsolatot jelenti – többek között az egyik legfontosabb kérdés, hogy az implantátum felületi morfológiájának módosításával lehet-e valamilyen módon gyorsítani a csontseb gyógyulásának folyamatát. A felületi érdesítés kérdéskörével számos szerző foglalkozott már [9–13]. A felszín mikrostruktúrájának módosításával a közvetlen csont–implantátum kapcsolat kialakulásában résztvevő felületek nagyságát növelhetjük. Tudjuk, hogy az érdesített felületen – ellentétben a simább felülettel – a csontképzés folyamata gyorsabban megy végbe, mivel a felszínen merőlegesen megtapadó kollagénrostok az integrációban szerepet játszó blasztos sejteket mintegy a felszínre vezetik. Az implantátumok felületén a kívánt formájú mikro szerkezet kialakítása jól irányítható módon, különböző módszerekkel lehetséges. Ehhez, a széles körben alkalmazott „homokfúvás + savazás" és a „plazma-ráfúvásos" technikák mellett kézenfekvőnek kínálkozik a lézeres felületkezelési módszer. A megváltoztatott mikrostruktúra

Érkezett: 2004. február 9.
Elfogadva: 2004. július 15.

mellett a felület tisztaságának megtartása természetesen a továbbiakban is rendkívül fontos alapkövetelmény marad [14–17].

Az implantátum felszínén kialakuló egészséges hámtapadást szintén a felületi morfológia befolyásolja [18]. A kötőszöveti rostok a sima felszínhez nem képesek közvetlenül kapcsolódni, tapadásuk glikoprotein rétegek segítségével történik. Bár a rostok tapadása szempontjából az érdesített felszín ideálisabb lenne, az implantátum nyaki részének felszínét mégis ajánlatos polírozni a plakk-felhalmozódás elkerülésének érdekében [19].

Az elmúlt években a szilárd felszínek lézerrel történő felületi érdesítésére számos eljárást dolgoztak ki [20], és vizsgálatok bizonyítják, hogy az implantátum-anyag lézeres felületkezelése során a kívánt morfológia, a felület legkisebb mértékű szennyeződése mellett érhető el [21, 22]. Nd:YAG lézeres megmunkálás során többszörös besugárzás hatására, a titán felszínén „koronaszerű" peremképződmények alakulnak ki [23], és beszámoltak arról is, hogy az ilyen lézeres kezelés a titán oxidációját váltja ki [24, 25]. Az excimer lézeres kezelések egyik előnye a többi lézerrel szemben az, hogy az ultraibolya (UV) hullámhossznak köszönhetően a kezelés egyúttal a felület sterilizálását is eredményezi. A lézerek jelentős potenciális lehetőséget nyújtanak a felületmódosítások terén, és ezért egyre kiterjedtebben alkalmaznak az iparban lézeres technológiákat. Ugyanakkor az orvosi alkalmazások által támasztott magasabb igények megkövetelik e technika hatásainak (mechanikai és kémiai jellemzők) teljes megismerését és a módszer tökéletesítését.

Jelen vizsgálatunk célja az volt, hogy titán próbatesteken excimer lézerrel olyan felszíneket alakítsunk ki, amelyek egyrészt a csontránövés, másrészt a hámtapadás kialakulása és fenntarthatósága számára biztosítanak optimális feltételeket.

Vizsgálati anyag és módszer

Vizsgálatainkhoz dentális implantátumok alapanyagául szolgáló, 1,25 mm vastag és 8 mm átmérőjű CP1 tisztasági fokú titánkorongokat használtunk. A minták felszínén a gépi megmunkálásból származó 0,1-2,0 μm mélységű barázdák szabad szemmel is megfigyelhető, koncentrikus körök formájában jelentek meg. A lézerkezelés előtt a korongokat ultrahanggal, detergensben tisztítottuk, majd desztillált vizes leöblítés után etanolban mostuk.

A felület polírozását ArF excimer lézerrel (Lambda Physics EMG 201, hullámhossz: 193 nm, impulzushossz: 18 ns, energiasűrűség: 100 mJ) végeztük. A lézernyaláb homogén részét téglalap alakú aperturán keresztül, 5 cm fókusztávolságú kvarclencsével képeztük le a mintára. 3,6 mm^2-es besugárzott területet különböző lézerimpulzus-sorozatokkal kezeltük, atmoszférikus körülmények között. A titán felületének simítása érdekében két paramétert változtattunk egymástól függetlenül: egyrészt a lézerfénynek a minta felületére eső energiasűrűségét, amelyet megfelelő kalibráló szűrők alkalmazásával 1,5–5,0 J/cm^2 értékhatárokon belül változtattuk, másrészt a lézer impulzusok számát, amelyek a mérések során 10, 100 és 1000 voltak.

A titánfelszín érdességének növelését lokális lézeres anyageltávolítással valósítottuk meg. Ehhez a felületsimításhoz hasonló berendezést használtuk, csak annyi változtatással, hogy ebben az esetben egy rézrácsot helyeztünk a lézersugarak útjába, és a leképezést a minta síkjára 4 cm fókusztávolságú kvarclencsével végeztük. A felületi energiasűrűség (8,5 J/cm^2) meghaladta a polírozásnál használt értéket. Ebben az estben 250, 500 és 1000 lézer impulzust alkalmaztunk.

A következő lépésben a felület módosításához ultrarövid impulzusú KrF excimer lézert használtunk (hullámhossz: 248 nm, félértékszélesség: 0,5 ps, impulzusenergia: 10 mJ). Ezt a kísérleti berendezést a [26]-os cikkben mutatták be részletesen. A titán-minta és a lencse fókuszpontja egy átlátszó üveg (Suprasil) ablakkal felszerelt, alacsony nyomású (10 Pa) vákuumkamrában volt elhelyezve, mivel ennél a lézernél a lencse fókuszában olyan nagy intenzitás alakul ki, ami a levegőben plazmát kelt, ezzel gátolva a fény továbbhaladását. Ebben a kísérletsorozatban 2,4 J/cm^2 energiasűrűség mellett 1000 lézer impulzust alkalmaztunk.

A minták felszínének morfológiáját először optikai mikroszkóp segítségével vizsgáltuk (Nikon Optiphot 100S fémipari mikroszkóp). A nagy felbontású szekunder elektron-emissziós képeket pásztázó elektron-mikroszkóppal (Hitachi S-2400) vettük fel. A mélyedéseket jobban láthatóvá tettük a minták 75°-os szögben való megdöntésével. A felszín topográfiáját a szubmikrométeres tartományban atomi erő mikroszkóppal (AFM) vizsgáltuk (TopoMetrix Explorer TM, kontakt üzemmód). A felület érdességét az úgynevezett átlagos érdeséggel (Ra) jellemeztük, melyet a TopoMetrix szoftver határozott meg. Ez az érték a felszín pontjainak átlagos eltérését adja meg nanométerben az átlagos magassághoz képest.

A titán-felszín kémiai összetételének vizsgálatát röntgen fotoelektron spektroszkópiával (XPS) végeztük. Az Al K_α primér sugárzásából keletkező fotoelektronokat félgömb elektron energia analizátor detektálta (Kratos XSAM 800). A kötési energiákat a C (1s) csúcs helyzetének figyelembevételével kalibráltuk. Az XPS spektrumok változásait többször megismételt, 10 perces Ar-ion bombázások után mértük. Az argon-ionokat 3 keV-os feszültséggel gyorsítottuk, a beeső ionsugár áramsűrűsége 4 μA/cm^2 volt. Tízperces Ar-ion bombázás körülbelül 10 nm vastagságú anyagot távolított el a minta felszínéről. Széles tartományú és nagy felbontású, részletes spektrumokat készítettünk a jellegzetes csúcsokról (Ti 2p, O 1s és N 1s).

A lézerkezelt és kezeletlen minták kristályszerkezetének összehasonlítására röntgendiffrakciós spektrumokat vettünk fel, a Cu K_α sugárzás segítségével ($\lambda = 0{,}154$ nm). A röntgendiffrakciós vizsgálatokat Philips PW 1830 röntgen generátorral felszerelt (40 kV, 25 mA) por diffraktométerrel (PW 1877, Philips) végeztük.

Eredmények

ArF lézeres felületsimítást végeztünk a mintákon 10 lézerimpulzussal. A polírozás hatékonyságát növelni tudtuk az energiasűrűség 1,5 J/cm^2-től 5 J/cm^2-es értékig való növelésével. Az elektronmikroszkópos felvételeken jól láthatóak azok a 10 µm-nél kisebb, a korongok titánrúdból való levágása során keletkező felszíni bemaródások *(1a. ábra)*, amelyek a lézerkezelés hatására eltűntek a minta felszínéről *(1b. ábra)*. A nagyobb struktúrák

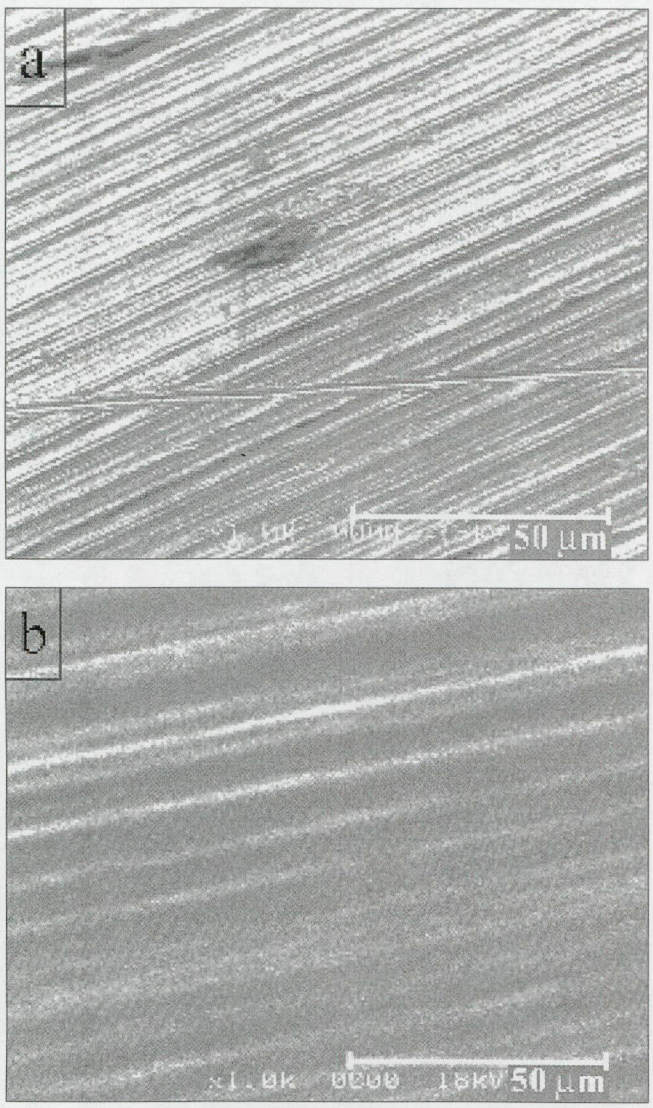

1. ábra. Gépileg megmunkált, kezeletlen (a) és ArF lézerrel simított titán-minta (b) felszínéről készült SEM felvétel. A polírozás 3,5 J/cm^2 energiasűrűséggel és 10 lézerimpulzussal történt.

mélysége jelentősen csökkent, bár a hullámos szerkezet még felismerhető a polírozott felszínen *(1b. ábra)*. Az atomi erő mikroszkópos felvételek segítségével a felületi érdesség kvantitatív meghatározására is lehetőségünk nyílt *(2. ábra)*. Az eredeti, megmunkált felszín érdessége Ra = 256 nm volt *(2a. ábra)*. A polírozott felszín érdessége 5 J/cm^2 energiasűrűségű, 10 impulzussal megvilágí-

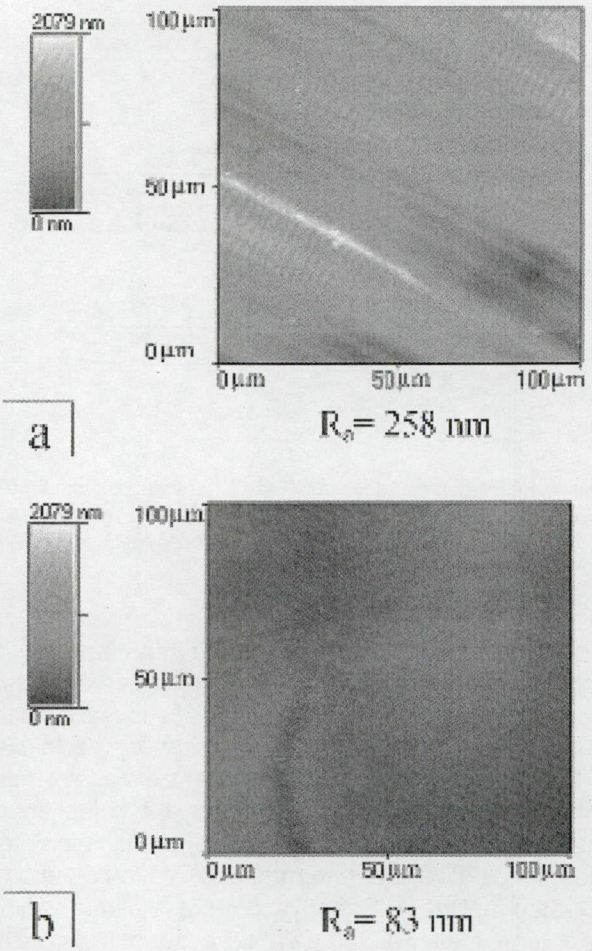

2. ábra. AFM topográfia-felvétel a kezeletlen (a) és ArF lézerrel polírozott felületről. A simítás 5 J/cm^2 energiasűrűséggel, 10 lézerimpulzussal történt.

tott lézernyaláb esetében szignifikánsan lecsökkent Ra = 25 nm értékre *(2b. ábra)*. Ez az érték megfelel korábbi irodalmi adatoknak [27], ahol a plakk-felhalmozódás és -érés elkerülésének érdekében az optimális felületi érdességet Ra ≤ 88 nm-ben határozták meg.

Az XPS mérések spektrumai igazolják az oxigén, a nitrogén és a szén jelenlétét mind a lézerkezelt, mind pedig a kezeletlen minták estében *(3. ábra)*. Ezeknek az elemeknek a jelenléte a titán-implantátumok felületére általában jellemző [28]. A foszfor és a klór jelenlétét nyomokban szintén kimutattuk [29, 30]. A *3. ábra* felső része az argon-besugárzás nélküli, az alsó része pedig az Ar-ionnal 10 percig bombázott felületről készült görbéket mutatja. A lézerkezelés a felszín kémiáját csak bizonyos tekintetben változtatta meg. A C 1s csúcs jelenléte a felszín szén-tartalmú szennyeződésére utal, amely a korongok kémiai tisztításából vagy a levegő szerves anyagaival történő kontaminációjából adódik [30, 31]. Az excimer lézeres kezelés hatására a C 1s csúcs nagymértékben lecsökkent, ami alátámasztja a lézer hatékony tisztítási képességét.

A lézerkezelt és a kezeletlen minták jellegzetes, nagy felbontású Ti 2p spektrumainak 10, 20 és 30 perces Ar-

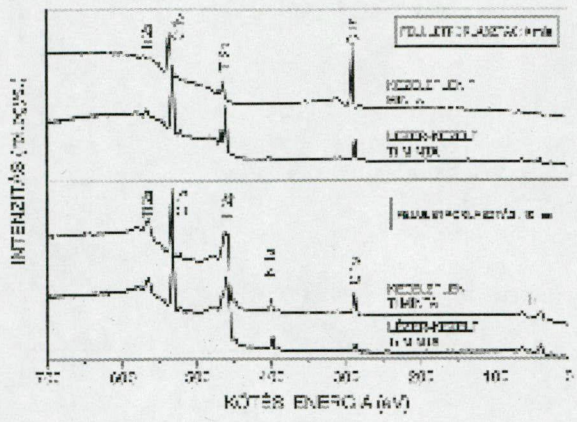

3. ábra. Kezeletlen és ArF lézerrel kezelt titán-minták felületéről készült XPS spektrumok képe Ar-ion ágyúzás előtt (felső rész), illetve 10 perces besugárzás után (alsó rész).

ion bombázás utáni görbéit a *4. ábra* mutatja. Az első 10 perces besugárzás utáni állapotról felvett spektrumok mindkét estben három jellegzetes csúccsal rendelkeznek, 464,7, 459 és 455,6 eV kötési energia értékeknél. A Ti $2p_{1/2}$ és a Ti $2p_{3/2}$ csúcsok helyzete a felszínen található TiO_2-re utal [32]. Az alacsonyabb kötési energiánál megjelenő váll (Ti $2p_{3/2}$ csúcs), a TiN jelenlétét támasztja alá [33]. Ez nem meglepő, hiszen a vékony TiO_2 réteg mellett TiN szennyeződés is található a mintában, amely feltehetőleg az alapanyagból származik [34]. Az alapanyagban lévő N jelenlétét alátámasztja a N 1s csúcs növekedése az argon-ion besugárzás hatására *(3., 4. ábra)*.

A legfontosabb információt a második és a harmadik Ar-ion besugárzás után felvett görbék tartalmazzák *(4. ábra)*. A kezeletlen felszínről készült spektrum 460 és 454 eV kötési energiáknál két csúcsot tartalmaz, ami a tiszta fém titán jelenlétére utal [33, 35]. A lézerkezelt minta esetében viszont, a második és harmadik porlasztási eljárás után is még mindig a titán oxidációs állapotára jellemző három csúcs van jelen, vagyis a lézeres polírozás során lézeres oxidáció is lejátszódott, az oxid-réteg vastagsága legalább kétszeresére nőtt. Ez alátámasztja a lézerek használhatóságát az implantátumok osszeointegrációjának hatékonyabbá tételében [13].

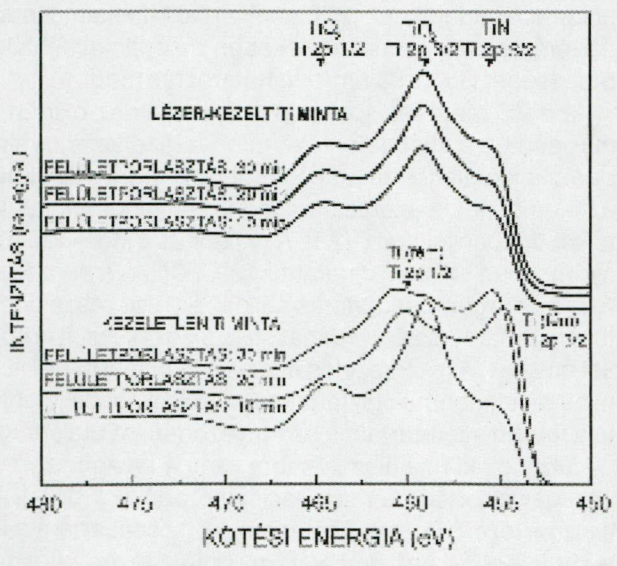

4. ábra. Nagy felbontású XPS Ti 2p spektrum 10, 20 és 30 perces Ar-ion ágyúzást követően, kezeletlen és lézerkezelt minta esetében.

A lézeres kezelés megváltoztathatja a hőeffektusnak kitett titán-minta kristályos szerkezetét. Szobahőmérsékleten a hexagonális α-titán a domináns szerkezet, míg 1158 K fölött ez a forma átalakul köbös β-titánná. A titán kristályos struktúrájában létrejött esetleges változásokat a lézerkezelt és kezeletlen minták, illetve az α-titán XRD spektrumainak összehasonlításával követtük nyomon *(5. ábra)*. A kezeletlen minta görbéje leginkább az α-titánra jellemző [24, 36], de a $2\theta = 31{,}61°$, 34,59°, 36,13°, 47,53° és az 56,29° értékeknél található csúcsok más kristályformák jelenlétét is igazolják. A 34,59° és 38,42° értéken található diffrakciós csúcsok valószínű felszíni szennyeződésekből adódnak, mivel a lézerkezelés hatására ezeknek a csúcsoknak az intenzitása jelentősen lecsökkent. A lézerkezelt minták *(5. ábra)* felszínéről készült XRD spektrumok szintén az α-formára jellemző intenzitásokat mutatják [37], ami arra enged következtetni, hogy az eredeti α-titán kristályszerkezet megmaradt, de ugyanakkor a lézerkezelés a felszín tisztulását is eredményezte.

A kezeletlen minta esetében a nem-α-titánból származó csúcsok eredete még nem teljesen tisztázott. A 38,42° értéken mért csúcs származhatna a β-titánból (38,48°), de az egyéb β-titánra jellemző értékek (55,54°

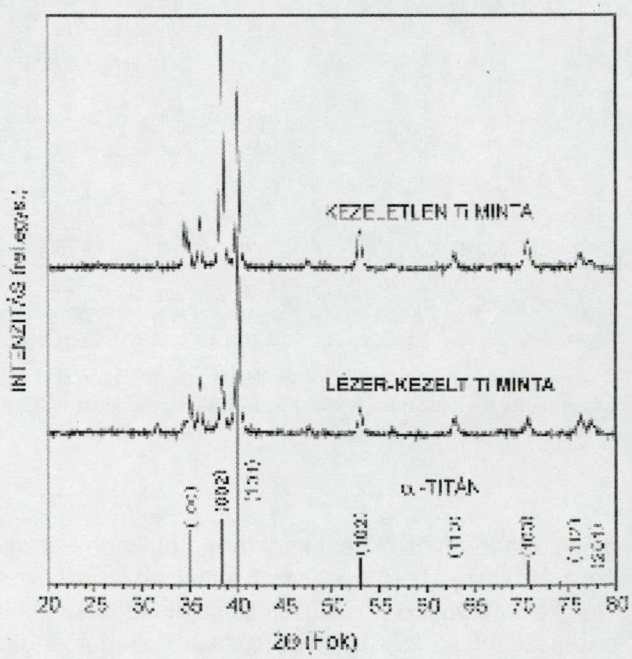

5. ábra. Kezeletlen és ArF lézerrel kezelt mintákról készült röntgendiffrakciós spektrumok. A kép alján a tiszta α-titán referencia intenzitásai láthatók.

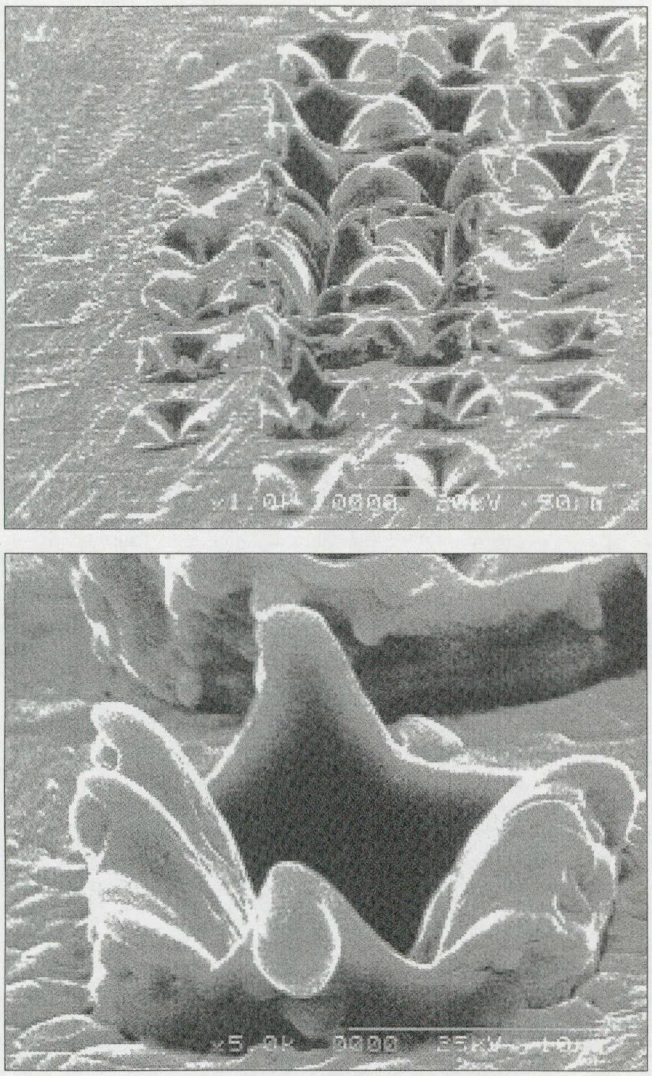

6. ábra. Titán-minta felszínén 18 ns-os ArF excimer lézerrel kialakított kráterek különböző nagyítású SEM képe. 250 lézerimpulzus, 8,5 J/cm2 energiasűrűség.

A perem nélküli kráterek speciális polimerek és kerámiák esetében gond nélkül könnyen kialakíthatók rövid hullámhosszúságú excimer lézerekkel, ellentétben a fémekkel, ahol a viszonylag nagy hővezetési képesség miatt nemcsak a megvilágított felszínt fűtjük fel, hanem az alatta lévő tartományt is. Emiatt a lézerimpulzus időtartama alatt a robbanásszerűen elpárolgó felszín alatt az olvadás következtében egy folyadékréteg keletkezik, mely kifröccsenése hozza létre a kitüremkedéseket, peremeket. Fél-pikoszekundumos lézerimpulzusok alkalmazásával a peremek kialakulása fémeknél is elkerülhető *(7. ábra)*. Csökkentve a hődiffúziós hossz értékét [20, 38–42], elérhetjük a perem nélküli bemélyedések keletkezését, és ezáltal nő az eljárásunk hatékonysága. 0,5 ps KrF excimer lézeres besugárzás következtében, 1000 lézer impulzus mellett és 2,4 J/cm^2 energia-

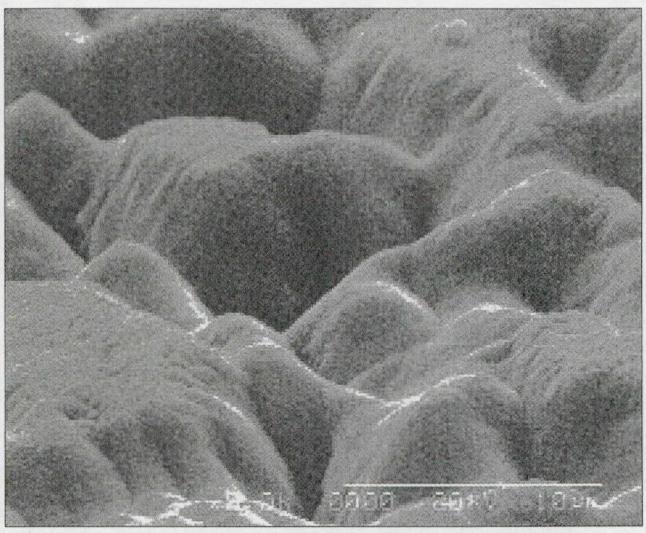

7. ábra. 0,5 ps-os KrF excimer lézerrel kialakított ablációs bemélyedések SEM képe. 1000 lézerimpulzus, 2,4 J/cm2 energiasűrűség.

és 69,60°) teljes mértékben hiányoznak a spektrumból. Más titán-oxidok, mint például az anatáz (25,32°), vagy a rutil (27,37°) sem lehet e csúcsok forrása, mivel a spektrumról ezek más karakterisztikus vonalai szintén hiányoznak [36]. Valószínűsítjük, hogy e csúcsok nem sztöchiometrikus titán-vegyületek kristályformáiból származnak (oxidok, nitridek vagy karbonátok), amelyeket az XPS vizsgálat is kimutatott.

ArF excimer lézerrácson keresztül történő leképezésével a titán-minta felszínén jellegzetes, egymástól körülbelül 25 μm távolságra lévő felszíni bemélyedések keletkeztek *(6a. ábra)*. A felszínen, azokon a helyeken képződtek lyukak, ahol a lézernyaláb energiasűrűsége meghaladta az ablációs küszöbértéket. Az impulzusok számának emelésével, az ablációs lyukak mélysége is nőtt. Ezzel egy időben a kráterek szélein nemkívánatos horgas kitüremkedések keletkeztek *(6b. ábra)*. 250 lézer impulzust alkalmazva 8,5 J/cm^2 energiasűrűségnél, a bemélyedések mélysége 10 μm, a peremek magassága pedig legfeljebb 8 μm.

sűrűségnél a horgas kitüremkedések megjelenése teljesen elkerülhető. A felület struktúrája a követelményeknek eleget tesz és az osszeointegrációban szereplő felszín nagysága jelentősen megnőtt.

Megbeszélés, következtetések

Titán-minták felszínét, annak kémiai összetételét és morfológiáját excimer lézerrel módosítottuk, egyrészt políroztuk, másrészt ablációs eljárással érdesítettük. A SEM és AFM vizsgálatok azt mutatták, hogy 3–5 J/cm^2 energiasűrűségű nanoszekundumos homogén nyalábok hatékonyan simították a felszínt. A felszínpolírozás folyamatának két lehetséges magyarázata van. A lézeres besugárzás hatására a felületi anyag megolvad és elpárolog, majd a visszahűlés után a kisimult folyadékfelszín megszilárdul. Egy másik lehetséges magyarázat szerint [20], a lézersugár az érdes felület kiemelkedéseit sokkal hatékonyabban képes felmelegíteni, mint a mélyedéseket,

ahol a hő diffúziója hatékonyabb. Ez azt eredményezi, hogy a magasabban fekvő területeken hatékonyabb az anyageltávolítás, és ezáltal lesz simább a felület.

Az XPS és XRD vizsgálatok kimutatták, hogy a szén-tartalmú szennyeződés a felületen jelentősen lecsökkent, vagyis a lézerkezelés a titán-minták felszínét tisztította. Az XPS vizsgálatok alapján megállapíthatjuk, hogy az excimer lézeres besugárzás hatására a titán felszínén lévő titán-dioxid réteg jelentősen megvastagodott.

Az XRD mérések eredménye, hogy a ns-os lézer a titánból készült implantátum-korong kristályszerkezetét, a hőkezelésnek kitett területen nem változtatta meg, megmaradt az eredeti α-forma. Az implantátumok esetében az eredeti kristályszerkezet megtartása alapvető fontosságú, az előnytelen feszültségek kialakulásának elkerülése érdekében.

A titán-minta felszínén a ns-os ArF excimer lézer 20 μm átmérőjű és 10 μm mélységű, peremmel rendelkező bemélyedéseket alakított ki. Ennél a módszernél bebizonyosodott, hogy az ablációt kiterjedt párolgás és olvadás kíséri. Az alkalmazott energiasűrűség tartományban plazma képződik, és az alatta lévő olvadék kifröccsenve, a széleken peremet alakít ki [23]. Ez a hatás nemkívánatos és hátrányosan befolyásolhatja az osszeointegrációt, mivel egyrészt retenciós részként szolgálhatnak a kórokozók számára, másrészt ezek a részek a felhasználás során letörhetnek az implantátum felszínéről, és szennyezhetik biológiai környezetüket. A törékeny kitüremkedések kialakulásának elkerülése érdekében 0,5 ps-os excimer lézert használtunk, és bebizonyítottuk, hogy ezzel a lézerrel az olvadék peremszerű felrakódása elkerülhető, ugyanakkor a megfelelő felületi struktúra megmarad és a tapadási felület jelentősen megnő.

Köszönetnyilvánítás

Köszönettel tartozunk dr. Oszkó Albertnek (SZTE, TTK Szilárdtest és Radiokémiai Intézet) az XPS vizsgálatokért, dr. Patzkó Ágnesnek (SZTE, TTK, Kolloidkémiai Tanszék) az XRD mérésekben nyújtott segítségéért és dr. Szatmári Sándornak (SZTE, TTK, Kísérleti Fizikai Tanszékének vezetője) a 0,5 ps-os KrF lézer használatáért.

Irodalom

1. Williams Df: Implants in dental and maxillofacial surgery. *Biomaterials* 1981;2:133
2. Lemons Je: Dental implant biomaterials. *J Am Dental Assoc* 1990; 121:716–719.
3. Craig Rg: *Restorative Dental Materials.* In: Powers JM, Craig RG, editors, St. Louis, Mosby Inc 1989. p. 169
4. Meffert Rm, Langer B, Fritz Me: Dental implants: a review. *J Periodontol* 1992; 63:859–870.
5. Brånemark Pi, Adell R, Albrektsson T, Lekholm U, Lundkvist S, Rockler B: Osseointegrated titanium fixtures in the treatment of edentulousness. *Biomaterials* 1983; 4:25–28.
6. Albrektsson T: The response of bone to titanium implants. CRC Critical Reviews in Biocompatibility 1985; 1:53.
7. Lautenschlager EP, Monaghan P: Titanium and titanium alloys as dental materials. Int Dental Journal 1993; 43:245–253.
8. Michel R: Trace metal analysis in biocompatibility testing. *CRC Critical Reviews in Biocompatibility* 1987; 3:235.
9. Eriksson C, Lausmaa J, Nygren H: Interactions between human whole blood and modifed TiO_2-surfaces: Influence of surface topography and oxide thickness on leukocyte adhesion and activation. *Biomaterials* 2001; 22:1987–1996.
10. Buser D, Schenk RK, Steinmann S, Fiorellini JP, Fox CH, Stich H: Influence of surface characteristics on bone integration of titanium implants - a histomorphometric study in miniature pigs. *J Biomed Mater Res* 1991; 25:889–902.
11. Wong M, Eulenberger J, Schenk R, Hunziker E: Effect of surface-topology on the osseointegration of implant materials in trabecular bone. *J Biomed Mater Res* 1995; 29:1567–1575.
12. Wennerberg A, Ektessabi A, Albrektsson T, Johansson L, Andersson B: A 1-year follow-up of implants of differing surface roughness placed in rabbit bone. *Int J Oral Max Imp* 1997; 12:486–494.
13. Boyan BD, Batzer R, Kieswetter K, Liu Y, Cochran DL, Szmuckler-Moncler SS, Dean DD, Schwartz Z: Titanium surface roughness alters responsiveness of MG63 osteoblast-like cells to 1 alpha,25-(OH)(2)D-3. *J Biomed Mater Res* 1998; 39:77–85.
14. Binon PP, Weir DJ, Marshall SJ: Surface analysis of an original Brånemark implant and three related clones. *Int J Oral Max Imp* 1992; 7:168–175.
15. Olefjord I, Hansson S: Surface analysis of four dental implant systems. *Int J Oral Max Imp* 1993; 8:32–40.
16. Cochran DL: A comparison of endosseous dental implant surfaces. *J Periodontology* 1999; 70:1523–1539.
17. Uitto VJ, Larjava H, Peltonen J, Brunette DM: Expression of fibronectin and integrins in cultured periodontal-ligament epithelial-cells. *J Dent Res* 1992; 71:1203–1211.
18. Hansson H, Albrektsson T, Brånemark PI: Structural aspects of the interface between tissue and titanium implants. *J Prosth Dent* 1983; 50:108–113.
19. Quirinen M, Bollen CM, Papaioannou W, Van Eldere J, van Steenberghe D: The influence of titanium abutment surface roughness on plaque accumulation and gingivitis: short-term observations. *Int J Oral Max Imp* 1996; 11:169–178.
20. Bäuerle D: *Laser Processing and Chemistry.* Berlin, Heidelberg, New York, Tokyo: Springer-Verlag, 2000.
21. Gaggl A, Schultes G, Müller WD, Kärcher H: Scanning electron microscopical analysis of laser-treated titanium implant surfaces – a comparative study. *Biomaterials* 2000; 21:1067–1073.
22. Pető G, Karacs A, Pászti Z, Guczi L, Divinyi T, Joób A: Surface treatment of screw shaped titanium dental implants by high intensity laser pulses. *Appl Surf Sci* 2001; 7524:1–7.
23. György E, Mihailescu IN, Serra P, Pérez del Pino A, Morenza JL: Crown-like structure development on titanium exposed to multipulse Nd:YAG laser irradiation. *Appl Phys A* 2002; 74:755–759.
24. Perez del Pino, Serra P, Morenza JL: Oxidation of titanium through Nd:YAG laser irradiation. *Appl Surf Sci* 2002; 197-198:887–890.
25. Nánai L, Vajtai R, George TF: Laser-induced oxidation of metals: state of art. *Thin Solid Films* 1997; 298:160–164.
26. Szatmari S, Schäfer FP: Simplified laser system for the generation of 60 fs pulses at 248 nm. *Opt Commun* 1988; 68:196–202.
27. Rimondini L, Farè S, Brambilla E, Felloni A, Consonni C, Brossa F, Carrassi A: The effect of surface roughness on early in vivo plaque colonization on titanium. *J Periodontol* 1997; 68:556–562.
28. Ameen AP, Short RD, Johns R, Schwach G: The surface analysis of implant materials 1. The surface composition of a titanium dental implant material. *Clin Oral Implan Res* 1993; 4:144–150.
29. Brånemark PI, Zarb GA, Albrektsson T: *Gewebeintegrierter Zahnersatz.* Berlin, Chicago, London, Rio de Janeiro, Tokio: Quintessenz Verlags-GmbH, 1985. p. 109–111.
30. Lausmaa J, Kasemo B: Surface spectroscopic characterization of titanium implant materials. *Appl Surf Sci* 1990; 44:133–146.
31. Sawase T, Hai K, Yoshida K, Baba K, Hatada R, Atsuta M: Spectroscopic studies of three osseointegrated implants. *J Dentistry* 1998; 26:119–124.

32. Kilpadi DV, Raikar GN, Liu J, Lemons JE, Vohra Y, Gregory JC: Effect of surface treatment on unalloyed titanium implants: Spectroscopic analyses. *J Biomed Mater Res* 1998; 40:646–659.
33. NIST XPS Database, 2000 (http://srdata.nist.gov/xps)
34. Park JY, Gemmell CH, Davies JE: Platelet interactions with titanium: modulation of platelet activity by surface topography. *Biomaterials* 2001; 2671–2682.
35. Arys A, Philippart C, Dourov N, He Y, Le QT, Pireaux JJ: Analysis of titanium dental implants after failure of osseointegration: combined histological, electron microscopy, and X-ray photoelectron spectroscopy approach. *J Biomed Mater Res* 1998; 43:300–312.
36. Sul YT, Johansson CB, Petronis S, Krozer A, Jeong Y, Wennerberg A, Albrektsson T: Characteristics of the surface oxides on turned and electrochemically oxidized pure titanium implants up to dielectric breakdown: the oxide thickness, micropore configurations, surface roughness, crystal structure and chemical composition. *Biomaterials* 2002; 23:491–501.
37. Sailer R, McCarthy G: *ICCD Grant-in-Aid.* North Dakota USA: Fargo, 1993
38. Kruger J, Kautek W: The femtosecond pulse laser: a new tool for micromachining. *Laser Physics* 1999; 9:30–40.
39. Banks PS, Feit MD, Rubenchik AM, Stuart BC, Perry MD: Material effects in ultra-short pulse laser drilling of metals. *Appl Phys A* 1999; 69:S377–380.
40. Zhu X, Naumov AY, Villeneuve DM, Corkum PB: Influence of laser parameters and material properties on micro drilling with femtosecond laser pulses. *Appl Phys A* 1999; 69:S367–371.
41. Tonshoff HK, Momma C, Ostendorf A, Nolte S, Kamlage G: Microdrilling of metals with ultrashort laser pulses. *J Laser Appl* 2000; 12:23–27.
42. Békési J, Klein-Wiele Jh, Simon P: Efficient submicron processing of metals with femtosecond UV pulses. *Appl Phys A* 2003; 76:355–357.

Dr. Pelsőczi I, Dr. Bereznai M, Dr. Tóth Z, Dr. Turzó K, Dr. Radnai M, Dr. Bor Z, Dr. Fazekas A:

Surface Modifications of Titanium Implant Material Induced by Excimer Laser Pulses

The biointegration of dental and orthopaedic implants depends mainly on the morphology and physical-chemical properties of their surfaces. Accordingly, the development of the desired microstructure is a relevant requirement in the bulk manufacture. Besides the widely used sandblasting plus acid etching and plasma-spray coating techniques, the laser surface modification method offers a plausible alternative. In order to analyze the influence of the laser treatment, the surfaces of titanium samples were exposed to excimer laser irradiation. The aim of this study was to develop surfaces that provide optimal conditions for bone-implant contact, bone growth, formation and maintenance of gingival attachment. For this purpose, holes were ablated on the surface of samples by nanosecond (18 ns, ArF) and also sub-picosecond (0,5 ps, KrF) laser pulses. Using pulses of ns length, due to melt ejection, crown-like protrusions were formed at the border of the holes, which made them sensitive to mechanical effects. To avoid these undesirable crown-like structures ultrashort KrF excimer laser pulses were successfully applied. On the other hand, titanium samples were laser-polished in favour of formation and connection of healthy soft tissues. Irradiation by a series of nanosecond laser pulses resulted in an effective smoothening as detected by atomic force microscopy (AFM). By inhibiting plaque accumulation this favours formation of gingival attachment. X-ray photoelectron spectroscopy (XPS) studies showed that laser treatment, in addition to micro-structural and morphological modification, results in decreasing of surface contamination and thickening of the oxide layer. X-ray diffraction (XRD) analysis revealed that the original α-titanium crystalline structure of the laser-polished titanium surface was not altered by the irradiation.

Key words: titanium, osseointegration, excimer laser ablation; surface modification; surface roughness